

**DEFLAGRATION-TO-DETONATION TRANSITION (DDT) STUDIES:
EFFECT OF NON-UNIFORM OBSTACLE DISTRIBUTION ON DDT**

A Dissertation

by

CAMILO ANDRES ROSAS-MARTINEZ

Submitted to the Office of Graduate and Professional Studies of
Texas A&M University
in partial fulfillment of the requirements for the degree of

DOCTOR OF PHILOSOPHY

Chair of Committee,	M. Sam Mannan
Co-Chair of Committee,	Eric L. Petersen
Committee Members,	Hae-Kwon Jeong
	Zhengdong Cheng
Head of Department,	Ibrahim Karaman

May 2016

Major Subject: Materials Science and Engineering

Copyright 2016 Camilo Andres Rosas-Martinez

ABSTRACT

Most of the previous work has been guided towards the understanding of this phenomenon under a uniform obstacle distribution, *i.e.*, same obstacle shape, blockage ratio, and gap between obstacles. However, industrial facilities lack this uniform obstruction arrangement. This research aimed to gain a better understanding of which non-uniform obstacle distribution enhances or weakens the flame acceleration. For this research, a 2.77 m long detonation tube with an internal diameter of 0.04 m was utilized. For the purpose of this investigation, a rig characterization was first performed to determine if a series of explosions under the same conditions was repeatable; the obtained responses showed similar behavior. Then, a Taguchi design of experiments was used. In this matrix, the parameters that were modified were: fuel type, obstacle shape, blockage ratio, and obstacle distribution. In general, each experiment consisted of nine obstacles inserted into the first meter of the detonation tube. The obstruction in each experiment had the same shape, but different blockage ratio and spacing between the obstacles. It was found that block-shaped obstacles with a decreasing blockage ratio and a “*staggered*” obstacle distribution had the highest tendency to promote the flame acceleration and, consequently, minimize the run-up distance to obtain a detonation. In contrast, experiments that had ring-shaped obstacles with an increasing blockage ratio and a “*variation*” obstacle distribution have an adverse effect on the flame acceleration and, consequently, maximize the distance at which DDT is observed.

Finally, the responses obtained from a Computational Fluid Dynamics (CFD) model were compared against data available in the literature and the experimental data obtained in this research. Even though this CFD model does not predict precisely the onset of DDT, it estimates the likelihood for having the onset of a detonation. In general, the CFD code predicts that the scenario that promotes a faster flame acceleration uses block-shaped obstacles with an equal blockage ratio and a “*staggered*” obstacle distribution. While the scenario that slows down the flame acceleration is given by ring-shaped obstacles with an increasing blockage ratio and a “*variation*” obstacle distribution. These trends agree with those from the experiment.

DEDICATION

To my parents, Carlos Felipe and Patricia, without whom I would not be where I am today;

To my siblings; To Stephanie; To my love, Maria Paula; and, To all my friends and family who helped me through this process

ACKNOWLEDGEMENTS

I would like to acknowledge Dr. Mannan for the opportunity to become a part of the Mary Kay O'Connor Process Safety Center. Thanks for your guidance and for leading me into different learning experiences that have allowed me to have a gigantic personal and professional development.

I also would like to thank Dr. Petersen for his guidance, support and encouragement. Thanks for your patience and dedication. You inspired me and guided me when I needed the most. Thank you for let me be part of the combustion group.

I would like to thank my committee members: Dr. Cheng and Dr. Jeong for their participation and assistance during the doctorate program.

I am deeply thankful to my team leaders: Dr. Carreto, Dr. Nayak and Dr. Laboureur for their support in each stage of my doctorate program. Thanks to Dr. Mashuga and Dr. Davis (from GexCon) for all his advice and long conversations we had on my research. Thanks to Dr. Glover for his advice, availability and guidance on my research. Thanks to the current and former members of the Mary Kay O'Connor Process Safety Center. Specially, thanks to Valerie Green, Mary Cass, Donna Startz, Tricia Hasan, Alanna Scheinerman and Amarette Renieri for their patience and support.

I would like to give special thanks to my friends Anibal Morones, Emiliano Vivanco and Dr. Mathieu, for helping me out when I had any issue with the experimental equipment. Thanks to Alberto, Alba and Josh for your encouragement and support during difficult times.

I would like to thank my parents, for their encouragement and for guiding me whenever I need the most. Thanks to my siblings Juan Carlos and Santiago Felipe; especially Juan Carlos for giving me his advice and for being an inspiration for me. Special thanks to Maria Paula, my fiancée, for all her patience and support throughout my doctorate program.

Thanks to all my friends and family, for being part of my academic development and for being there when I needed you the most. Thanks to Felipe Muñoz for believing in me and helping me after my undergrad.

Finally, thanks to God for guiding me throughout this process, for the strength and knowledge to complete my studies and for giving me the opportunity of being here and becoming an Aggie.

NOMENCLATURE

DDT	Deflagration-to-Detonation Transition
CFD	Computational Fluid Dynamics
ρ	Density
u	Velocity
\dot{m}	Mass flux
P, p	Pressure
h	Enthalpy
q	Chemical energy release
x_i	Composition
C_p	Specific heat at constant pressure
C_v	Specific heat at constant volume
γ	Specific heat ratio
R	Gas constant
T	Temperature
c_0	Speed of sound
BR	Blockage ratio
d	Orifice diameter
D	Tube diameter
λ	Cell size
L	Length of the detonation tube

ϕ	Equivalence ratio
CJ	Chapman-Jouguet
P_{CJ}	Chapman-Jouguet pressure
V_{CJ}	Chapman-Jouguet velocity
DPDX	Non-dimensional spatial pressure gradient
X_{CV}	Grid resolution
DDTLS	Deflagration-to-Detonation Transition length scale
LSLIM	Geometric length scale

TABLE OF CONTENTS

	Page
ABSTRACT	ii
DEDICATION	iv
ACKNOWLEDGEMENTS	v
NOMENCLATURE.....	vii
TABLE OF CONTENTS	ix
LIST OF FIGURES.....	xii
LIST OF TABLES	xxii
1. INTRODUCTION.....	1
1.1. Combustion Mechanisms	4
1.1.1. Deflagration.....	4
1.1.2. Onset of Detonation	5
1.1.3. Deflagration to Detonation Transition (DDT)	6
1.2. Gas Dynamic Theory of Detonations.....	8
1.2.1. Rayleigh Line and Hugoniot Curve	9
1.2.2. Chapman-Jouguet Theory	11
2. BACKGROUND.....	14
3. MOTIVATION AND PROBLEM STATEMENT	22
3.1. Motivation	22
3.2. Problem Statement	23
3.3. Research Objectives	25
4. EXPERIMENTAL	27
4.1. Detonation Tube.....	27
4.2. Data Acquisition Systems	28
4.3. Design of Experiments	30
4.4. Design of Obstacles.....	37
5. RIG CHARACTERIZATION.....	38

5.1.	Hydrogen–Oxygen Mixtures With an Equivalence Ratio of 1.0	38
5.2.	Hydrogen–Oxygen Mixtures With an Equivalence Ratio of 0.25	44
5.3.	Summary	50
6.	EXPERIMENTAL RESULTS	52
6.1.	Experiment 1	53
6.2.	Experiment 2	56
6.3.	Experiment 3	58
6.4.	Experiment 4	61
6.5.	Experiment 5	63
6.6.	Experiment 6	65
6.7.	Experiment 7	67
6.8.	Experiment 8	69
6.9.	Experiment 9	71
6.10.	Discussion	73
6.10.1.	Velocity Results	73
6.10.2.	Pressure Results.....	81
6.10.3.	Summary	88
6.11.	Validation	91
6.11.1.	Maximum Run-up Distance Layout.....	91
6.11.2.	Minimum Run-up Distance Layout.....	94
6.12.	Conclusions	97
7.	DEFLAGRATION-TO-DETONATION TRANSITION (DDT): PREDICTING DDT IN HYDROCARBON-AIR MIXTURE EXPLOSIONS WITH DATA AVAILABLE FROM THE LITERATURE	100
7.1.	FLACS Background.....	102
7.2.	Selection of Scenarios	105
7.3.	Results and Discussion.....	107
7.3.1.	Confined Geometries.....	107
7.3.2.	Unconfined, Open Geometries	113
7.4.	Summary	123
8.	DEFLAGRATION-TO-DETONATION TRANSITION (DDT): PREDICTING DDT IN FUEL-OXYGEN SYSTEMS USING EXPERIMENTAL DATA	125
8.1.	Methodology	125
8.2.	Simulation Results.....	126
8.2.1.	Scenario 1	127
8.2.2.	Scenario 2	131
8.2.3.	Scenario 3	134
8.2.4.	Scenario 4.....	138
8.2.5.	Scenario 5	141

8.2.6.	Scenario 6.....	144
8.2.7.	Scenario 7.....	148
8.2.8.	Scenario 8.....	151
8.2.9.	Scenario 9.....	155
8.3.	Discussion.....	158
8.4.	Summary.....	164
8.5.	Conclusions.....	165
9.	CONCLUSIONS AND FUTURE WORK.....	166
9.1.	Conclusions.....	166
9.2.	Future Work.....	168
	REFERENCES.....	171

LIST OF FIGURES

	Page
Figure 1. Graphic description of a deflagration (expansion wave). The red line represents the reaction front and the black line represents the shock front. Adapted from [5].	4
Figure 2. Graphic description of a detonation (compression wave). The red line represents the reaction front and the black line represents the shock front. Adapted from [5].	6
Figure 3. Rayleigh line and Hugoniot curve. Adapted from [5].	11
Figure 4. CJ solutions. Adapted from [5].	13
Figure 5. Photograph of the detonation tube at Texas A&M University.	28
Figure 6. Original layout of the pressure transducers, units are in m.	28
Figure 7. New layout of the pressure transducers positions along the tube, units in m.	29
Figure 8. Selection of basic obstacle shapes used in this study. a) half washer-shaped obstacle with a blockage ratio of 25%. b) block-shaped obstacle with a blockage ratio of 40%. c) ring-shaped obstacle with a blockage ratio of 80%. All the obstacles have a thickness of 0.25 in. Dimensions shown are in units of inches.	32
Figure 9. Experimental results for different fuel-oxygen mixtures for no obstacles and $\phi=1$ for all mixtures. a) Experimental results for a H_2-O_2 explosions with $P_0 = 20$ kPa. Figures b) and c) show the average pressure and velocity results, respectively, for the H_2-O_2 experiments with $P_0 = 20$ kPa. Figures d) and e) illustrate the average pressure and velocity results, respectively, for $C_2H_2-O_2$ explosions with $P_0 = 9.3$ kPa and $C_2H_4-O_2$ explosions with $P_0 = 17$ kPa.	34
Figure 10. Pressure results obtained for a Hydrogen-Oxygen mixture ($\phi = 1$) explosion with half washer-shaped obstacles, an equal blockage ratio, and a gap between obstacles of 3D. Each frame shows the results obtained for the transducers described within the figures (T1 – T17).	39
Figure 11. Overall progression of the combustion wave for a Hydrogen-Oxygen mixture ($\phi = 1$) explosion with half washer-shaped obstacles, an equal blockage ratio and a gap between obstacles of 3D.	41

Figure 12. Summary of experimental results for Hydrogen-Oxygen mixture explosions ($\varphi = 1$) in the characterization study. Figures a) and b) show the pressure and velocity results, respectively, for the 10 experiments, and Figures c) and d) illustrate the average pressure and velocity results, respectively. The error bars represent one standard deviation obtained for each transducer.	42
Figure 13. Variability of the run-up distances obtained for 10 repeat hydrogen-oxygen mixture ($\varphi = 1$) explosions with an initial pressure of 20 kPa. The obstacle configuration used in these experiments was: half-washer-shaped obstacles with a uniform blockage ratio (40%) and with a gap between obstacles of 3D.	44
Figure 14. Pressure results obtained for a Hydrogen-Oxygen mixture ($\varphi = 0.25$) explosion with half washer-shaped obstacles, an equal blockage ratio, and a gap between obstacles of 3D. Each frame shows the results obtained for the transducers described within the figures (T1 – T17).	45
Figure 15. Overall progression of the combustion wave for a Hydrogen-Oxygen mixture ($\varphi = 0.25$) explosion with half washer-shaped obstacles, an equal blockage ratio and a gap between obstacles of 3D.	47
Figure 16. Summary of experimental results for Hydrogen-Oxygen mixture explosions ($\varphi = 0.25$) in the characterization study. Figures a) and b) show the pressure and velocity results, respectively, for the four experiments, and Figures c) and d) illustrate the average pressure and velocity results, respectively. The error bars represent one standard deviation obtained for each transducer.	48
Figure 17. Variability of the run-up distances obtained for four repeat hydrogen-oxygen mixture ($\varphi = 0.25$) explosions with an initial pressure of 20 kPa. The obstacle configuration used in these experiments was: half-washer-shaped obstacles with a uniform blockage ratio (40%) and with a gap between obstacles of 3D.	49
Figure 18. Obstacle layout for Experiment 1 – Ring-shaped obstacles with an increasing blockage ratio and a “ <i>variation</i> ” obstacle distribution. The first obstacle is located at 0.16 m away from the ignition point. The gap between the first two obstacles is 2D. The gap between the second and third obstacle is 3D. The gap between the next pair of obstacles is 1D. The location for the upcoming obstacles is repeated following the same order. Units are given in meters.	53
Figure 19. Experimental pressure and velocity results for Experiment 1, a hydrogen-oxygen mixture ($\varphi = 1$) explosion with ring-shaped obstacles, an increasing	

blockage ratio, and a placement of obstacles as follows: once, twice, and three times the internal diameter of the detonation tube. T_n represent the response obtained for that pressure transducer location.	54
Figure 20. Summary of the experimental results for Experiment 1, the hydrogen-oxygen mixtures with ring-shaped obstacles, an increasing BR, and a variation obstacle distribution.	55
Figure 21. Obstacle layout for Experiment 2 – Half-washer-shaped obstacles with an equal blockage ratio and a “ <i>uniform</i> ” obstacle distribution. The gap between the obstacles is 2D. Units are given in meters.	57
Figure 22. Summary of the experimental results for Experiment 2—hydrogen-oxygen mixtures with half washer-shaped obstacles, an equal BR, and a uniform obstacle distribution.	57
Figure 23. Obstacle layout for Experiment 3 – Block-shaped obstacles with a decreasing blockage ratio and a “ <i>staggered</i> ” obstacle distribution. The gap between the first three obstacles is 1D each. Each set is separated by a gap of 5D. The location for the upcoming obstacles is repeated following the same order. Units are meters.	59
Figure 24. Summary of the experimental results for Experiment 3—hydrogen-oxygen mixtures with block-shaped obstacles, decreasing BR, and a staggered obstacle distribution.	59
Figure 25. Obstacle’ layout for experiment 4 – ring-shaped obstacles with an equal blockage ratio and a “ <i>staggered</i> ” obstacle distribution. The gap between the first three obstacles is 1D. This is then followed by a gap of 5D. The location for the upcoming obstacles is repeated following the same order. Dimensions are in m.	61
Figure 26. Summary of the results for Experiment 4—ethylene-oxygen mixtures with ring-shaped obstacles, equal BR, and a staggered obstacle distribution.	62
Figure 27. Obstacle layout for Experiment 5 – half-washer-shaped obstacles with a decreasing blockage ratio and a “ <i>variation</i> ” obstacle distribution. The gap between the first two obstacles is 2D. The gap between the second and third obstacles is 3D. The gap between the next pair of obstacles is 1D. The location for the upcoming obstacles is repeated following the same order. Units are given in meters.	63
Figure 28. Summary of the results for Experiment 5—ethylene-oxygen mixtures with half-washer-shaped obstacles, decreasing BR, and a variation obstacle distribution.	64

Figure 29. Obstacle layout for Experiment 6 – block-shaped obstacles with an increasing blockage ratio and a “ <i>uniform</i> ” obstacle distribution. The gap between the obstacles is 2D. Units are given in meters.....	65
Figure 30. Summary of the Experiment 6—ethylene-oxygen mixtures with block-shaped obstacles, increasing BR, and a uniform obstacle distribution.....	66
Figure 31. Obstacle layout for Experiment 7 – ring-shaped obstacles with a decreasing blockage ratio and a “ <i>uniform</i> ” obstacle distribution. The gap between the obstacles is 2D. Units are given in meters.....	68
Figure 32. Summary of the results for Experiment 7—acetylene-oxygen mixtures with ring-shaped obstacles, decreasing BR, and a uniform obstacle distribution.....	68
Figure 33. Obstacle layout for Experiment 8 – Half-washer-shaped obstacles with an increasing blockage ratio and a “ <i>staggered</i> ” obstacle distribution. The gap between the first three obstacles is 1D each. This is then followed by a gap of 5D. The location for the upcoming obstacles is repeated following the same order. Units are given in meters.	70
Figure 34. Summary of the results for Experiment 8—C ₂ H ₂ -O ₂ mixture with half-washer-shaped obstacles, increasing BR, and a staggered obstacle distribution.....	70
Figure 35. Obstacle layout for Experiment 9 – block-shaped obstacles with an equal blockage ratio and a “ <i>variation</i> ” obstacle distribution. The gap between the first two obstacles was 2D. The gap between the second and third obstacle was 3D. The gap between the next pair of obstacles was 1D. The location for the upcoming obstacles is repeated following the same order. Units are given in meters.....	72
Figure 36. Summary of the results for Experiment 9—an acetylene-oxygen mixture with block-shaped obstacles, equal BR, and a variation obstacle distribution.....	72
Figure 37. Sensitivity analysis for the wave velocity for different (a) location and (b) magnitude variables having fuel type as the parameter of interest.....	76
Figure 38. Sensitivity analysis for the wave velocity for different (a) location and (b) magnitude variables having obstacle shape as the parameter of interest.....	77
Figure 39. Sensitivity analysis for the wave velocity for different (a) location and (b) magnitude variables having blockage ratio as the parameter of interest.	78

Figure 40. Sensitivity analysis for the wave velocity for different (a) location and (b) magnitude variables having obstacle distribution as the parameter of interest.....	79
Figure 41. Sensitivity analysis for the pressure for different (a) location and (b) magnitude variables having fuel type as the parameter of interest.....	83
Figure 42. Sensitivity analysis for the pressure for different (a) location and (b) magnitude variables having the obstacle shape as the parameter of interest.....	84
Figure 43. Sensitivity analysis for the pressure for different (a) location and (b) magnitude variables having the blockage ratio as the parameter of interest. ...	85
Figure 44. Sensitivity analysis for the pressure for different (a) location and (b) magnitude variables having the obstacle distribution as the parameter of interest.....	86
Figure 45. Results for the ethylene–oxygen mixture using the results for maximum run-up distance shown in Table 9.....	91
Figure 46. Results for the acetylene–oxygen mixture using the results for maximum run-up distance shown in Table 9.....	93
Figure 47. Results for the ethylene–oxygen mixture using the configuration for minimum run-up distance shown in Table 9.	95
Figure 48. Results for acetylene–oxygen mixtures using the results for minimum run-up distance shown in Table 9.....	96
Figure 49. Estimated explosion overpressures based on blast damage (left) [46] and predicted using FLACS (right) for the Buncefield fuel storage depot explosion.....	102
Figure 50. Flame front (top) and shock front (bottom) snapshots e (ID 0.3 – C ₂ H ₄ , $\phi = 0.56$) at 160.9 ms. Note that the flame front (interface between the red and blue in the top image) has reached the exit of the shock tube as well as the associated shock front (pressures > 12 barg locally) in the bottom image.....	110
Figure 51. DPD _X snapshot e (ID 0.3 – C ₂ H ₄ , $\phi = 0.56$) at 160.9 ms. Note that the lower threshold value for DPD _X (dark blue) is given as 1.....	111
Figure 52. Flame front (Top) and Shock front (Bottom) snapshots - (ID 0.3 – H ₂ , $\phi = 3.58$) at ~24.5 ms. Note that the flame front (interface between the red and	

blue in the Top image) has reached approximately 2.7 m from end of the shock tube as well as the associated shock front (pressures >10 barg locally) in the bottom image.	111
Figure 53. DPDX snapshot e (ID 0.3 – H ₂ , $\phi = 3.58$) at ~24.5 ms. Note that the lower threshold value for DPDX (dark blue) is given as 1. The image shows that a detonation is likely (<i>e.g.</i> , DPDX > 5).	112
Figure 54. Layouts of the scenarios used by BP for their experiments (left 4 rows of pipes configuration and right 7 rows of pipes configuration). Adapted from [77].	114
Figure 55. PMAX (Left) and DPDX (Right) snapshots - (4 rows of pipes configuration – C ₂ H ₄ , $\phi = 1.0$) at ~129 ms. Note the pressures were observed to be less than 0.4 barg and no DDT was observed (DPDX < 1)....	115
Figure 56. PMAX (Left) and DPDX (Right) snapshots - (7 rows of pipes configuration – C ₂ H ₄ , $\phi = 1.0$) at ~123 ms. Note the pressures were observed to be less than 0.7 barg and no DDT was observed (DPDX < 1)....	115
Figure 57. PMAX (Left) and DPDX (Right) snapshots - (4 rows of pipes configuration – H ₂ , $\phi = 0.8$) at ~48 ms. Note the pressures were observed to be less than 4 barg and no DDT was observed within the geometry (DPDX < 1).....	116
Figure 58. PMAX (Left) and DPDX (Right) snapshots - (4 rows of pipes configuration – H ₂ , $\phi = 1.0$) at ~51 ms. Note the pressures were observed to be less than 3 barg and no DDT was observed within the geometry (DPDX < 1).....	117
Figure 59. PMAX (Left) and DPDX (Right) snapshots - (4 rows of pipes configuration – H ₂ , $\phi = 1.2$) at ~65 ms. Note the pressures were observed to be less than 2 barg and no DDT was observed within the geometry (DPDX < 1).....	117
Figure 60. PMAX (Left) and DPDX (Right) snapshots - (4 rows of pipes configuration – H ₂ , $\phi = 1.6$) at ~61 ms. Note the pressures were observed to be less than 2 barg and no DDT was observed within the geometry (DPDX < 1).....	118
Figure 61. PMAX (Left) and DPDX (Right) snapshots - (4 rows of pipes configuration – H ₂ , $\phi = 1.7$) at ~61 ms. Note the pressures were observed to be less than 2 barg and no DDT was observed within the geometry (DPDX < 1).....	118

Figure 62. PMAX (Left) and <i>DPDX</i> (Right) snapshots - (7 rows of pipes configuration – H ₂ , $\phi = 0.8$) at ~35 ms. Note the pressures were observed to be greater than 14 barg and DDT is likely to occur (<i>DPDX</i> > 10).....	120
Figure 63. PMAX (Left) and <i>DPDX</i> (Right) snapshots - (7 rows of pipes configuration – H ₂ , $\phi = 1.0$) at ~38 ms. Note the pressures were observed to be greater than 10 barg and DDT is likely to occur (<i>DPDX</i> > 10).....	120
Figure 64. PMAX (Left) and <i>DPDX</i> (Right) snapshots - (7 rows of pipes configuration – H ₂ , $\phi = 1.2$) at ~50 ms. Note the pressures were observed to be greater than 10 barg and DDT is likely to occur (<i>DPDX</i> > 10).....	121
Figure 65. PMAX (Left) and <i>DPDX</i> (Right) snapshots - (7 rows of pipes configuration – H ₂ , $\phi = 1.6$) at ~46 ms. Note the pressures were observed to be greater than 10 barg and DDT is likely to occur (<i>DPDX</i> > 10).....	121
Figure 66. PMAX (Left) and <i>DPDX</i> (Right) snapshots - (7 rows of pipes configuration – H ₂ , $\phi = 1.7$) at ~46 ms. Note the pressures were observed to be greater than 9 barg and DDT is likely to occur (<i>DPDX</i> > 10).....	122
Figure 67. Overpressure for measurements parallel (left) and perpendicular (right) to wall 4 rows of pipes configuration – H ₂ , $\phi = 1$).	123
Figure 68. <i>DPDX</i> profile obtained using ring-shaped obstacles with an increasing blockage ratio and a “ <i>variation</i> ” obstacle distribution – Previous the modification of the flame velocity.....	127
Figure 69. <i>DPDX</i> profile obtained using ring-shaped obstacles with an increasing blockage ratio and a “ <i>variation</i> ” obstacle distribution – After the modification of the flame velocity.....	129
Figure 70. Comparison between the experimental and the simulation results for Scenario 1 – H ₂ -O ₂ mixtures with ring-shaped obstacles, an increasing BR, and a variation obstacle distribution. a) prior modification of the flame velocity, b) after the modification of the flame velocity.	129
Figure 71. <i>DPDX</i> profile obtained using half-washer-shaped obstacles with an equal blockage ratio and a “ <i>uniform</i> ” obstacle distribution – Previous the modification of the flame velocity.....	131
Figure 72. <i>DPDX</i> profile obtained using half-washer-shaped obstacles with an equal blockage ratio and a “ <i>uniform</i> ” obstacle distribution – After the modification of the flame velocity.....	132

Figure 73. Comparison between the experimental and the simulation results for Scenario 2 – H ₂ -O ₂ mixtures with half-washer-shaped obstacles, an equal BR, and a uniform obstacle distribution. a) prior modification of the flame velocity, b) after the modification of the flame velocity.	133
Figure 74. DPDX profile obtained using block-shaped obstacles with a decreasing blockage ratio and a “ <i>staggered</i> ” obstacle distribution – Previous the modification of the flame velocity.....	134
Figure 75. DPDX profile obtained using block-shaped obstacles with a decreasing blockage ratio and a “ <i>staggered</i> ” obstacle distribution – After the modification of the flame velocity.....	136
Figure 76. Comparison between the experimental and the simulation results for Scenario 3 – H ₂ -O ₂ mixtures with block-shaped obstacles, decreasing BR, and a staggered obstacle distribution. a) prior modification of the flame velocity, b) after the modification of the flame velocity.	137
Figure 77. DPDX profile obtained using ring-shaped obstacles with an equal blockage ratio and a “ <i>staggered</i> ” obstacle distribution – Previous the modification of the flame velocity.....	138
Figure 78. DPDX profile obtained using ring-shaped obstacles with an equal blockage ratio and a “ <i>staggered</i> ” obstacle distribution – After the modification of the flame velocity.....	139
Figure 79. Comparison between the experimental and the simulation results for Scenario 4 – C ₂ H ₄ -O ₂ mixtures with ring-shaped obstacles, an equal BR, and a staggered obstacle distribution. a) prior modification of the flame velocity, b) after the modification of the flame velocity.	140
Figure 80. DPDX profile obtained using half-washer-shaped obstacles with a decreasing blockage ratio and a “ <i>variation</i> ” obstacle distribution – Previous the modification of the flame velocity.....	141
Figure 81. DPDX profile obtained using half-washer-shaped obstacles with a decreasing blockage ratio and a “ <i>variation</i> ” obstacle distribution – After the modification of the flame velocity.....	142
Figure 82. Comparison between the experimental and the simulation results for Scenario 5 – C ₂ H ₄ -O ₂ mixtures with half-washer-shaped obstacles, decreasing BR, and a variation obstacle distribution. a) prior modification of the flame velocity, b) after the modification of the flame velocity.....	143

Figure 83. DPDX profile obtained using block-shaped obstacles with an increasing blockage ratio and a “uniform” obstacle distribution – Previous the modification of the flame velocity.....	145
Figure 84. DPDX profile obtained using block-shaped obstacles with an increasing blockage ratio and a “uniform” obstacle distribution – After the modification of the flame velocity.....	146
Figure 85. Comparison between the experimental and the simulation results for Scenario 6 – C ₂ H ₄ -O ₂ mixtures with block-shaped obstacles, increasing BR, and a uniform obstacle distribution. a) prior modification of the flame velocity, b) after the modification of the flame velocity.	147
Figure 86. DPDX profile obtained using ring-shaped obstacles with a decreasing blockage ratio and a “uniform” obstacle distribution – Previous the modification of the flame velocity.....	148
Figure 87. DPDX profile obtained using ring-shaped obstacles with a decreasing blockage ratio and a “uniform” obstacle distribution – After the modification of the flame velocity.....	149
Figure 88. Comparison between the experimental and the simulation results for Scenario 7 – C ₂ H ₂ -O ₂ mixtures with ring-shaped obstacles, decreasing BR, and a uniform obstacle distribution. a) prior modification of the flame velocity, b) after the modification of the flame velocity.	150
Figure 89. DPDX profile obtained using half-washer-shaped obstacles with an increasing blockage ratio and a “staggered” obstacle distribution – Previous the modification of the flame velocity.....	152
Figure 90. DPDX profile obtained using half-washer-shaped obstacles with an increasing blockage ratio and a “staggered” obstacle distribution – After the modification of the flame velocity.....	153
Figure 91. Comparison between the experimental and the simulation results for Scenario 8 – C ₂ H ₂ -O ₂ mixtures with half-washer-shaped obstacles, increasing BR, and staggered obstacle distribution. a) prior modification of the flame velocity, b) after the modification of the flame velocity.	154
Figure 92. DPDX profile obtained using block-shaped obstacles with an equal blockage ratio and a “variation” obstacle distribution – Previous the modification of the flame velocity.....	155

Figure 93. DPDX profile obtained using block-shaped obstacles with an equal blockage ratio and a “ <i>variation</i> ” obstacle distribution – After the modification of the flame velocity.....	156
Figure 94. Comparison between the experimental and the simulation results for Scenario 9 – C ₂ H ₂ -O ₂ mixtures with block-shaped obstacles, equal BR, and a variation obstacle distribution. a) prior modification of the flame velocity, b) after the modification of the flame velocity.	157
Figure 95. Sensitivity analysis for the pressure for different (a) location and (b) magnitude variables having fuel type as the parameter of interest.....	159
Figure 96. Sensitivity analysis for the pressure for different (a) location and (b) magnitude variables having the obstacle shape as the parameter of interest.....	160
Figure 97. Sensitivity analysis for the pressure for different (a) location and (b) magnitude variables having the blockage ratio as the parameter of interest. .	161
Figure 98. Sensitivity analysis for the pressure for different (a) location and (b) magnitude variables having the obstacle distribution as the parameter of interest.....	162

LIST OF TABLES

	Page
Table 1. Description of the parameters and its levels.....	30
Table 2. Design of experiments matrix utilized for this study	31
Table 3. Description of the obstacles machined.....	37
Table 4. CJ conditions obtained from the Shock and Detonation Toolbox [56] for the fuel-oxygen systems utilized in these experiments	52
Table 5. Summary of experimental results for the velocity data. Speeds are given relative to the calculated CJ velocity.	74
Table 6. Ranking of variables as a function of the parameters modified in the experiments, where “1” is most significant and “4” is least significant.	80
Table 7. Summary of experimental results for the pressure data. Pressures are given relative to their respective CJ levels.	82
Table 8. Ranking of experiment parameters for the various pressure response variables measured in the experiments.	87
Table 9. Maximum and minimum run-up distance scenarios	88
Table 10. Maximum and minimum distance when the experimental pressure exceeds the CJ pressure for the first time.....	90
Table 11. Summary of the scenarios simulated in FLACS	107
Table 12. Experiments performed by Peraldi <i>et al.</i> [36].....	108
Table 13. Summary of results from the simulations	109
Table 14. CJ pressure for different concentrations of hydrogen	119
Table 15. Summary of the simulation results for the pressure data. Pressures are given relative to their respective CJ levels.	158
Table 16. Ranking of variables as a function of the parameters modified in the simulations, where “1” is most significant and “4” is least significant.	163
Table 17. Maximum and minimum run-up distance scenarios	164

1. INTRODUCTION

Explosions are still one of the major concerns for the different chemical, petrochemical, mining, transport, and other industries. The hazards derived from explosions require the development and maintenance of safety measures aimed to prevent and mitigate explosions [1,2]. Upon ignition of an explosive mixture, a combustion wave, which transforms the reactants into products, propagates away from the ignition source. During this process, there is a release of potential energy stored in the chemical bonds of the reactant molecules, which is then converted into thermal and kinetic energy for the combustion products [3-6].

In general, for an explosion to occur there are two possibilities. The first one is that the explosion occurs due to a high energy ignition source. This scenario will lead to a direct initiation of a detonation (when the combustion wave travels at supersonic speeds) [7]. The second scenario, which is the more likely situation, occurs due to a low energy ignition source. In this case, a deflagration (combustion wave that travels at subsonic speeds) will develop first [8]. However, a self-propagating deflagration is unstable and presents an acceleration tendency subsequent to its ignition [9]. If the appropriate conditions are present, the flame can accelerate and undergo an abrupt transition from deflagration to detonation [5].

In terms of industrial safety, DDTs are undesirable events, and when they occur, the consequences of the explosion can go beyond the facility boundaries [10]. Therefore, it is imperative to reduce the likelihood of obtaining DDTs. For this purpose, experimental

studies have been guided towards the understanding of this phenomenon, and it has been found that for DDTs to occur, several variables play key roles: *e.g.*, confinement, obstruction, sensitivity of the mixture to detonate [11-21]. Obstruction (shape and blockage ratio) is a physical parameter that can be easily modified. It is therefore important to determine how a larger or smaller blockage ratio affects the onset of detonation as well as the interaction between the detonation wave and the obstacle. In order to get a better understanding of the role played by the obstruction, several researchers [5,13,15-17,19-21] performed experiments with a uniform distribution of obstacles (same shape, blockage ratio and separation distance between the obstacles). From these tests, it was found that an optimal value to reduce the run-up distance to obtain DDT exists when the blockage ratio is ~43% and the gap distance between obstacles is one tube diameter.

However, this obstacle uniformity is not present at any industrial facility. On the contrary, obstructions, such as pipe racks, vessels, pumps, and turbines, create a non-uniform distribution of obstacles and, consequently, might affect the total distance required to obtain DDT. Therefore, this research was focused on the effect of non-uniform distribution of obstacles.

Currently, there is not a publicly available computational tool capable of integrating the combustion regime of deflagration and detonation into one module. All models treat these combustion processes independently. This situation is mainly because the mechanisms of propagation of a deflagration (diffusion of heat and mass) and of detonation (adiabatic compression) are very different. When DDT occurs, this change is represented by a discontinuity, which occurs very rapidly and is shown by a sudden

increase in the overpressure. However, this gap in research has not stopped the evolution of CFD models. In general, the onset of detonation occurs when the flame front catches up to the pressure front. Some CFD models are capable of showing when this occurs, despite the fact that they do not reproduce the discontinuity from deflagration to detonation. Therefore, it is possible to use these models to predict how likely DDT is to occur and the possible run-up distance where DDT is achieved [22,23]. As this methodology is relatively new, a comparison between experimental and estimated data must be performed. The variables to look at are pressure and run-up distance to obtain DDT. For the purpose of this research, the CFD model that was used was FLACS.

In the following sections, a brief introduction to gas-dynamics is given, followed by a literature review and the distinction between deflagration and detonation including flame acceleration mechanisms that could potentially trigger the transition from deflagration to detonation. This will allow the identification of the mechanisms for DDT to occur in two different situations: in a smooth-walled tube and in a tube filled with obstacles. Once this has been described, an overview of the facility (detonation tube) and the experimental methodology utilized in this research is presented. Then, the experimental results are shown and described in detail, followed by an introduction to the CFD model used in this research. Prior to the use of FLACS, a validation process was performed against available data found in the literature. Then, a comparison between the experimental results obtained in this research and the results obtained with the CFD model is provided.

1.1. Combustion Mechanisms

1.1.1. Deflagration

In general, deflagrations are described by the lower branch of the Hugoniot curve. In this section of the curve, the pressure and density behind the flame are lower than in the initial state (p_0, ρ_0) . A deflagration occurs whenever a combustion wave travels at subsonic speed with respect to the unburned gas ahead of the flame. Being a subsonic wave, downstream disturbances can propagate upstream and influence the initial state of the reactants. This disturbance propagation makes the deflagration a combustion process that depends not only on the initial state of the mixture, but also on the rear boundary conditions [24]. For instance, if a deflagration is propagating from the closed end of a tube where the particle velocity must be zero, then the decrease of density across the flame front leads to a displacement of the reactants ahead of it. The flame will then push the reactants, forcing them to move in the same direction as the flame. This process is illustrated in Figure 1.

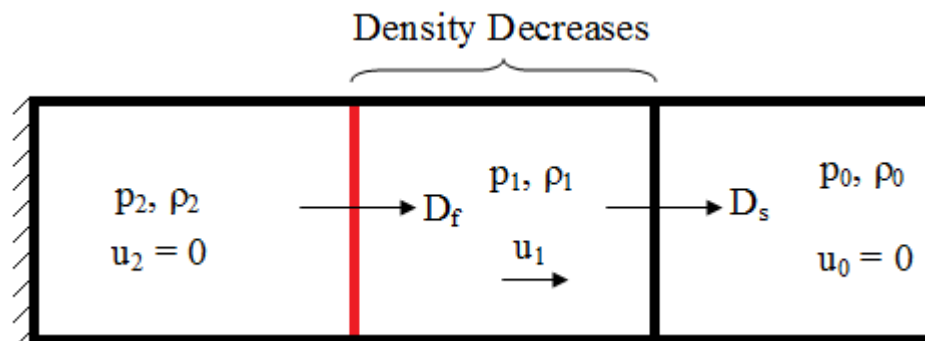


Figure 1. Graphic description of a deflagration (expansion wave). The red line represents the reaction front and the black line represents the shock front. Adapted from [5].

Furthermore, the decrease in the density of the mixture across the flame causes the formation of compression waves. When the compression waves catch up with one another, they form a precursor wave. Such a wave sets the reactants behind it into motion, modifying the initial state of the reactants. As can be observed in Figure 1, another characteristic of deflagration is the existence of a gap between the shock and reaction front. The reason for this gap to exist is that the pressure in the products is higher than the initial pressure (p_0). This pressure difference implies that the momentum of the gas between the shock and the flame front must increase with time; in other words, the flame and pressure front speeds are different. Consequently, the gap between them will increase. Moreover, it is important to note that the mechanism of propagation of deflagrations is to propagate into the flammable mixture via diffusion of heat and mass [4,5].

1.1.2. Onset of Detonation

Detonations occur when the combustion wave travels at supersonic speeds with respect to the unburned gas ahead of the flame. This condition forces the pressure and temperature to increase drastically within a small period of time (typically microseconds). During a detonation, the reactants ahead of the wave are not disturbed until the pressure and reaction front reach them. Detonations are compression waves, where the density increases across the wave and the products of the reaction move in the same direction of the wave motion (Figure 2). Moreover, the reaction front and the shock front are coupled together; the separation distance is extremely small, and it is difficult to distinguish between them. Detonations can be considered self-sustained propagating waves, where the ignition mechanism of the reactants ahead of the wave is caused by the adiabatic

compression of the shock front which interacts first with the reactants and then with the reaction front [25].

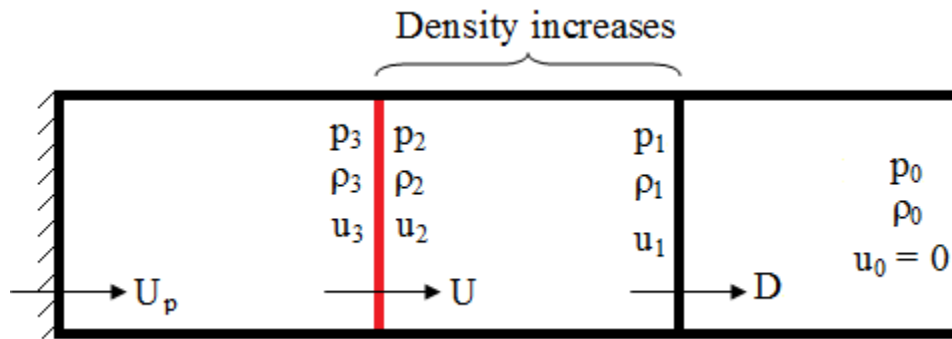


Figure 2. Graphic description of a detonation (compression wave). The red line represents the reaction front and the black line represents the shock front. Adapted from [5].

The onset of detonation occurs when the appropriate conditions have been achieved in the turbulent flame zone. This means that the detonation by itself does not depend on the flame acceleration process that was needed to achieve such conditions. For instance, in a transition from deflagration to detonation in a smooth-walled tube, the required conditions in the turbulent flame zone are achieved once the deflagration has accelerated up to some critical velocity, *e.g.*, typically half the CJ velocity of detonation or the CJ deflagration speed [26].

1.1.3. *Deflagration to Detonation Transition (DDT)*

It is possible for the combustion process to undergo an abrupt DDT. In such processes, a flammable mixture is ignited with a low energy source followed by the occurrence of a deflagration. However, if appropriate conditions are satisfied, *e.g.*,

turbulence and localized auto-explosions, the flame front will keep accelerating until it couples together with the shock front, which leads to detonation.

Experiments have been performed in the literature to determine how the transition from deflagration to detonation occurs. For instance, Moen [24] describes that once a deflagration starts, it is possible to observe that the pressure front and the reaction front are apart from each other. When obstacles are present in the detonation tube, the overall velocity of the combustion wave will tend to increase due to the flame folding and stretching, which increases the surface area of the flame and, consequently, increases the amount of material that participates in the reaction. Additionally, the presence of obstructions in the path of the combustion wave helps the creation of pockets of compressed and un-reacted mass at high temperatures that can be ignited via shock interactions. Typically, these shocks are known as Mach stems, which are shock fronts that travel at supersonic speed and have sufficient energy to auto-ignite unburned pockets of gases. When this pocket of mass is successfully ignited, it has the potential to create an auto-explosion, which leads to a rapid acceleration of the flame front. As discussed by Lee [5], the presence of the localized auto-explosions is one of the necessary conditions to have a successful deflagration-to-detonation transition.

During a deflagration, the combustion process is influenced by turbulence. For instance, if the turbulence is excessive, the combustion process will quench. This effect occurs mainly because the flame travels extremely fast and does not have enough time to fold/stretch and burn all the hot-pockets of compressed gases. The combustion process will also quench if the turbulence is insufficient. This occurs since a deflagration is not

self-sustainable. However, when the system has adequate turbulence, the flame will have enough time to fold/stretch and burn all the gas, even by localized auto-explosions in the hot-pockets. This mechanism enhances the flame speed until the flame front and the shock front are coupled together [7,8,25].

1.2. Gas Dynamic Theory of Detonations

For a specific initial state and boundary conditions, the properties of the combustion wave can be obtained by solving the conservation equations across the wave. Applying the basic conservation equations of mass, momentum, and energy in the following system, one obtains:

$$\rho_o u_o = \rho_1 u_1 = \dot{m} \quad (1)$$

$$p_o + \rho_o u_o^2 = p_1 + \rho_1 u_1^2 \quad (2)$$

$$h_o + q + \frac{u_o^2}{2} = h_1 + \frac{u_1^2}{2}; \text{ where } q = \sum_i^{\text{Reactants}} x_i h_{f_i}^\circ - \sum_j^{\text{Products}} x_j h_{f_j}^\circ \quad (3)$$

This result demonstrates that the enthalpy in equation 3 only depends on the specific heat of the mixture, determined by the composition. Although the product composition is hard to determine, generally carbon dioxide and water are considered the final products. One major assumption from this point on is that the value of the chemical energy release (q) is known and constant. Assuming that $h = c_p T$, and the ideal gas law applies ($P = \rho RT$, $c_p - c_v = R$ and $\gamma = c_p/c_v$), the enthalpy can be written as [5,24]:

$$h = \frac{\gamma}{\gamma - 1} \frac{p}{\rho} \quad (4)$$

Thus, if the initial state of the mixture is known, four equations will be available. However, when solving for five unknown properties (u_0 , u_1 , p_1 , ρ_1 and h_1), one more equation is required, which is described in the following section.

1.2.1. Rayleigh Line and Hugoniot Curve

If Equations 1 and 2 are combined, a new relationship is obtained for the mass flux per unit area:

$$\dot{m}^2 = \frac{p_1 - p_0}{\frac{1}{\rho_0} - \frac{1}{\rho_1}} \quad \rightarrow \quad \dot{m} = \sqrt{\frac{p_1 - p_0}{\frac{1}{\rho_0} - \frac{1}{\rho_1}}} \quad (5)$$

This equation shows that there are two possible scenarios. First, if $p_1 > p_0$, it requires $1/\rho_0 > 1/\rho_1$ for \dot{m} to be real. This case refers to the compression solution, or the detonation waves. Second, if $p_1 < p_0$, it requires $1/\rho_0 < 1/\rho_1$ for \dot{m} to be real. This refers to the expansion solution, or the deflagration waves. Furthermore, the equations can be simplified by introducing two, new dimensionless variables $x = \rho_0/\rho_1$ and $y = p_1/p_0$, which can be rewritten as:

$$\dot{m} = \sqrt{\left(\frac{y-1}{1-x}\right) * p_0 * \rho_0} \quad (6)$$

By applying the definition of sound speed, $c_0 = \sqrt{\gamma_0 p_0 / \rho_0}$ and the definition of the Mach number, $M_0 = u_0 / c_0$, equation 6 can be rewritten as:

$$\gamma_0 M_0^2 = \frac{y-1}{1-x} \quad \rightarrow \quad y = (1 + \gamma_0 M_0^2) - (\gamma_0 M_0^2)x \quad (7)$$

Equation 7 is known as the Rayleigh line, and it states that the thermodynamic path of transition takes place from state (1, 1) to a different state, as shown in Figure 3. As it

has been shown, the Rayleigh line was obtained from manipulating the basic conservation of mass and momentum equations. This equation by itself is only useful in predicting whether the combustion process is a detonation or a deflagration; it is not possible to determine the characteristics of the deflagration or detonation. In order to obtain more meaningful results, a relationship between the conservation equations of momentum and energy has to be found. From equation 5, the expression for the velocities u_0 and u_1 can be obtained as follows:

$$u_i^2 = \frac{1}{\rho_i^2} \left(\frac{p_1 - p_0}{\frac{1}{\rho_0} - \frac{1}{\rho_1}} \right) \quad (8)$$

where i is 0 for reactants and 1 for products. Now, by plugging equation 8 into equation 3, one obtains the following relation:

$$h_1 - (h_o + q) = \frac{1}{2} \frac{(p_1 - p_0)(\rho_0 + \rho_1)}{\rho_0 \rho_1} \quad (9)$$

Equation 9 is known as the Hugoniot curve. This equation represents the locus of the downstream state for a given upstream state [5]. By plotting equations 7 and 9 on the same graph, the type and characteristics of the combustion process can be determined.

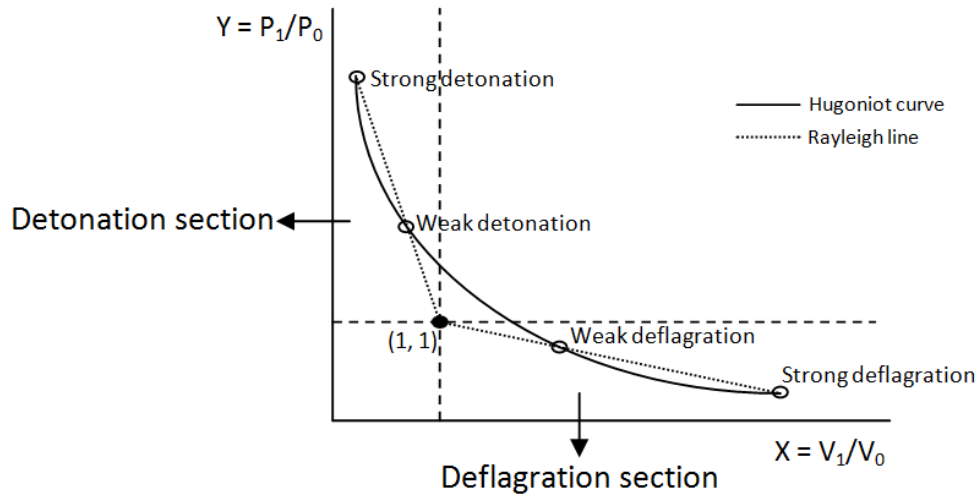


Figure 3. Rayleigh line and Hugoniot curve. Adapted from [5].

As shown in Figure 3, there are two types of detonation and two types of deflagration. In general, a strong detonation occurs when the flow behind the wave is subsonic, allowing any expansion wave to enter the reaction zone and, consequently, weaken the detonation. A weak detonation occurs when the flow behind the wave is supersonic. In practice, this type of detonation rarely occurs. In the case of deflagrations, the opposite behavior is observed. For instance, a weak deflagration occurs when the velocity behind and in front of the wave is subsonic. This means that any disturbance can alter the condition of the reactants ahead of the wave. A strong deflagration, on the contrary, occurs when the velocity behind the wave is supersonic [5,7,8,24,25].

1.2.2. *Chapman-Jouguet Theory*

The Chapman-Jouguet (CJ) theory predicts the velocity of detonation of an explosive mixture. Chapman and Jouguet worked independently and obtained the same

results through different approaches. Chapman chose the minimum-velocity solution [27], while Jouguet studied the variation of entropy along the Hugoniot curve and discovered a minimum [28]. Jouguet also showed that the minimum entropy solution corresponds to the sonic condition of detonation downstream. From this, it is possible to conclude that the CJ theory refers to sonic detonations. As described earlier in this report, there are two different types of detonations, depending on the speed behind the front; however, if the velocity behind the wave is sonic, a CJ detonation occurs as shown in Figure 4 [2].

Graphically, the CJ speed can be determined for a detonation and a deflagration. For instance, if the Rayleigh line is tangent to the Hugoniot curve, two possible speeds can be obtained, one for detonation (minimum velocity) and the other one for deflagration (maximum velocity). Mathematically, by using the Hugoniot equation (Equation 9) and Equation 4, the Hugoniot equation can be rewritten in terms of γ :

$$y = \frac{\frac{\gamma_0 + 1}{\gamma_0 - 1} - x + 2 \frac{q}{p_0 v_0}}{\frac{\gamma_0 + 1}{\gamma_0 - 1} x - 1} \quad (10)$$

The slope of Rayleigh line and the Hugoniot curve is calculated as:

$$\left(\frac{dy}{dx}\right)_R = -\frac{y-1}{1-x} \quad \left(\frac{dy}{dx}\right)_H = -\frac{y + \frac{\gamma_1 - 1}{\gamma_1 + 1}}{x - \frac{\gamma_1 - 1}{\gamma_1 + 1}} \quad (11)$$

At the tangency point, these two formulas should be equal.

After some mathematical manipulation, the CJ solution is obtained by:

$$y_{CJ} = \frac{-x_{CJ}}{\gamma_1 - (\gamma_1 + 1)x_{CJ}} \quad (12)$$

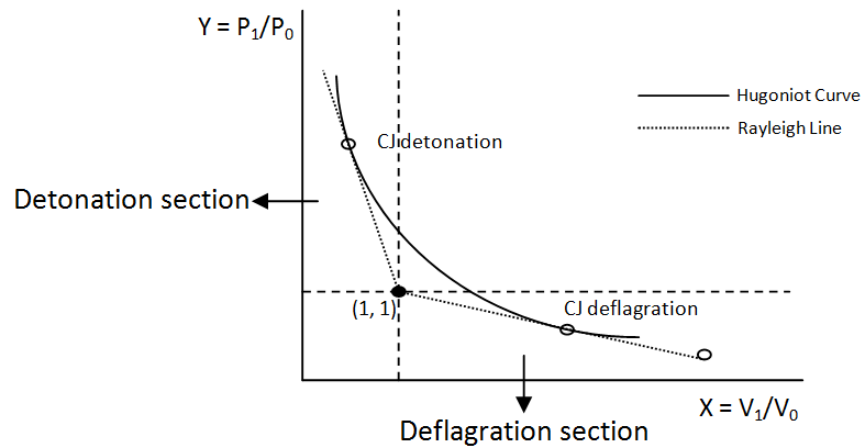


Figure 4. CJ solutions. Adapted from [5].

In general, the CJ speed for detonation is in good agreement with experimental data; however, the CJ speed for deflagration is not well represented by this solution. One possible cause of this behavior is that during a deflagration, the initial state of the reactants ahead of the wave is modified by the rear boundary conditions and the dynamics of the products. Nonetheless, the CJ theory is still widely used due to its great accuracy in predicting the CJ conditions: speed, temperature, and pressure. However, it is criticized because it does not provide a strong mathematical or physical argument that justifies the criterion used for the selection of the solution [7].

2. BACKGROUND

When ignition in a premixed fuel-oxidizer mixture occurs, a combustion wave forms and propagates in the direction of the reactants. This wave can be classified as a deflagration or a detonation. A detonation cannot be produced simultaneously with ignition, unless a high energy is supplied as the ignition source. In other words, a detonation is typically produced via a deflagration-to-detonation transition (DDT). Therefore, in order to obtain DDT a flame acceleration mechanism must take part in this process. As flame can accelerate by many means, *e.g.*, shock-flame interactions, increase in the flame area Landau-Darrieus¹ instability, among others; it also depends on the combustible mixture itself. For instance, it is easier to detonate a mixture of hydrogen-air than methane-air, due to the higher burning velocity of hydrogen-air (about eight times greater than the methane-air burning velocity). Therefore, since many parameters can affect the formation of DDT it is practically impossible to establish a simple theory that predicts at what specific conditions DDT will occur [5].

Experimentally, DDTs are achieved in detonation tubes. This layout provides sufficient confinement to create shock waves followed by detonation waves. Still, for mixtures that present difficulty to detonate in a smooth-walled tube *i.e.*, methane-air mixtures, it is necessary to put some obstructions (or obstacles) in the path of the propagating flame. When obstacles are present in the system, the detonation tube is known

¹ Landau-Darrieus instability: All propagating flames are gas-dynamically unstable due to the diffuser (or nozzle) effect of diverging (or converging) streamlines ahead of a perturbed flame front. The decrease (or increase) in the approaching flow velocity then results in the growth of flame perturbations [5].

as a rough-walled tube. The main purpose of introducing obstacles in the system is to reduce the run-up distance to obtain DDT by increasing the turbulence, the burning rate and the flame area.

Previous experimental research has dealt with obstruction in a detonation tube consisting of uniform distribution with regular patterns, *e.g.*, obstacles with the same shape along the tube and the same blockage ratio. For instance, as early as 1923, Laffite [29] showed that when a strip of coarse sand is deposited on the tube wall, the run-up distance to obtain DDT is considerably reduced.

Chapman and Wheeler (1926) [30] demonstrated that the inclusion of obstacles can increase flame speeds to the order of hundreds of meters per second, even with mixtures that are difficult to detonate. Following the obstacle experiments made by Chapman and Wheeler, Shchelkin (1940) [31] put a spiral-coiled wire into a tube. The results from these experiments were surprising as he was able to reduce the distance to obtain DDT by approximately two orders of magnitude less than in a smooth-walled tube. Similarly, Guénoche (1949) [32] studied the detonation velocity in $C_2H_2-O_2$ mixtures in detonation tubes with different diameters, using various wire diameters and pitches in his experiments. The primary conclusion of this study was that the velocity of the detonation decreases when the roughness in the tube increases, *i.e.*, ratio of the wire diameter to the tube diameter and when the frequency of the repeated obstacle increases.

After it was proven that the obstacles have a key role on reducing the run-up distance to obtain detonations, various researchers started experimenting with different substances to verify if the expected behavior was what really occurred experimentally. For

instance, Brochet (1966) [33] carried out similar experiments to those performed by Guénoche in $C_3H_8-O_2-N_2$ mixtures.



The general purpose of this study was to analyze the effect of nitrogen dilution, as well as the effect of obstacles on this mixture. The effect of nitrogen in this case was to reduce the detonation velocity and pressure. As it was expected, for smooth-walled tubes with low concentration of nitrogen a multi-headed spin detonation was observed; however, when this concentration was increased a single-headed spin was then observed ($z \geq 14$). When the Shchelkin spiral was included in the system, large velocity deficits were observed, and again, the single-head spin detonation takes place at high concentrations of nitrogen ($z \geq 8$). Brochet also noticed that when the concentration of nitrogen was $z \geq 10$, a separation gap between the shock front and the reaction front started to appear; however, the distance of this gap did not increase, as both the shock front and the reaction front traveled at the same speed. From this study, it was possible to conclude that the spiral can also have an adverse effect on the detonation and accelerates its approach towards the limits and failure of detonation.

Teodorczyk *et al.* (1988) [34] obtained Schlieren photographs that allowed them to study how a detonation wave propagates once an obstacle has been passed. In their experiments, they observed how a failed detonation subsequently became an overdriven detonation, *e.g.*, the pressure and velocity of propagation of the detonation wave are greater than the values predicted by the CJ theory, and the influence of obstacles to form a detonation front.

In the case when a detonation wave propagates over an obstacle, once the detonation wave passes the obstacle, the expansion wave generates a noticeable gap between the shock and reaction front, causing the detonation to fail. Once the shock is reflected from the tube wall, this reflection changes to a Mach stem, *i.e.*, weak waves that when combined are capable to create a supersonic flow. This Mach stem is sufficiently strong to auto-ignite the unburned fuel. When auto-ignition occurs, the Mach stem becomes an overdriven detonation, which then expands and engulfs the decaying detonation.

Additionally, Teodorczyk *et al.* [35], captured how a detonation is initiated from a reflected shock wave which originated from the obstacle. Initially, the shock is deflected around the obstacle and then a couple of frames after, the shock merges with the leading shock front and then forms a detonation. The detonation front then engulfs the mixture behind the diffracted shock. One of the purposes of having obstacles in the system is to scatter any incident shock front and then create Mach stems that will ultimately cause local ignition of a detonation. From these studies, it was possible to conclude that detonations which occur in an obstacle-filled tube constantly fail by shock diffraction around the obstacles and reinitiate due to shock reflections that create Mach stems capable of auto-igniting the unburned mixture and, subsequently, create localized formations of detonations.

Further studies were performed with mixtures that are less sensitive to detonation than fuel-oxygen mixtures; *i.e.*, fuel-air mixtures, consequently larger diameter tubes were needed in order to obtain detonations. In the experiments performed by Peraldi *et al.*

(1988) [36], a series of regularly spaced orifice plates, *i.e.*, ring-shaped obstacles, were used. These obstacles were spaced one tube diameter apart from each other. In order to determine the roughness in the system given by the obstacles, the concept of blockage ratio was established.

$$BR = 1 - \left(\frac{d}{D}\right)^2 \quad (14)$$

Here, d refers to the orifice diameter and D to the tube diameter.

In Peraldi's experiments [36], they found that there are different propagation regimes to the different mixture sensitivities. In order to characterize the mixture sensitivity, Peraldi used the detonation cell size λ . Additionally, they obtained the detonation velocity as a function of hydrogen concentration for tubes with different diameter, *i.e.*, 5, 15 and 30 cm. Their study allowed them to determine that, in general, the wall roughness does not appear to have much influence on the propagation of a detonation as in some of the experiments, a large velocity deficit was observed. This regime is known as quasi-detonation regime. This regime is characterized by having the shock and reaction front coupled together as one, *e.g.*, as in detonations, but both fronts travel at low speeds compared to the speeds predicted by the CJ theory.

Moreover, when the detonation cell size is of the order of the orifice opening, *i.e.*, $\lambda \approx d$, Peraldi and coworkers [36] noticed that a transition from the quasi-detonation regime to a lower-velocity regime takes place. This lower-velocity regime is known as the choked or sonic regime, mainly because the velocity of the detonation wave is close to the value that corresponds to the speed of sound of the combustion products. From these experiments, they also determined that as the velocity of the mixture decreases, the

mechanism of propagation changes from adiabatic compression to turbulent diffusion. Another important observation that this study concluded was that the bigger the tube diameter, the velocity of the combustion process is closer to the values reported by the CJ theory [36].

Further experiments performed by Lyamin *et al.*, (1991) [37] and Makris *et al.*, (1993 and 1995) [38,39] consisted of the study of the propagation of detonations in a porous medium consisting of a densely packed bed of solid particles with the same size and uniformly distributed throughout the system. Mostly, these experiments focused on the study of the variation of the detonation velocity with the equivalence ratio of different fuel-air and fuel-oxygen mixtures. The blockage that was used in these experiments consisted of a packed bed of ceramic spheres with a 12.7 mm diameter. The conclusion of these experiments was similar to the study performed by Peraldi *et al.*, [36], where basically the mixture sensitivity to detonation plays an important role; however, the mechanism of DDT is different, as the path that takes the detonation is not a straight line as it is in a detonation tube.

Makris in 1993 [38] distinguished three different cases. In the first one, the combustion wave propagates uniformly throughout the obstacles and there is no failure of the detonation. From his results, he estimated that the propagation velocity of the detonation is very close to the CJ value. In the second case, it was observed that the cell structure is less uniformly distributed. This result occurs mainly because the mixture is less sensitive to DDT. Still, it is possible to determine areas where there is local failure

followed by the re-initiation of the detonation. Finally, the third case, the mixture proves difficulty to detonate and the combustion process is merely a fast deflagration [38].

Teodorczyk *et al.*, (2008) [35] performed experiments with hydrogen-air mixtures in a small, obstructed channel. These experiments were performed in a similar manner to the ones described previously; *i.e.*, uniformly distributed obstacles with the same blockage ratio along the tube during experiments; however, these tests were done in a rectangular cross-section channel. Moreover, three different blockage ratios were tested, *i.e.*, 0.25, 0.50 and 0.75, and different compositions were explored. They concluded that when using a higher blockage ratio the obstacle separation distance should be larger to increase the likelihood to obtain DDT.

Kuznetsov *et al.*, (1999) [40] performed several experiments using three tubes with different internal diameters of 0.174 m, 0.35 m and 0.52 m and a square cross-section channel. In these experiments, different blockage ratios were used, *i.e.*, 0.09, 0.1, 0.3, 0.6 and 0.9. The mixtures used for these tests were hydrogen-air and hydrogen-oxygen mixtures diluted with nitrogen, argon, helium and carbon dioxide. They concluded that when having a small blockage ratio there was no quenching of the combustion process. However, when the blockage ratio is bigger than 0.6, a relatively more unstable and slow regime was observed, compared to when the blockage ratio is smaller than 0.6.

Lee *et al.*, (2004) [41] and Ciccarelli *et al.*, (2005) [13] performed a series of experiments which led to similar conclusions. For instance, Lee noticed that when a blockage ratio between 0.3 and 0.6 was used and sufficient space was left between the obstacles, the run-up distance to obtain DDT was reduced. Following a similar trend,

Ciccarelli found that when the blockage ratio was 0.4, the spacing between the obstacles had little effect on the flame acceleration; however, when the blockage ratio exceeds this value, the obstacle spacing has a significant effect on the flame acceleration. Moreover, he determined that the optimal obstacle spacing is one tube diameter.

Finally, Cross and Ciccarelli [42] performed experiments for hydrogen-air and ethylene-air mixtures at atmospheric conditions in a 6.1 m long and 0.1 m diameter tube using different obstacles configurations. Three obstruction arrangements utilized in these tests were: obstacles located downstream of the detonation wave towards the right-end of the detonation tube (with 4.11 m of the detonation tube filled with obstacles), the obstruction filled the right-half of the detonation tube and, the obstacles were located within the first and second half of the tube. This study aimed to determine the DDT limits and to understand the quasi-detonation propagation mechanism.

3. MOTIVATION AND PROBLEM STATEMENT

3.1. Motivation

As mentioned earlier, explosions are one of the major concerns across the different industries. Currently, there are various mitigation barriers to prevent the acceleration of deflagrations and, consequently, the transition to detonations, *e.g.*, explosion relief, inert gases (the higher the specific heat, the more effective the inert gas is), and explosion suppression systems [2]. However, one should look from the design perspective and determine how the randomness of different geometries and the non-uniform distribution of obstacles placed along the facility have an effect on the run-up distance to obtain a DDT [43].

Previous experimental studies [5,13,16,19-21] have shown the importance of obstacles in the reduction of the run-up distance to obtain DDT. For example, Ciccarelli concluded that in a uniform distribution of obstacles, a blockage ratio of approximately 43% is the optimal value to minimize the distance to obtain detonation [13,36]. Additionally, Blanchard *et al.* [44] studied the effect of the ignition position in the run-up distance to obtain detonation in a smooth-walled tube. From this study, it was concluded that the onset to detonation distance was minimized when the flammable mixture was ignited 0.9 m away from the pipe end wall. These studies have allowed for a good understanding on the run-up distance to achieve detonation; however, the majority of studies that deal with obstacles in detonation tubes are performed under the ideality that all the obstacles have the same shape and blockage ratio. In terms of safety and in an

industrial facility, this is not usually the case. Generally, facility layouts include a series of non-uniform shapes and distribution of obstacles, *e.g.*, pipe racks, pipelines, and vessels of different sizes. Therefore, there is an urgent need to understand how the onset of detonation is affected due to the inclusion of these non-uniform conditions and to determine whether or not this randomness reduces the run-up distance to obtain detonation and other features of the DDT process such as the peak pressure and the peak velocity.

In general, conventional Computational Fluid Dynamics (CFD) models are not capable of predicting the abrupt transition from deflagration to detonation [23]. However, from the combustion process, it is possible to determine if the flame front captures the pressure front at some point. If it does, the basic principle of detonation is achieved, *i.e.*, coupling between the flame and pressure front. If this situation is addressed correctly, it will be possible to perform facility siting studies and determine how the facility layout should be, avoiding a possible DDT [45].

3.2. Problem Statement

Even though the probability of DDT taking place in an industrial facility is relatively small, history has proven that this type of explosion still occurs, leaving undesirable consequences for the facility, population, and environment. Buncefield (UK, 2005), Caribbean Petroleum Refining Tank Explosion (Puerto Rico, 2009), and Jaipur (India, 2009) are a few examples of these incidents. A common feature from these oil depots (located onshore) is the massive amounts of petrochemicals stored [10,46,47]. In these incidents, a vapor cloud of a flammable substance was formed and subsequently ignited. Initially, a deflagration took place; however, the layout of such facilities allowed

sufficient turbulence, generated by the obstacles, for the flame front to accelerate. Moreover, the substances that leaked were not very reactive; however, the total amount of leaked gasoline was enough to allow detonation in a confined environment. From these incidents, it has been observed that obstacles play a key role in reducing the run-up distance to achieve detonation.

Generally, oil depots are designed to have significant separation distances between vessels. Also, there are not many pipe racks that could add turbulence in the system; however, DDTs are still observed. This is not the case in the rest of the industry. For instance, offshore platforms are built with a substantial number of obstacles. This obstruction can eventually lead to a detonation. Even though offshore facilities are designed with safety gaps, as mentioned above, once a detonation is triggered the combustion process is self-sustainable. Consequently, if a vapor cloud has surpassed the safety gap and reached the other obstructed area, it is very likely that if the cloud is ignited and DDT is achieved, the detonation will persist [2].

In general, when facility siting studies are being performed, the portion of the cloud that does not participate in the explosion is not taken into account by such analysis. For this reason, CFD models should be used for these studies. For instance, a deflagration is a non-self-sustainable combustion process, and there are requirements in the system for the deflagration to maintain its propagation (*e.g.*, turbulence); a detonation is a self-sustainable combustion process, and once it is triggered all the fuel is going to be consumed. Current CFD models are not capable of predicting the abrupt change from deflagration to detonation due to the small period of time when the transition takes place.

However, CFD models are able to predict and show the situation when the flame front captures the pressure front and leads to a DDT. By allowing the visualization of the position of the flame front and the pressure front, in time CFD models should be capable to predict whether or not DDT takes place in a specific scenario. For this purpose, this research aims to produce fundamental data for both fundamental understanding and for the validation of numerical models; and to make a comparison between experimental and numerical results, in which the main variables to analyze are the pressure and the likelihood to have a DDT.

3.3. Research Objectives

As part of this research, an existing test rig was utilized for the DDT study. However, rig modifications were required, and it was important that the results were repeatable since multiple repeats of a given set of conditions were needed. Therefore, a rig characterization was needed to determine if with the current facility and methodology the general behavior of the combustion wave, the pressure, and velocity results produced similar trends and were repeatable.

As this research aimed to get a better understanding on how the onset of detonation and the flame acceleration are affected by a non-uniform distribution of obstacles, an experimental study was carried out. This was done by the implementation of a design of experiments matrix, in which the factors of interest were properly studied in an efficient manner.

Finally, the comparison of numerical tools to predict the likelihood of having a detonation is an important long-term goal of this research. Therefore, an initial comparison

between available data in the literature and then with the experimental data gathered in this study were performed. This provides insight into a new methodology to study how likely a certain scenario might transition into a detonation.

4. EXPERIMENTAL

4.1. Detonation Tube

The detonation tube used in this study is 2.77 m long and has an internal diameter of 3.8 cm. The ratio of the tube length to the tube diameter, L/D , is equal to 73. The wall thickness of the tube is 1.1 cm and it was built using 304 stainless steel. This tube has an expansion volume in the end-wall on the other side of the ignition point, which consists of the following pieces: the end-wall, the back-wall, and multiple spacers with different widths: 12.7 mm, 25.4 mm, 3.175 mm, and 6.35 mm. Figure 5 shows the detonation tube.²

As observed in Figure 5, the detonation tube is mounted on two steel I-beams and four pipe clamps which are welded to the I-beams. The purpose of this mounting is to securely hold the detonation tube in place during an experiment [48]. As for the ignition mechanism, a glow plug (AC Delco 60G) was used and operated at 10 A in all the tests. Experimentally, it has been observed that, under these conditions, ignition occurs within 10–20 seconds once power has been supplied to the glow plug.

²The detonation tube is located at the Turbo Machinery Laboratory and is part of the Combustion Research Group.



Figure 5. Photograph of the detonation tube at Texas A&M University.

4.2. Data Acquisition Systems

In order to identify where the change from deflagration to detonation is actually occurring, the original layout of the pressure transducers, shown in Figure 6, might not give sufficient information for sensitive mixtures, *i.e.*, hydrogen–oxygen mixtures.

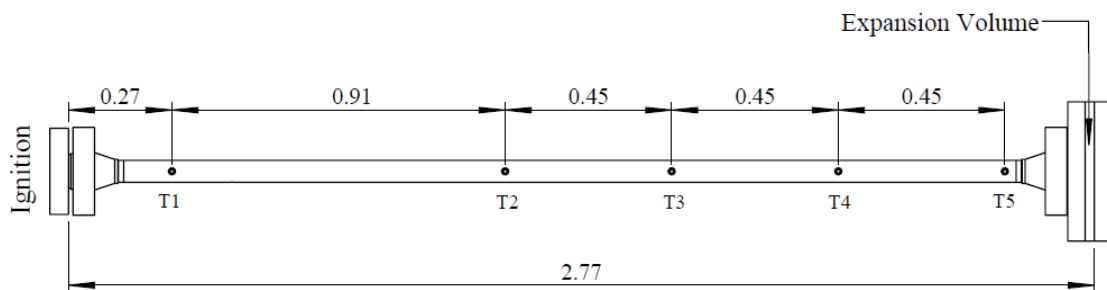


Figure 6. Original layout of the pressure transducers, units are in m.

Therefore, there was a need to add more pressure transducers, especially in the area where the obstacles are present. In the case of sensitive mixtures, the onset of detonation occurs in this section of the tube. This will help to determine with more accuracy where the transition from deflagration to detonation occurs. The new location of the pressure transducers is shown in Figure 7.

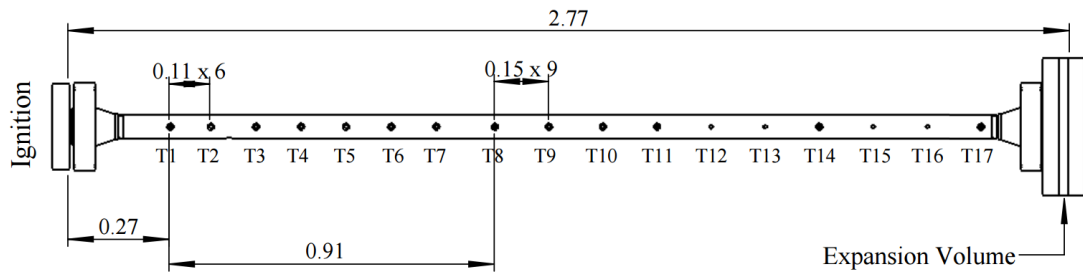


Figure 7. New layout of the pressure transducers positions along the tube, units in m.

As can be observed in Figure 7, between T1 and T8, a total of six new positions for pressure transducers were allotted. Then, between T8 and T11, T11 and T14, and T14 and T7, two new positions for pressure transducers have been distributed between each pair. This brings the total to 17 pressure transducers along the detonation tube.

The transducers used (PCB 113B22) have a measurement range of 34.5 MPa, a rise time of less than 1 μ s, and a resonance frequency \geq 500 kHz. In order to record the data of each experiment, two different oscilloscopes are available. The first is a four-channel oscilloscope (model GDS-2064) and it is able to record up to 5,000 pts/channel. The second oscilloscope is a two-channel HP Infinium Oscilloscope and it is able to record

up to 25,000 pts/channel. Both oscilloscopes are typically used at a sampling rate of 1 MS/s [49].

4.3. Design of Experiments

The objective of this study was to evaluate the effect the randomization of obstacles has on the run-up distance to obtain DDT and the acceleration of the flame. In this case, four parameters were established: fuel type, obstacle shape, blockage ratio and obstacle distribution. Each parameter has a total of three levels, as shown in Table 1.

Table 1. Description of the parameters and its levels.

Parameters	Level 1	Level 2	Level 3
Gas	Hydrogen	Ethylene	Acetylene
Obstacle Shape	Ring Shape	Half Washer	Block Shape
Blockage ratio	Increasing	Equal (~40%)	Decreasing
Obstacle's Distribution	Variation	Uniform	Staggered

A factorial design in this case is not ideal, as there will be a need to do a total of 81 experiments (3^4) to account for all the possible interactions within the variables. As there are 17 pressure transducers along the detonation tube and only four channels available for data acquisition, to capture all the data from a complete test it requires at least five experiments to gather the behavior of the explosion along the tube. Therefore, the amount of required experiments increases by a factor of five, which gives a total of 405 experiments. Additionally, each completed experiment must be repeated five times to have a degree of variability of a complete experiment. This brings to a total of 2025

experiments, which is impracticable. Therefore, a different design of experiments method should be used. For instance, the Taguchi methodology uses the least number of possible trials to provide accurate information and reproducible results. In this particular case, a L9 matrix was generated [50]. This allows one to obtain the necessary amount of data with only nine experiments; however, by introducing the experiment repetitions and the data gathering, a total of 225 experiment are needed, which is significantly less than with a factorial design of experiments. Therefore, the Taguchi methodology was chosen. In Table 2 the experimental matrix that was used for this study is shown.

Table 2. Design of experiments matrix utilized for this study.

Experiment	Fuel	Obstacle shape	Blockage Ratio	Obstacle Distribution
1	Hydrogen	Ring Shape	Increasing	Variation
2	Hydrogen	Half Washer	Equal	Uniform
3	Hydrogen	Block Shape	Decreasing	Staggered
4	Ethylene	Ring Shape	Equal	Staggered
5	Ethylene	Half Washer	Decreasing	Variation
6	Ethylene	Block Shape	Increasing	Uniform
7	Acetylene	Ring Shape	Decreasing	Uniform
8	Acetylene	Half Washer	Increasing	Staggered
9	Acetylene	Block Shape	Equal	Variation

As depicted in Table 2, several obstacles in different shapes (ring, block, and half washer) were machined from aluminum 7075. For each basic shape, three different sizes were manufactured to have 25%, 40%, and 80% blockage ratio (to satisfy the blockage ratio parameter in Table 2). Figure 8 shows a schematic of how the basic shapes of these

obstacles looked, and later in the paper, the obstacle layout is schematically described for each of the nine configurations in Table 2.

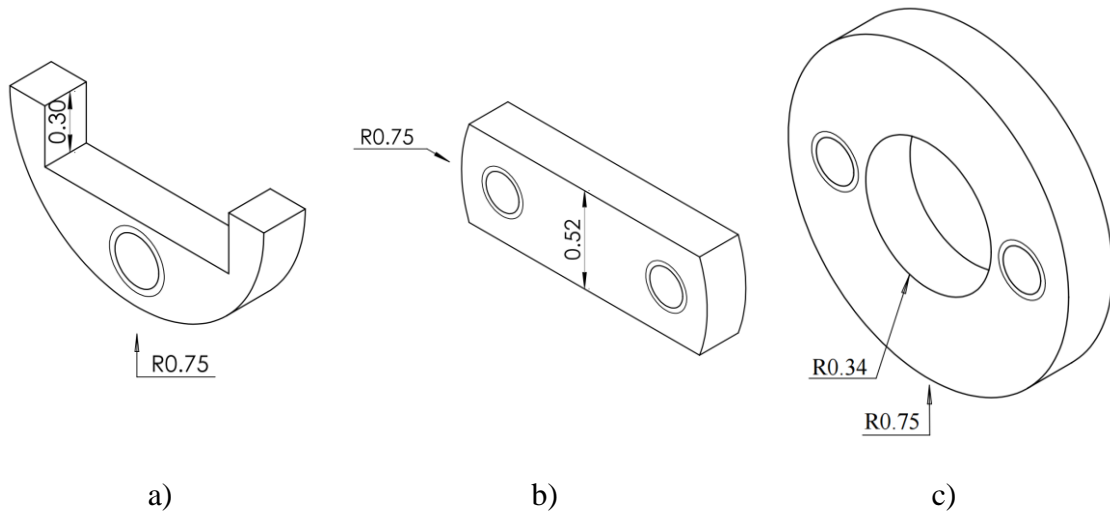


Figure 8. Selection of basic obstacle shapes used in this study. a) half washer-shaped obstacle with a blockage ratio of 25%. b) block-shaped obstacle with a blockage ratio of 40%. c) ring-shaped obstacle with a blockage ratio of 80%. All the obstacles have a thickness of 0.25 in. Dimensions shown are in units of inches.

Each of the experiments consisted of three sets of obstacles, and each set had three obstacles (for a total of nine obstacles) inserted into the first 0.8 m of the detonation tube; all of them for a given configuration had the same shape, but different blockage ratios and spacing between them, as in Table 2. For instance, there were three categories for blockage ratio: 1) increasing (from 25% to 80%), 2) equal (40%), and 3) decreasing (from 80% to 25%) blockage ratio. The three categories for spacing between obstacles were: 1) variation (one, two, and three times the internal diameter of the detonation tube); 2) uniform (a

spacing twice the internal diameter of the detonation tube); and, 3) staggered (all obstacles were spaced one internal diameter of the detonation tube followed by a gap of five times the internal diameter of the tube).

As the main objective of this research was to obtain the run-up distance to detonation and related information on the acceleration, magnitude, and stability, it was desirable that the fuel-oxygen mixtures experienced a deflagration-to-detonation transition within the limitations of the current facility. The selection of the fuels was carried out by previous experiments performed in the detonation tube [48] and by performing new experiments in which no obstacles were present within the detonation tube (smooth tube) for an ideal mixture with a fuel-to-oxidizer equivalence ratio of one ($\phi=1$). If detonation was achieved in any of these cases, the fuel was approved for the experimental matrix. Figure 9 shows the experimental results for these experiments. The error bars represent one standard deviation obtained for each measurement.

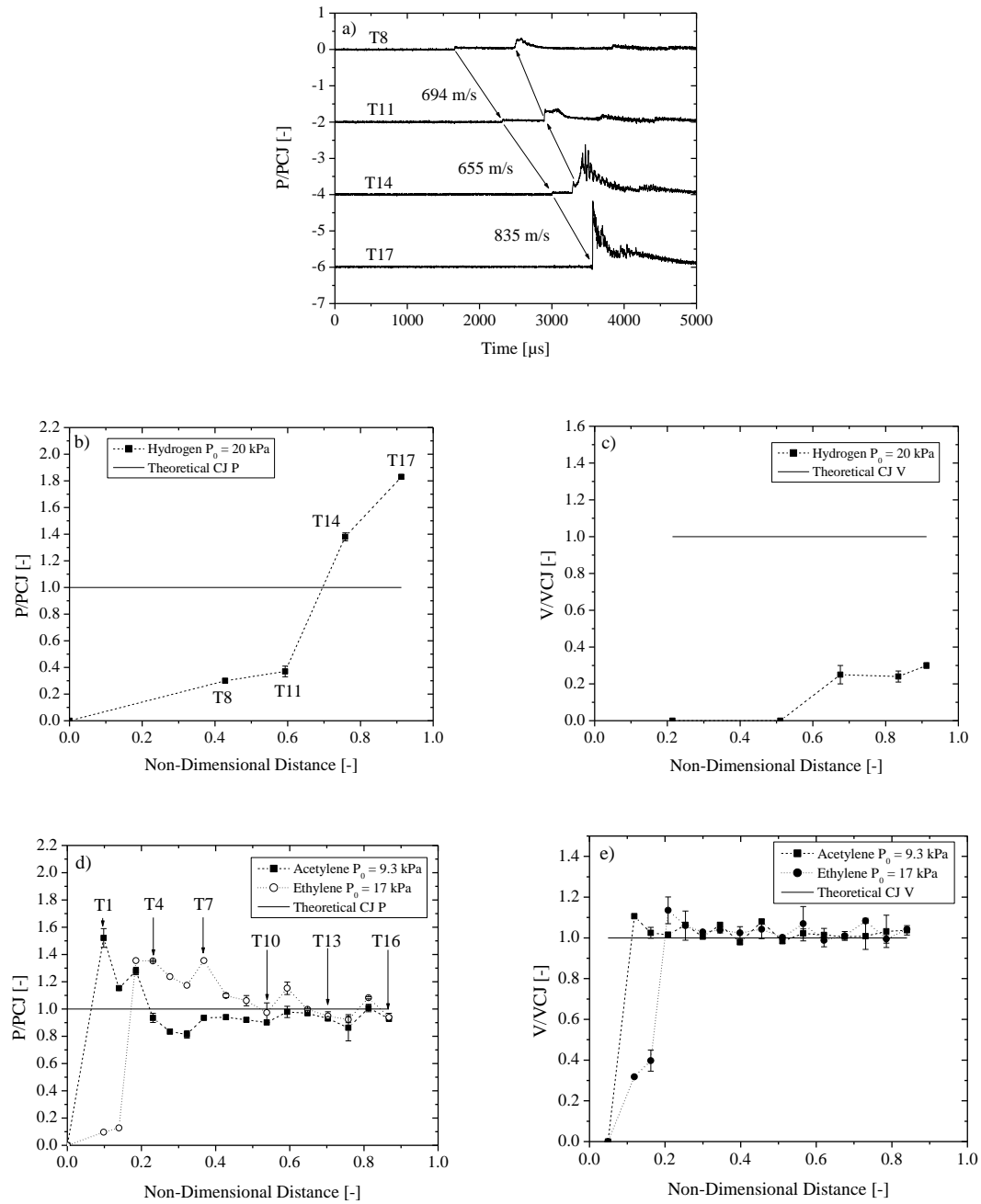


Figure 9. Experimental results for different fuel-oxygen mixtures for no obstacles and $\phi=1$ for all mixtures. a) Experimental results for a H_2-O_2 explosions with $P_0 = 20$ kPa. Figures b) and c) show the average pressure and velocity results, respectively, for the H_2-O_2 experiments with $P_0 = 20$ kPa. Figures d) and e) illustrate the average pressure and velocity results, respectively, for $C_2H_2-O_2$ explosions with $P_0 = 9.3$ kPa and $C_2H_4-O_2$ explosions with $P_0 = 17$ kPa.

As can be observed in Figure 9a through Figure 9c, the hydrogen-oxygen mixture reaches a speed of approximately 800 m/s at the location of the last probe (T17) [51]. This experiment illustrates a progressive flame acceleration accompanied by significantly high pressures (twice the CJ value). According to the Kuznetsov *et al.* [52] study, the detonation cell size for hydrogen-oxygen mixtures at these conditions is approximately 8.5 mm. The onset of detonation for this particular case is not expected, as the diameter of the tube is smaller than 13λ ($D \ll 13\lambda$) [4,20,36,52-54]. Previous experiments carried out by Polley [48], in the same facility used in this study, showed that a successful transition to detonation was achieved using this H₂-O₂ mixture with the use of obstacles. To guarantee that DDT was going to take place within the limits of the facility, Polley [48] utilized half washer-shaped obstacles with a blockage ratio of approximately 40%. With this information, the use of hydrogen-oxygen mixtures with a maximum initial pressure of 20 kPa was accepted.

As for ethylene-oxygen mixture, the experimental detonation cell size values reported by Strehlow [55] at similar test conditions to the ones used in this study (a maximum initial pressure used by Strehlow of 16.46 kPa) the detonation cell size was 2.9 mm. Following the same criterion defined by Peraldi *et al.*, [36,53,54] and based on this information, the critical diameter for DDT to take place in the present detonation tube is 3.76 cm. This calculated critical diameter is similar to the one used for this study (3.8 cm); therefore, DDT is expected. Additionally, it is important to mention that as the initial pressure increases, the detonation cell size is smaller, as is well known [52,55-57]. Experimentally, the fact that ethylene-oxygen mixtures were capable of detonating in the

smooth tube was corroborated by the data obtained for ethylene-oxygen mixture ($\phi=1$) tests shown in Figure 9d and Figure 9e. For instance, the tube had no congestion (smooth tube) and showed an overdriven detonation occurring between transducer ports T3 and T4. The detonation tends to stabilize at T9 (located 1.35 m away from the ignition source). The run-up distance obtained for this mixture at the specified conditions is 0.62 m away from the ignition source.

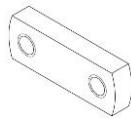
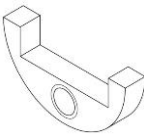

Finally, for acetylene-oxygen mixtures, the experimental detonation cell size value reported by Desbordes [58] at similar test conditions to the ones used in this study (9.3 kPa) was approximately 1.9 mm. According to the criterion specified previously, the critical tube diameter for the acetylene-oxygen mixture at these conditions is 2.46 cm. This diameter is significantly smaller than the diameter of the detonation tube used in this study. Consequently, with the current facility DDT is expected for acetylene-oxygen mixtures at the specified conditions. Experimentally, this was proven and the test results illustrated in Figure 9d and Figure 9e show that the pressure obtained at T1 and the velocity calculated between T1 and T2 are higher than the CJ conditions, describing an overdriven detonation. The pressure and velocity stabilize and oscillate near the CJ conditions at T6 (located at 0.9 m away from the ignition source). The run-up distance obtained for acetylene-oxygen mixtures ($\phi=1$) in the smooth tube is 0.40 m away from the ignition source. In this paper, the authors refer to the run-up distance as the distance at which the onset of detonation due to DDT is observed [59].

In summary, the run-up distance for the fuel-oxygen mixtures in the smooth detonation tube at the conditions tested are: a) $\text{H}_2\text{-O}_2$ is not applicable, b) $\text{C}_2\text{H}_4\text{-O}_2$ is 0.62 m, and c) $\text{C}_2\text{H}_2\text{-O}_2$ is 0.40 m away from the ignition source.

4.4. Design of Obstacles

As this research was focused on the effect the randomization of the obstructions has on the acceleration of the flame, which ultimately leads to DDT, several obstacles in different shapes (ring, half washer and block) with different blockage ratios (25%, 40% and 80%) were machined from aluminum 7075. Table 3 summarizes the properties of the obstacles.

Table 3. Description of the obstacles machined.

Shape	Blockage Ratio	Quantities Machined	Graphical Description
Block	0.25	4	
	0.4	9	
	0.8	4	
Half Washer	0.25	4	
	0.4	9	
	0.8	4	
Ring	0.25	4	
	0.4	9	
	0.8	4	

Each experiment had a total of nine obstacles inserted into the first 0.8-m of the detonation tube. All the obstacles used for each experiment had the same shape, and as mentioned previously, different blockage ratios and spacing between them.

5. RIG CHARACTERIZATION

As there were more transducers than available channels to record data, a repeatability study was performed. The purpose of this study was to determine whether or not the current facility and methods employed produced similar pressures and velocities for several repeat experiments carried out under the same conditions. This characterization study was made with two different mixtures: 1) stoichiometric hydrogen-oxygen mixtures and, 2) lean hydrogen-oxygen mixtures ($\phi = 0.25$). Both mixtures were at an initial pressure of 20 kPa. Additionally, a total of nine, half-washer obstacles with a blockage ratio of 40% were utilized and spaced approximately 3D from each other down the length of the detonation tube. At these conditions, the calculated CJ pressure is 350 kPa and the CJ velocity is 2747 m/s for the stoichiometric mixture and the calculated CJ pressure is 286 kPa and the CJ speed is 1,890 m/s for the leaner mixture [56,59].

5.1. Hydrogen–Oxygen Mixtures With an Equivalence Ratio of 1.0

A total of 10 experiments were performed; recall that between each experiment, the available pressure transducers were placed at different locations down the tube to obtain full coverage of the wave propagation (sharing one common port from test to test). Figure 10 shows the results of a complete set of experiments (from T1 to T17). Each frame represents a sub-experiment. In this case, only three pressure transducers were used in each sub-experiment. With this approach, the authors were able to gather more data and compare it with previous information collected.

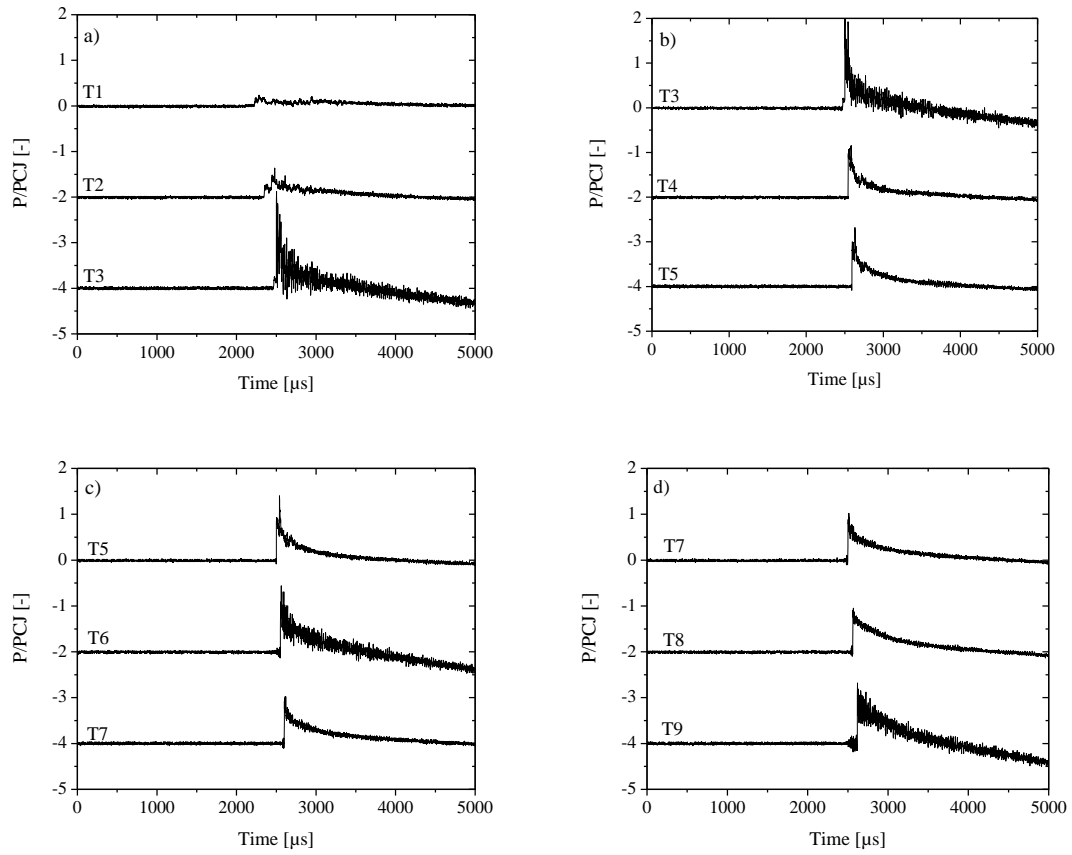


Figure 10. Pressure results obtained for a Hydrogen-Oxygen mixture ($\phi = 1$) explosion with half washer-shaped obstacles, an equal blockage ratio, and a gap between obstacles of 3D. Each frame shows the results obtained for the transducers described within the figures (T1 – T17).

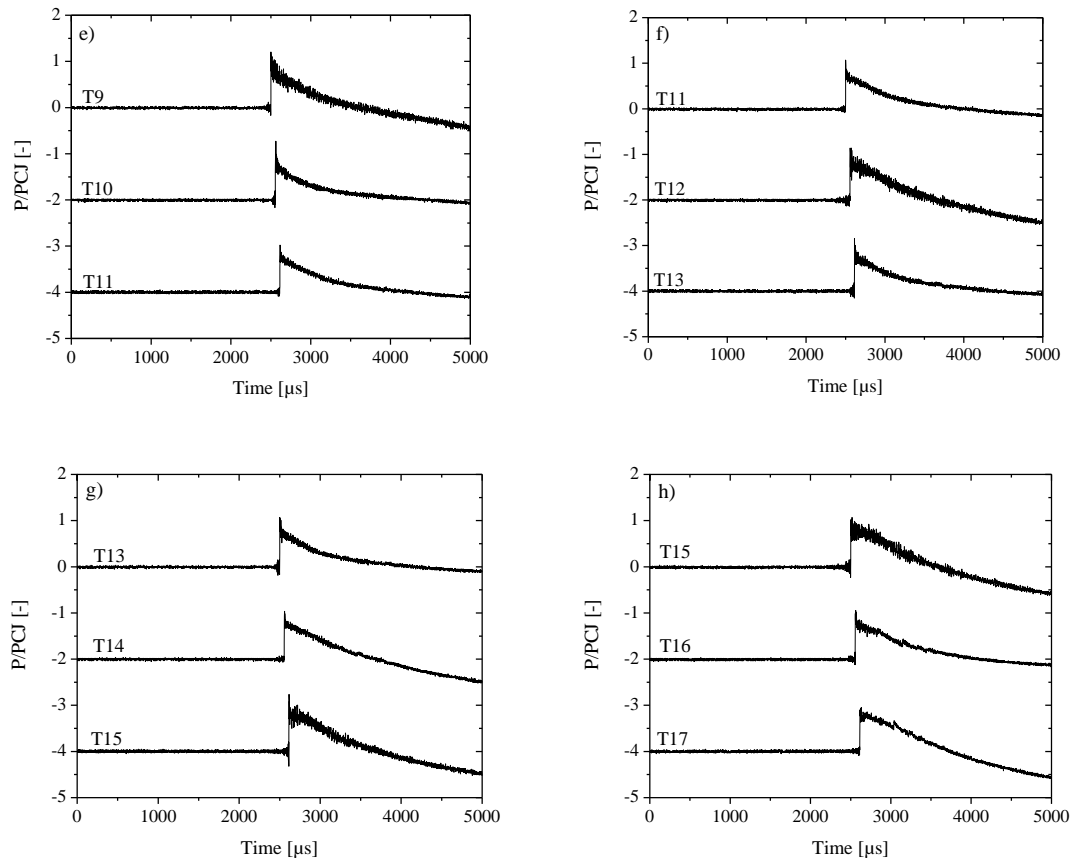


Figure 10. Continued.

As observed in Figure 10, with the positioning of the pressure transducers, it is possible to distinguish the slow and fast deflagration, the onset of the detonation (deflagration-to-detonation transition) and stable detonation regimes. For instance, T1 shows a typical reading of a slow deflagration, T2 illustrates a fast deflagration, T3 describes the onset of the detonation, and from T4 to T17 a stable detonation is observed. When the onset of the detonation was achieved, the pressure rose to approximately twice the CJ pressure. After this occurred, the pressure stabilized and oscillated near the CJ

pressure value. Figure 11 shows the overall progression of the combustion wave depicted by the detailed data from Figure 10.

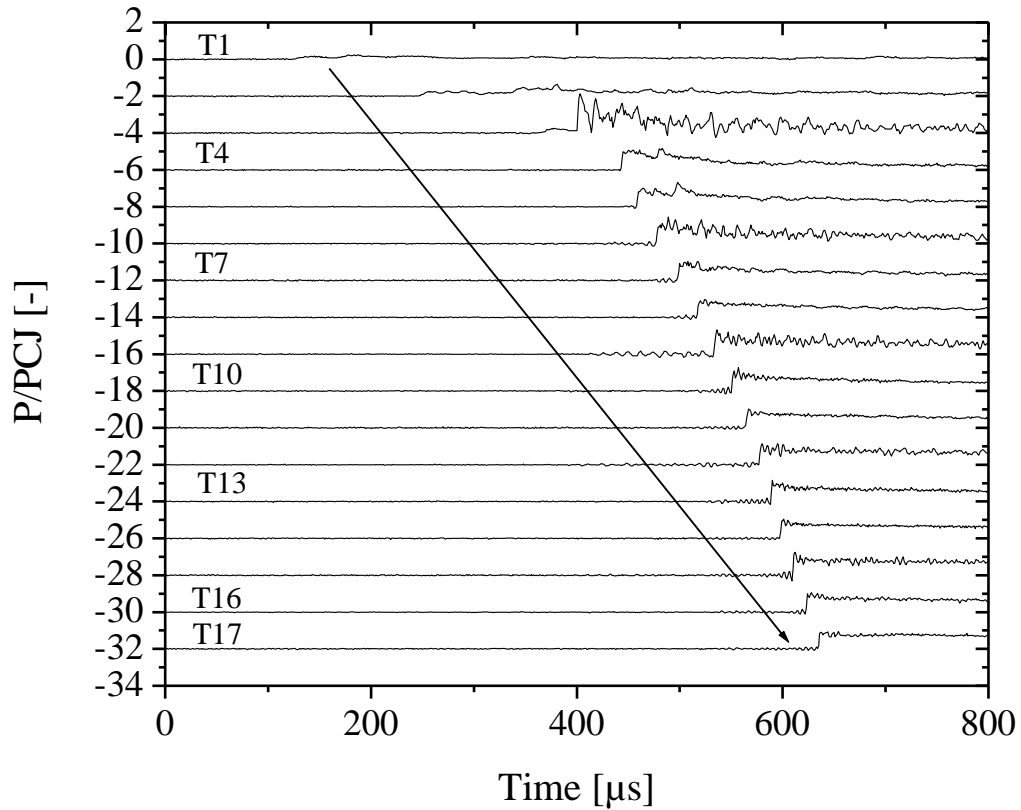


Figure 11. Overall progression of the combustion wave for a Hydrogen-Oxygen mixture ($\phi = 1$) explosion with half washer-shaped obstacles, an equal blockage ratio and a gap between obstacles of $3D$.

On the other hand, the speeds from the characterization tests show an interesting behavior. Firstly, it is important to note that the shock velocities were determined from the arrival times of the wave at a pair of pressure transducers. Additionally, for the purposes of this study, as there are no data available before T1, it is assumed that the speed at T1 is

zero. Between T1 and T2 the speed of the shock wave reaches approximately half the CJ velocity, then between T2 and T3 there is a small decrease in the shock velocity. As mentioned by Lee [5,48], the onset of the detonation occurs when the velocity of the deflagration is of the order of half the velocity of the detonation at equilibrium. This behavior is seen in Figure 12. The next data point for the velocity shows a significant acceleration in the combustion process, the speed exceeded the CJ velocity. From then on, the velocity oscillates near the CJ speed value. Figure 12 shows the experimental results of the 10 experiments. Additionally, an average of these results is shown with error bars representing one standard deviation obtained for each measurement.

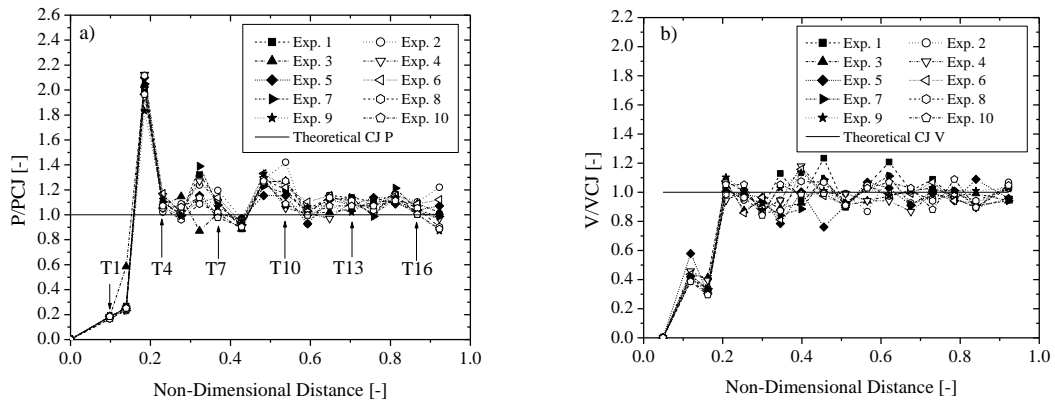


Figure 12. Summary of experimental results for Hydrogen-Oxygen mixture explosions ($\phi = 1$) in the characterization study. Figures a) and b) show the pressure and velocity results, respectively, for the 10 experiments, and Figures c) and d) illustrate the average pressure and velocity results, respectively. The error bars represent one standard deviation obtained for each transducer.

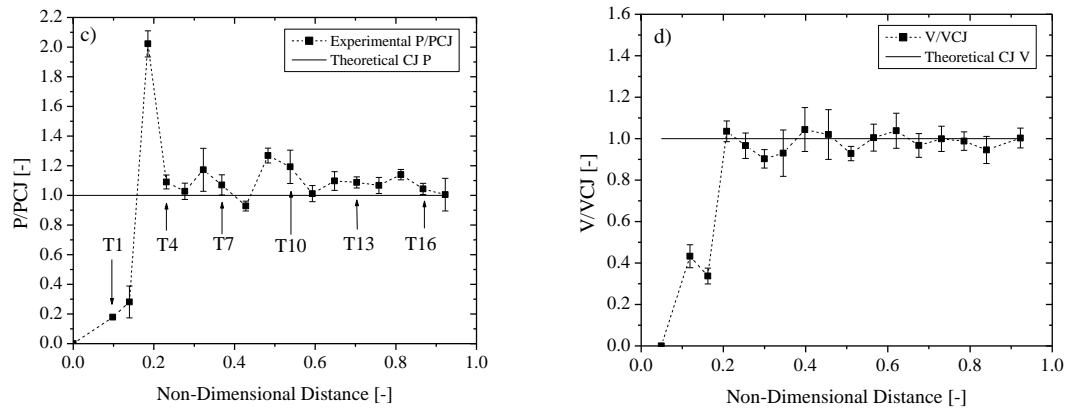


Figure 12. Continued.

Another important aspect to consider is that the obstacles are located up to about the fifth pressure transducer (location T5). This presence influences the initial trends (T1 to T5). For instance, the pressure results presented in Figure 12 show a peak pressure in the section where there is no obstruction at T9. This peak might be due to a localized auto-explosion that occurred around that area. Additionally, the speed results show a deceleration right after the onset of detonation is achieved. It is observed that once the detonation is formed, the presence of obstacles tends to slow down the combustion process. As the combustion proceeds into the smooth tube, there is a re-acceleration of the detonation wave. Once this takes place, the detonation becomes stable with small fluctuations near the CJ velocity. For this particular experiment, the run-up distance was approximately 0.57 m (obtained by the multiplication of the non-dimensional distance, 0.21, by the length of the detonation tube, 2.77 m) away from the ignition source. Figure 13 shows the run-up distances obtained for these 10 experiments.

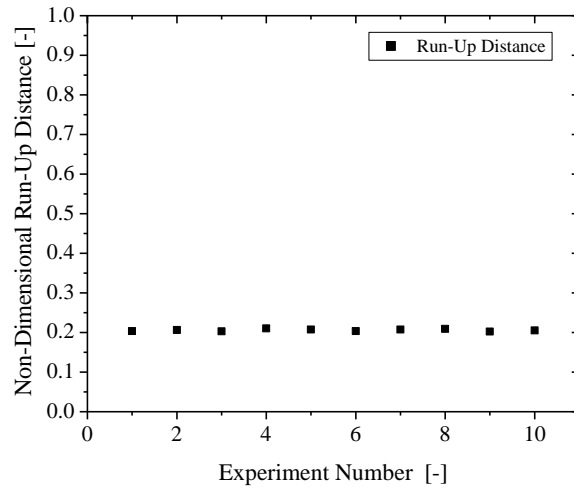


Figure 13. Variability of the run-up distances obtained for 10 repeat hydrogen-oxygen mixture ($\phi = 1$) explosions with an initial pressure of 20 kPa. The obstacle configuration used in these experiments was: half-washer-shaped obstacles with a uniform blockage ratio (40%) and with a gap between obstacles of 3D.

In general, experiments show good repeatability both in Figure 12 and in Figure 13. Similar trends in velocity and pressure were observed throughout all the experiments. Additionally, the run-up distances obtained for all the experiments within a given configuration presented no significant variation and were all located near the first quarter of the detonation tube.

5.2. Hydrogen–Oxygen Mixtures With an Equivalence Ratio of 0.25

A similar analysis to the one described in the previous sub-section was performed for this mixture. For a Hydrogen–Oxygen mixture with an equivalence ratio of 0.25 and an initial pressure of 20 kPa, the CJ pressure is 286 kPa and the CJ speed is 1,890 m/s [56]. However, in this case a total of four runs were made and a total of four pressure transducers were used for each sub-experiment.

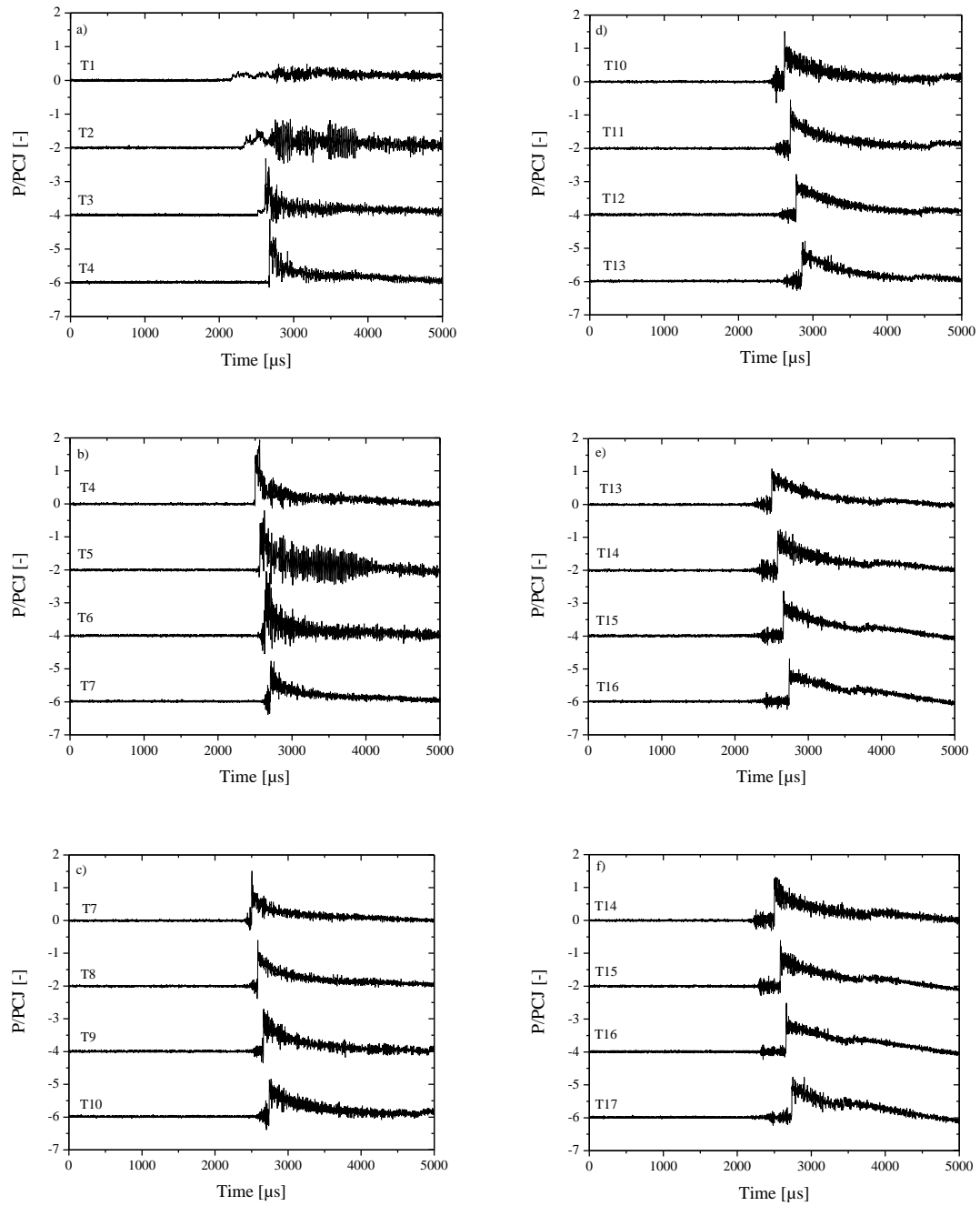


Figure 14. Pressure results obtained for a Hydrogen-Oxygen mixture ($\phi = 0.25$) explosion with half washer-shaped obstacles, an equal blockage ratio, and a gap between obstacles of 3D. Each frame shows the results obtained for the transducers described within the figures (T1 – T17).

Similar to the experimental results obtained in the previous sub-section, with the current positioning of the pressure transducers, it is possible to distinguish the different combustion regimes, *i.e.*, slow and fast deflagration, DDT and the stable detonation regime. For instance, T1 and T2 describe a slow deflagration, T3 and T4 illustrate a fast deflagration, T5 shows the onset of the detonation and from T5 to T17 a stable detonation is observed. When DDT is achieved, the pressure increased to approximately 1.8 times the CJ value. After this occurred, the pressure tends to stabilize near 1.5 times the CJ pressure. Figure 15 shows the overall progression of the combustion wave.

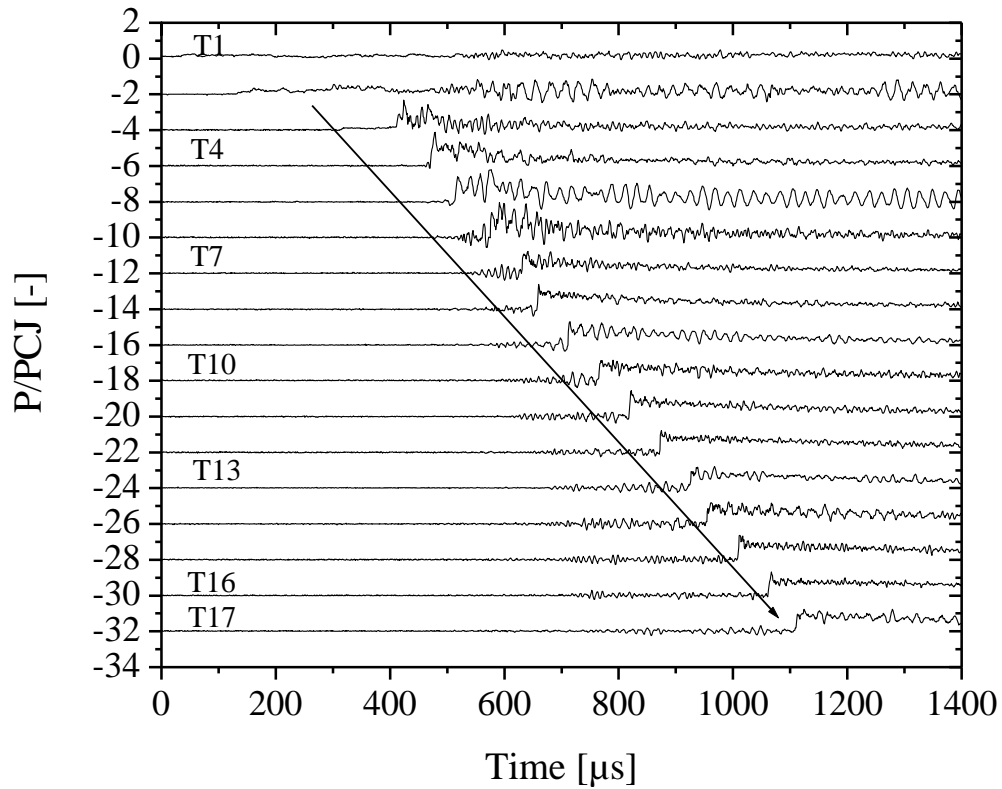


Figure 15. Overall progression of the combustion wave for a Hydrogen-Oxygen mixture ($\phi = 0.25$) explosion with half washer-shaped obstacles, an equal blockage ratio and a gap between obstacles of $3D$.

On the other hand, the experimental velocity obtained between T1 and T4 is nearly constant and close to half the CJ speed. Between T4 and T5 the velocity of the shock wave exceeds the CJ value. This means that the onset of the detonation occurs between T4 and T5. The next data points for the velocity show a significant deceleration in the combustion process; however, the velocity remains close to the CJ value. As the combustion propagates into the uncongested section of the detonation tube, the experimental velocity shows a clear tendency to stabilize near the CJ value. Figure 16 shows the experimental

results of the four experiments. Additionally, an average of these results is shown with error bars representing one standard deviation obtained for each measurement.

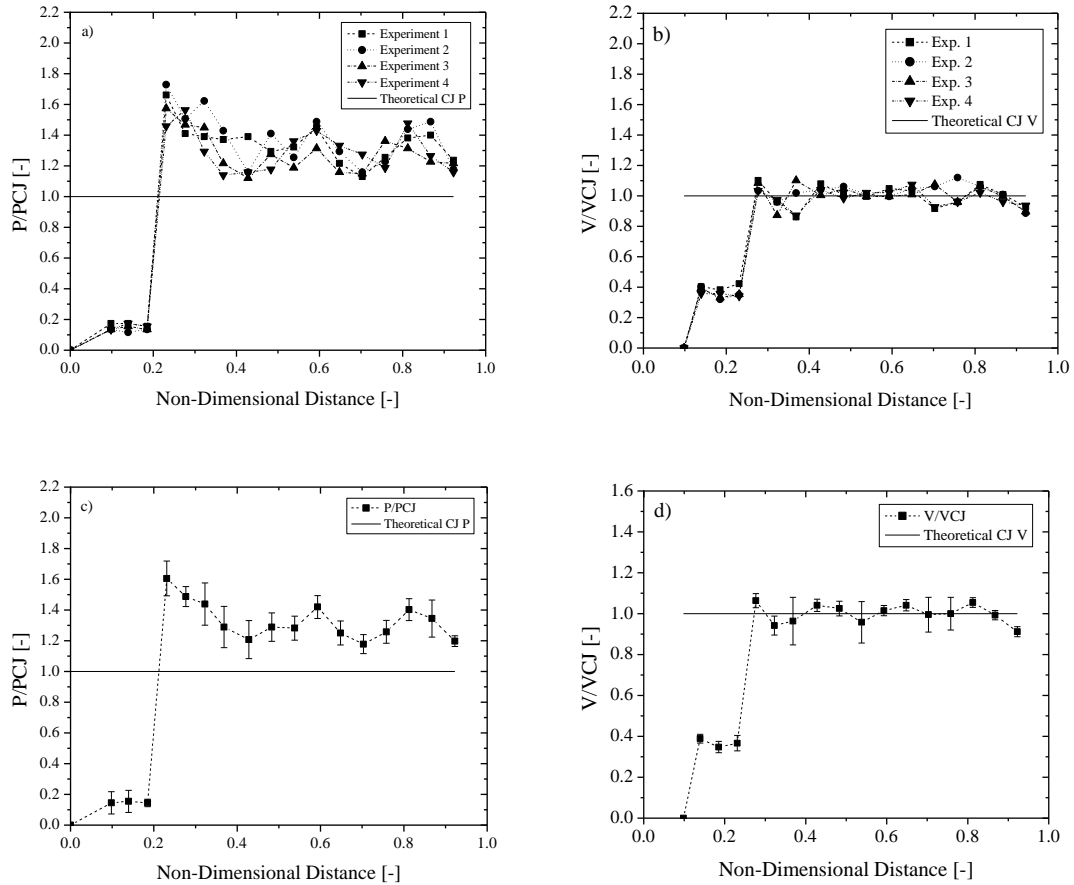


Figure 16. Summary of experimental results for Hydrogen-Oxygen mixture explosions ($\phi = 0.25$) in the characterization study. Figures a) and b) show the pressure and velocity results, respectively, for the four experiments, and Figures c) and d) illustrate the average pressure and velocity results, respectively. The error bars represent one standard deviation obtained for each transducer.

Figure 16d shows that the run-up distance is approximately 0.69 m (result obtained by the multiplication of the non-dimensional distance – 0.25, by the length of the detonation tube – 2.77 m) away from the ignition source. Figure 17 shows the run-up distances obtained for these four experiments.

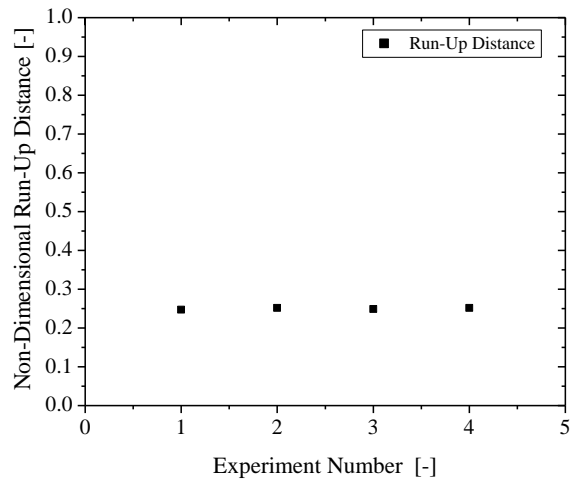


Figure 17. Variability of the run-up distances obtained for four repeat hydrogen-oxygen mixture ($\varphi = 0.25$) explosions with an initial pressure of 20 kPa. The obstacle configuration used in these experiments was: half-washer-shaped obstacles with a uniform blockage ratio (40%) and with a gap between obstacles of 3D.

In general, experiments show good repeatability both in Figure 16 and in Figure 17. Similar trends in velocity and pressure were observed throughout all the experiments, so only the averaged results are shown in the rest of the paper. Additionally, the run-up distances obtained for all the experiments within a given configuration presented no significant variation and were all located near the first quarter of the detonation tube.

Comparing Figure 13 with Figure 17, it is possible to infer the effect that the equivalence ratio has on the run-up distance to achieve detonation. For instance, the leaner the fuel concentration, the longer the distance necessary to obtain a detonation. For the experiments that had an equivalence ratio of one, the run-up distance was 0.57 m away from the ignition source and with the leaner fuel concentration ($\phi = 0.25$) the run-up distance was of 0.69 m away from the ignition source. This implies an increment of approximately 20% with respect to an ideal mixture ($\phi = 1.0$).

5.3. Summary

In this section, it was shown that the proposed layout of the pressure transducers allows the identification of the four combustion regimes, *i.e.*, slow deflagration, fast deflagration, onset of detonation (DDT) and stable detonation. Additionally, experiments with an equivalence ratio of 1.0 and 0.25 were performed. From these experiments, theoretical assumptions were proven. For instance, the fact that prior to the onset of detonation a deceleration of the shock to half the CJ speed was observed. Additionally, when the mixture is taken to the detonation limits, *e.g.*, when the equivalence ratio is 0.25 in hydrogen–oxygen mixtures, the detonation will tend to mitigate energy losses by giving higher pressure values than the ones defined by the CJ theory.

More importantly, these experiments prove that the experimental layout and procedure allow good repeatability on the results, *i.e.*, the run-up distance to obtain detonation with hydrogen–oxygen mixtures with an equivalence ratio of 1.0 was always at 0.57 m away from the ignition source, while for more diluted mixtures (equivalence ratio of 0.25) the run-up distance to obtain detonation occurred at 0.69 m away from the

ignition source. This proves that the leaner the fuel concentration is, the longer the distance necessary to obtain a detonation.

6. EXPERIMENTAL RESULTS

Experiments were performed at room temperature and stoichiometric fuel-oxygen mixtures. As seen in Table 2, the fuels selected for this study were hydrogen, ethylene, and acetylene. The initial pressure for these mixtures varied with the fuel. Schematics of each experiment are presented later in this paper. Table 4 summarizes the experimental conditions used as well as the CJ values for these mixtures at the specified condition.

Table 4. CJ conditions obtained from the Shock and Detonation Toolbox [56] for the fuel-oxygen systems utilized in these experiments.

	Hydrogen	Ethylene	Acetylene
Initial Pressure [kPa]	20	17	9.3
CJ Pressure [kPa]	354	517	285
CJ Speed [m/s]	2747	2287	2296

As mentioned above, a total of five repetitions were completed for each experiment, and the pressures and speeds were recorded up to T16 (T1-T4, T4-T7, T7-T10, T10-T13 and T13-T16). In each sub-experiment, data were recorded for four pressure transducers. The pressure transducers were randomly moved between the four adjacent probes, and no specific trend was followed for their placements. This degree of randomness in the placement of the transducers was done to ensure that they were capturing similar data and to avoid possible data misinterpretation that may have followed a certain transducer and port location. Results from each of the 9 experiments defined in Table 2 are presented, in order, in the following sections.

6.1. Experiment 1

The first experiment of the matrix consisted of igniting hydrogen-oxygen mixtures with an array of ring-shaped obstacles. In this case, the blockage ratio configuration used was “*increasing*”; therefore, the blockage ratio was augmenting from 25% to 80% within each set. The placement of the obstacles was “*variation*” and is described by the obstructions in each set being placed once, twice, and three times the internal diameter of the detonation tube. Figure 18 shows a schematic of the layout of the obstacles for this experiment.

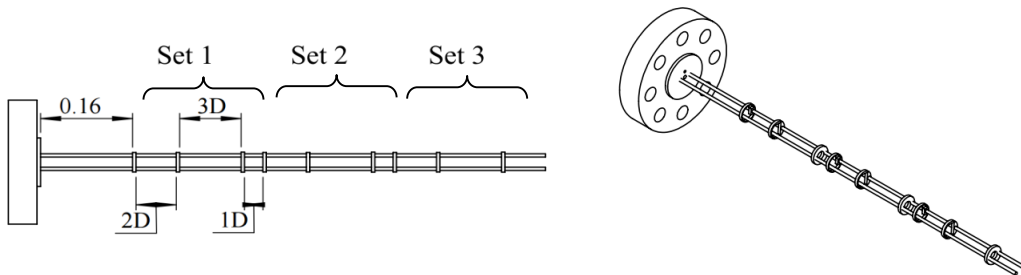


Figure 18. Obstacle layout for Experiment 1 – Ring-shaped obstacles with an increasing blockage ratio and a “*variation*” obstacle distribution. The first obstacle is located at 0.16 m away from the ignition point. The gap between the first two obstacles is 2D. The gap between the second and third obstacle is 3D. The gap between the next pair of obstacles is 1D. The location for the upcoming obstacles is repeated following the same order. Units are given in meters.

Figure 19 illustrates the results for a complete experiment with this configuration. The format of the sample response presented in Figure 19 is representative of the rest of the repeat experiments, and therefore only graphical statistical summaries are presented for the other eight experiments in the following subsections.

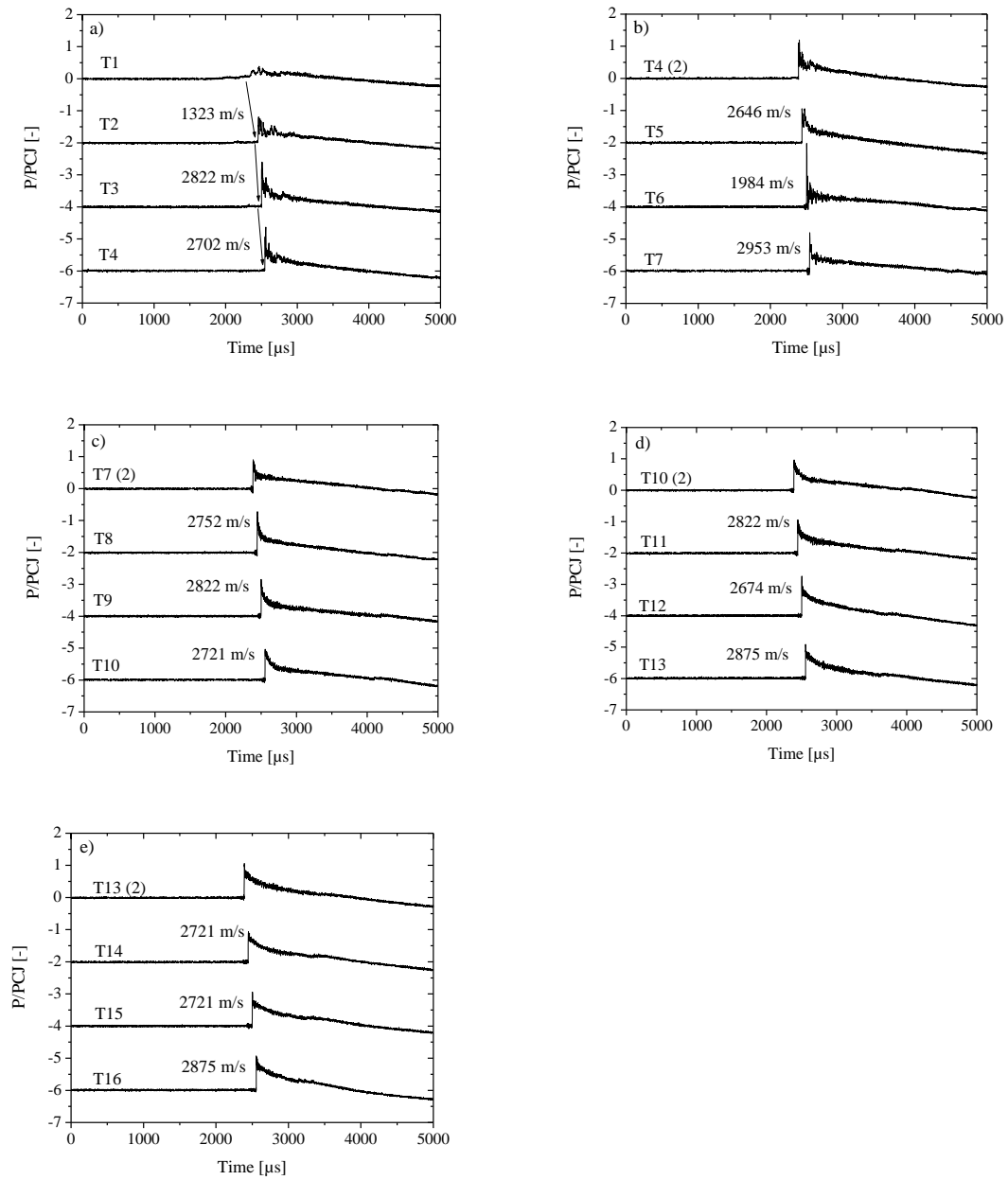


Figure 19. Experimental pressure and velocity results for Experiment 1, a hydrogen-oxygen mixture ($\phi = 1$) explosion with ring-shaped obstacles, an increasing blockage ratio, and a placement of obstacles as follows: once, twice, and three times the internal diameter of the detonation tube. T_n represent the response obtained for that pressure transducer location.

In Figure 19, T1 and T2 describe a deflagration combustion regime, and T3 shows a possible initiation of the detonation. However, it seems that after T3 the detonation fails. This event is illustrated by later readings (T4 and T5) which show a significant reduction in both the pressure and speed. On T6, a rapid increase in the pressure (up to nearly twice the CJ pressure) is observed, and between T6 and T7 a sudden re-acceleration of the combustion process is seen. From then on, a stable detonation is achieved. Figure 20 shows the summary of the pressure and velocity profiles. The error bars in these graphs represent one standard deviation obtained at each measurement point. This is the same for all the experimental results shown in the following sections.

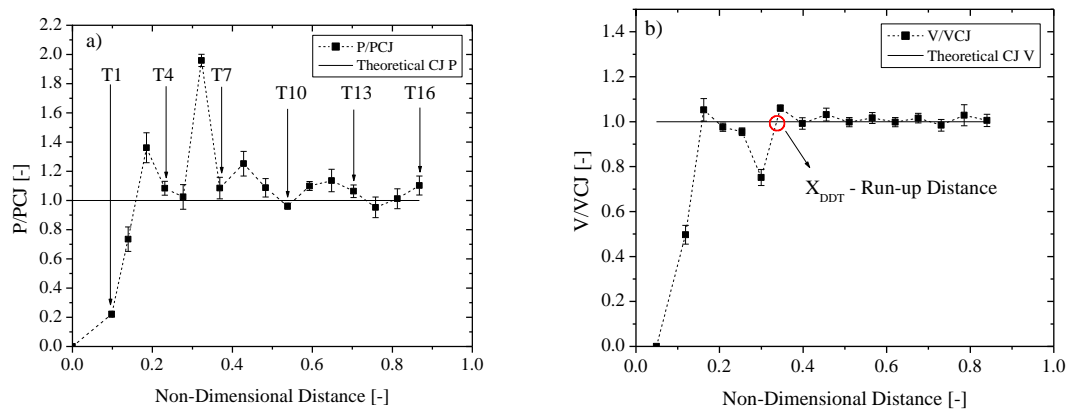


Figure 20. Summary of the experimental results for Experiment 1, the hydrogen-oxygen mixtures with ring-shaped obstacles, an increasing BR, and a variation obstacle distribution.

The pressure profile shown in Figure 20a illustrates a first peak at approximately the first fifth of the detonation tube (0.5 m away from the ignition source, T3) followed

by a decrease in the pressure magnitude. The velocity results show a similar trend. In this case, the CJ Speed is reached at T3; however, the experimental velocity reduces to nearly 0.7 times the CJ speed. The authors believe that excessive turbulence due to the obstacles with high blockage ratio do not allow the transition from deflagration to detonation to be successful. At the first third of the detonation tube (0.9 m away from the ignition source, T6), a secondary peak pressure is observed. This crest is also noticeable in the speed results; however, it occurs between T6 and T7. The velocity and pressure profiles reported downstream show that the detonation has become stable, in which relatively small fluctuations in the speed are observed.

6.2. Experiment 2

This experiment consisted of igniting hydrogen-oxygen mixtures with an array of half-washer-shaped obstacles. In this case, all the obstructions had a blockage ratio of 40%, and the obstacles were placed uniformly (with a gap of twice the internal diameter of the tube) throughout the first 0.8 m of the detonation tube. Figure 21 shows a schematic of the layout of the obstacles for Experiment 2. Figure 22 shows the summary of the pressure and velocity profiles obtained for this experiment.

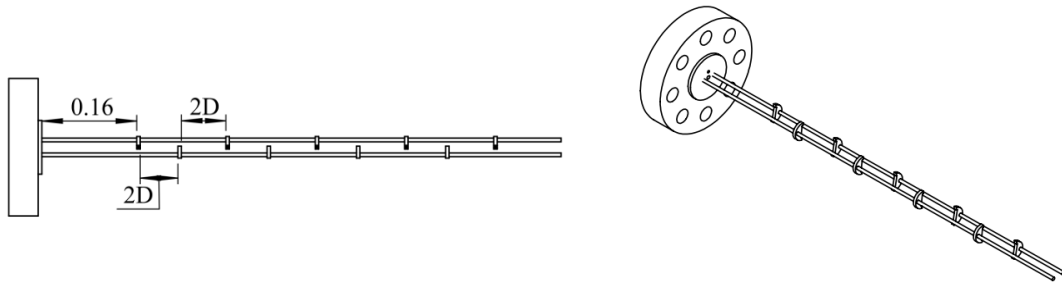


Figure 21. Obstacle layout for Experiment 2 – Half-washer-shaped obstacles with an equal blockage ratio and a “uniform” obstacle distribution. The gap between the obstacles is $2D$. Units are given in meters.

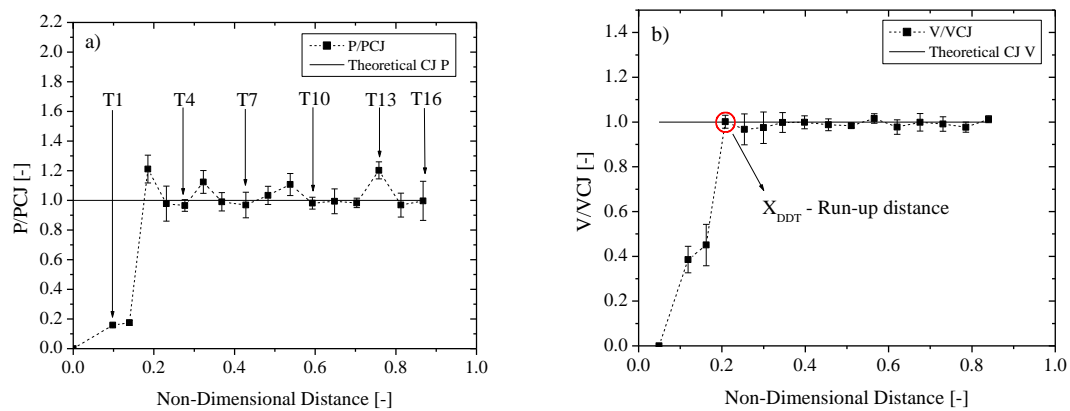


Figure 22. Summary of the experimental results for Experiment 2—hydrogen-oxygen mixtures with half washer-shaped obstacles, an equal BR, and a uniform obstacle distribution.

This second configuration shows a more stable detonation profile than the one obtained for Experiment 1 of the matrix. The pressure results described in Figure 22a show a relatively low pressure at the first and second transducers. Similarly, the values reported for the velocity between T1-T2 and T2-T3 are approximately within 0.5 times the CJ speed. Moreover, the pressure response obtained at T3 shows a significant increase (exceeding the CJ value). The experimental velocity obtained between T3 and T4 also

indicates that the CJ speed has been reached. Therefore, the onset of the detonation for this configuration was found to be at this location (approximately the first quarter of the detonation tube – 0.58 m away from the ignition source). The velocity profile reported downstream of the detonation tube shows very stable behavior, and some velocity fluctuations are observed; however, these occur near the CJ value.

As for the pressure, after T3 a reduction in its magnitude is observed. It is worth mentioning that the congested obstacle section is present until T5. From T6 until T16, there are no obstructions. Once the detonation is formed, the presence of obstacles seems to have an adverse effect on the pressure, *i.e.*, the pressure decreases to approximately the CJ values. As the combustion progresses into the uncongested region of the detonation tube, a secondary peak is observed; however, there is a tendency for the pressure to stabilize near the CJ value.

6.3. Experiment 3

The third experiment consisted of H₂-O₂ mixtures with an array of block-shaped obstacles. In this case, the blockage ratio used was “*decreasing*”; therefore, the blockage ratio was reducing from 80% to 25% within each set. The placement of the obstruction within the sets was “*staggered*”, which means that the obstacles were spaced at 1D followed by a gap of 5D. This arrangement was made in three groups, each group consisting of three obstacles. Figure 23 shows a schematic of the layout of the obstacles for Experiment 3. Figure 24 shows the summary of the pressure and velocity profiles.

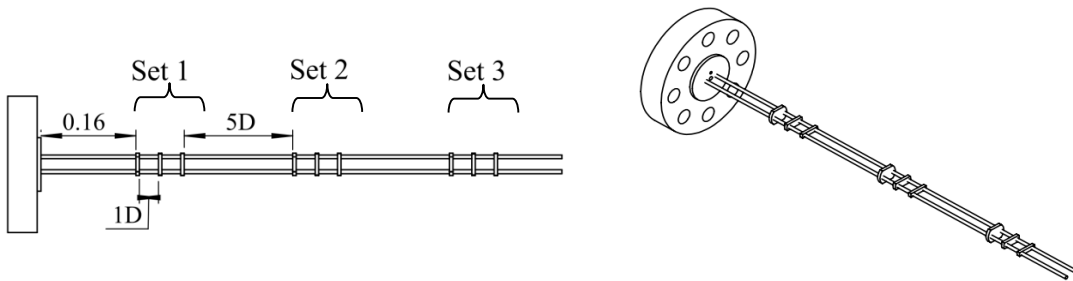


Figure 23. Obstacle layout for Experiment 3 – Block-shaped obstacles with a decreasing blockage ratio and a “staggered” obstacle distribution. The gap between the first three obstacles is 1D each. Each set is separated by a gap of 5D. The location for the upcoming obstacles is repeated following the same order. Units are meters.

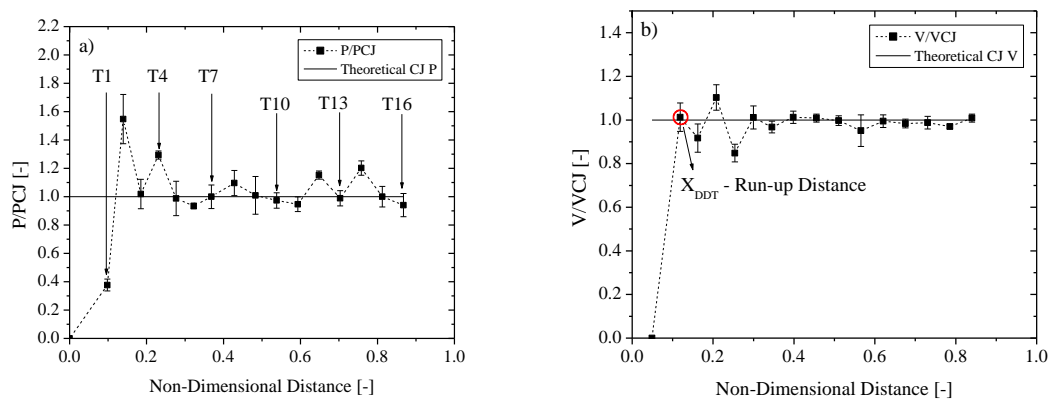


Figure 24. Summary of the experimental results for Experiment 3—hydrogen-oxygen mixtures with block-shaped obstacles, decreasing BR, and a staggered obstacle distribution.

The results obtained with this obstacle configuration show a deflagration at T1. At T2, a sudden increase in the pressure (1.5 times the CJ value) is observed. The velocity between T1 and T2 exceeds the CJ speed, as seen in Figure 24b. A reduction in the pressure and speed magnitudes is observed at T3 and between T2 and T3, respectively; however, the pressure remains above the CJ value. Secondary pressure and velocity peaks

were observed at T4 and between T3 and T4, respectively. Between T4 and T5 there is a rapid decrease in the velocity of the detonation wave to nearly 0.8 times the CJ value. It is worth mentioning that a blockage ratio of 80% was present before T4, and the next obstacle has a 40% blockage ratio. The authors believe that this sudden deceleration of the combustion process is given by the obstacle shape and positioning within the tube (block-shaped, aligned in the center of the tube). For the detonation wave to overcome the obstacle, the shock has to divert and around the obstacle. During this process, the formation of a pocket of unburned and compressed mass may be formed and, subsequently ignited via a retonation wave (a shock that moves into the burned gases) formed from the next obstacle present in the obstruction arrangement. This process leads to the formation of an auto-explosion which ultimately results in the acceleration of the detonation wave [42] and is observed in the experimental results in Figure 24b (between T5 and T6). From then on, the velocity profile reported downstream shows a very stable behavior with some minor velocity fluctuations near the CJ value. The onset of the detonation for this configuration was found to be between T1 and T2 (approximately the first tenth of the detonation tube – 0.33 m away from the ignition source).

The pressure profile described in Figure 24a shows significant variations when the combustion wave is propagating within the obstructed region of the detonation tube. As the detonation moves within the uncongested section, the pressure shows fewer fluctuations and an overall tendency to stabilize very close to the CJ value.

6.4. Experiment 4

This experiment consisted of igniting ethylene-oxygen mixtures with an array of ring-shaped obstacles. In this case, all the obstruction had a blockage ratio of 40%. The placement of the obstacles was “*staggered*”, which means that the ring-shaped obstacles were spaced one times the internal diameter of the detonation tube followed by a gap of 5D. This arrangement was made in three groups, each group consisting of three obstacles. Figure 25 shows a schematic of the layout of the obstacles for Experiment 4. Figure 26 shows the summary of the pressure and velocity profiles.

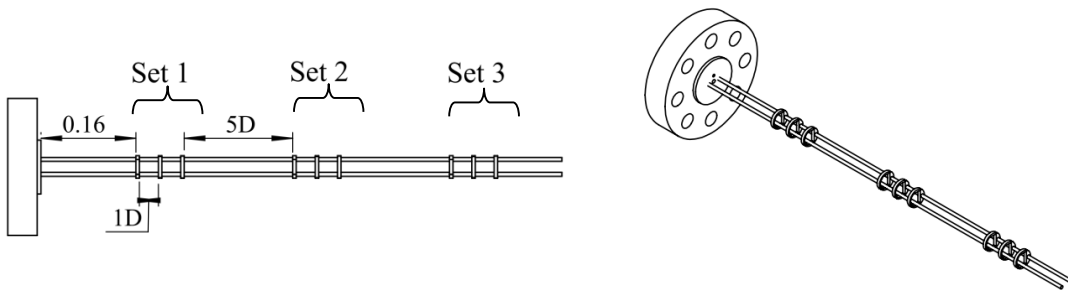


Figure 25. Obstacle' layout for experiment 4 – ring-shaped obstacles with an equal blockage ratio and a “*staggered*” obstacle distribution. The gap between the first three obstacles is 1D. This is then followed by a gap of 5D. The location for the upcoming obstacles is repeated following the same order. Dimensions are in m.

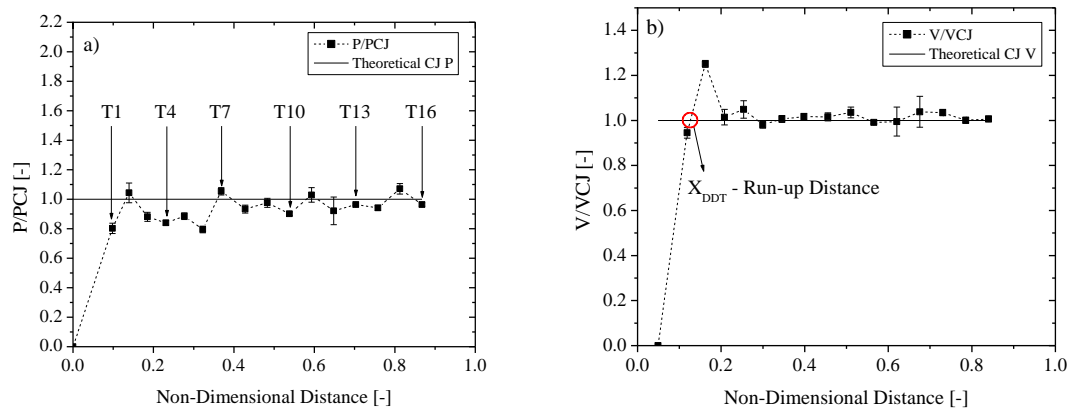


Figure 26. Summary of the results for Experiment 4—ethylene-oxygen mixtures with ring-shaped obstacles, equal BR, and a staggered obstacle distribution.

In this experiment, high pressures (approximately 0.8 times the CJ pressure) were obtained at T1. As the combustion progresses, at T2 the CJ pressure is achieved. The pressure results (Figure 26a) obtained within the obstructed section of the detonation tube (until T5) show that after the CJ pressure was reached at T2, a reduction in the pressure magnitude is observed. For instance, the pressure tends to stabilize at 0.85 times the CJ value. As the detonation wave moves into the uncongested section of the detonation tube, at T6 the pressure decreases to 0.8 times the CJ value. At T7, the pressure exceeds the CJ pressure. From then on, the pressure shows minor fluctuations near the CJ value.

As for the speed of the detonation wave, the velocity between T1 and T2 is relatively high (0.9 times the CJ value). As the wave progresses, between T2 and T3, the velocity exceeds the CJ speed, and an overdriven detonation is observed. After that, between T3 and T4 the detonation decelerates rapidly until it reaches the CJ velocity. From then on, the velocity profile reported downstream shows a very stable behavior with some

minor velocity fluctuations near the CJ value. The run-up distance for the transition from deflagration to detonation was estimated to be at 0.35 m away from the ignition source.

In this experiment, it is possible to observe that the obstacles enhance the flame acceleration; however, once DDT takes place, the pressure is adversely affected by the presence of the obstructions.

6.5. Experiment 5

The fifth experiment of the matrix consisted of ethylene-oxygen mixtures with an array of half-washer-shaped obstacles. In this case, the blockage ratio used was “*decreasing*”; therefore, the blockage ratio reduced from 80% to 25%. The placement of the obstacles was “*variation*” and is described by the obstruction being placed once, twice, and three times the internal diameter of the detonation tube. Figure 27 shows a schematic of the layout of the obstacles for this experiment. Figure 28 shows the summary of the pressure and velocity profiles.

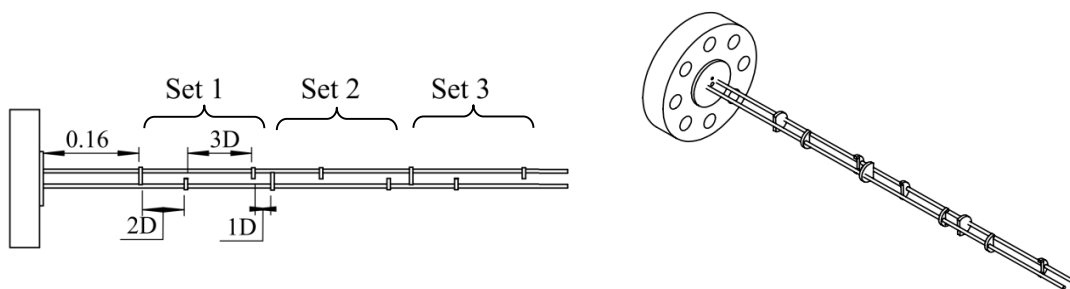


Figure 27. Obstacle layout for Experiment 5 – half-washer-shaped obstacles with a decreasing blockage ratio and a “*variation*” obstacle distribution. The gap between the first two obstacles is $2D$. The gap between the second and third obstacles is $3D$. The gap between the next pair of obstacles is $1D$. The location for the upcoming obstacles is repeated following the same order. Units are given in meters.

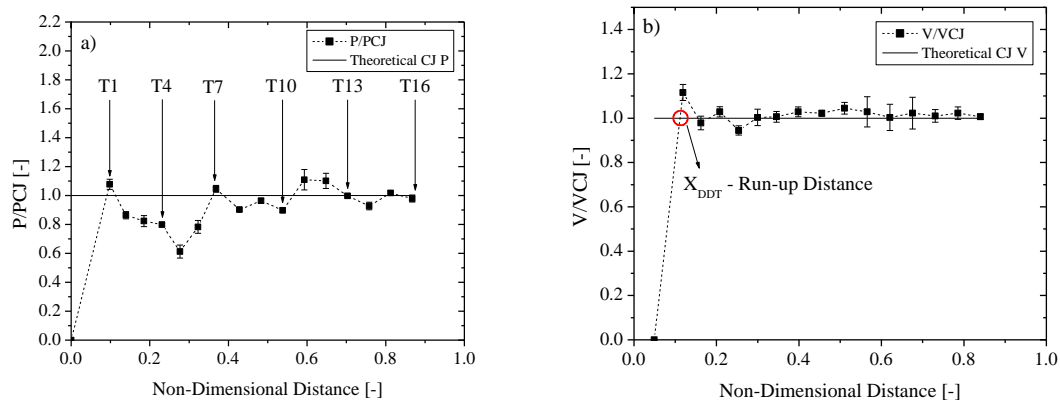


Figure 28. Summary of the results for Experiment 5—ethylene-oxygen mixtures with half-washer-shaped obstacles, decreasing BR, and a variation obstacle distribution.

In this experiment, high pressures (above the CJ pressure) were obtained at T1 (Figure 28a). However, in the obstructed section the pressure decays to nearly half the CJ pressure. This behavior, again, illustrates that the presence of obstacles once the detonation wave has been formed diminishes the pressure. As the combustion progresses into the unobstructed section, there is an increase in the pressure with a tendency to stabilize near the CJ value.

As it can be observed in Figure 28b, the experimental velocity between T1 and T2 exceeds the CJ value. This high velocity is followed by a deceleration of the combustion wave to the CJ speed (between T2 and T3). From then on, in the obstructed region of the detonation tube the velocity of the detonation presents some fluctuations; however, it oscillates near the CJ value. Once the detonation propagates into the uncongested region of the tube, the velocity tends to stabilize relatively near the CJ speed, but over this value.

Thus, with this layout a tendency to have an overdriven detonation is observed. The run-up distance for this scenario was estimated to be at 0.31 m away from the ignition source.

6.6. Experiment 6

Experiment 6 utilized an ethylene-oxygen mixture with an array of block-shaped obstacles. In this case, the blockage ratio configuration used was “*increasing*”; therefore, the blockage ratio was augmented from 25% to 80% within a set of three obstacles; the obstacles were placed uniformly (with a gap of twice the internal diameter of the tube) throughout the first 0.8 m of the detonation tube. Figure 29 shows a schematic of the layout of the obstacles for this experiment. Figure 30 shows the summary of the pressure and velocity profiles.

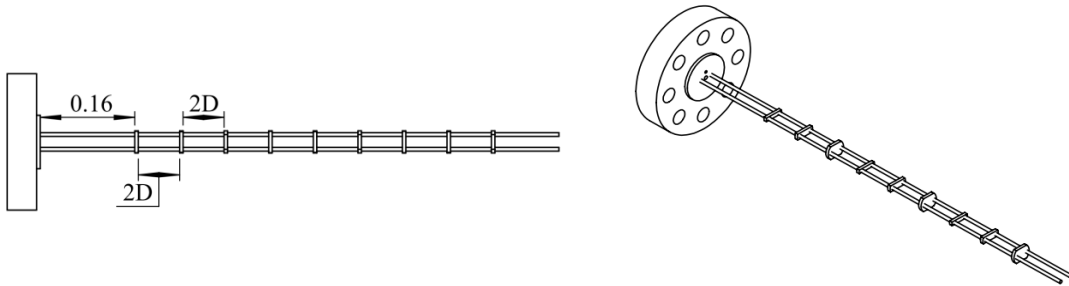


Figure 29. Obstacle layout for Experiment 6 – block-shaped obstacles with an increasing blockage ratio and a “*uniform*” obstacle distribution. The gap between the obstacles is $2D$. Units are given in meters.

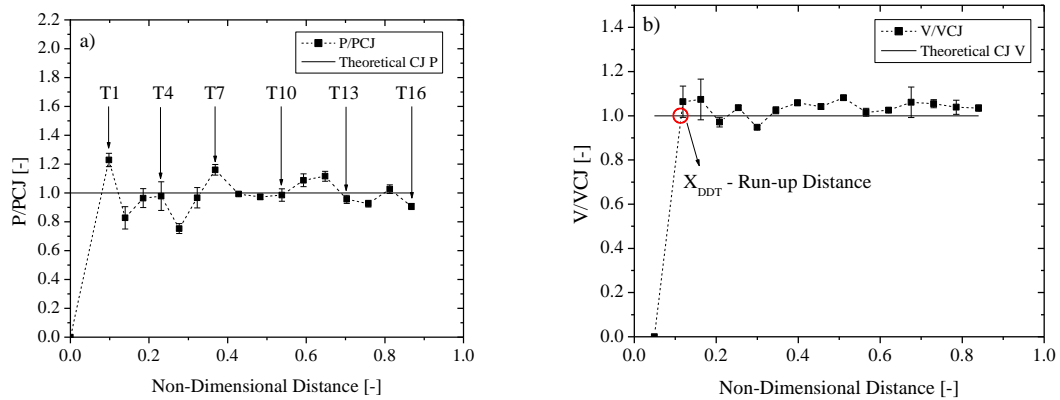


Figure 30. Summary of the Experiment 6—ethylene-oxygen mixtures with block-shaped obstacles, increasing BR, and a uniform obstacle distribution.

Figure 30a shows that the experimental pressure at T1 exceeds the CJ value. However, at T2 the pressure reduces to approximately 0.8 times the CJ pressure. As the combustion propagates in the congested region the pressure shows a tendency to be below the CJ value, especially at T5, which is located right before the last obstacle (80% blockage ratio) with a pressure of approximately 0.75 times the CJ value. Once the detonation moves into the uncongested region, these fluctuations in the pressure are significantly reduced and occur above and below the CJ pressure.

On the other hand, Figure 30b shows the experimental velocities obtained for this layout. The speed of the combustion wave obtained between T1 and T2 already exceeds the CJ value. This behavior is characteristic of an overdriven detonation. This unstable wave is sustained until the next monitor point (between T2 and T3). When the combustion propagated within the obstructed region of the tube, the detonation had a tendency to stabilize near the CJ speed. Once the combustion wave propagated into the uncongested

section of the tube, the experimental values obtained for the velocity tended to be above the CJ value. The authors believe that in this particular case the shock front is diverting progressively after each obstacle, leaving some unburned mass right after each obstacle. This compressed mass reacts with the blast waves formed from the interaction with the next obstacle that, in this case, presents a higher blockage ratio. Using the criteria mentioned by Ciccarelli and Cross [42], it is believed that the interaction between these Mach stems and the compressed gas will result in the formation of a detonation wave. These interactions make the combustion process unstable and, consequently, an overdriven detonation is expected and observed. The run-up distance for this experiment was estimated to be at 0.32 m from the ignition source.

6.7. Experiment 7

The seventh experiment of the matrix consisted of a $C_2H_2-O_2$ mixture with an array of ring-shaped obstacles. In this case, the blockage ratio used was “*decreasing*”; therefore, the blockage ratio was reduced from 80% to 25%, and the obstacles were placed uniformly (two times the internal diameter of the detonation tube) throughout the first 0.8 m of the detonation tube. Figure 31 shows a schematic of the layout of the obstacles for this experiment. Figure 32 shows the summary of the pressure and velocity profiles.

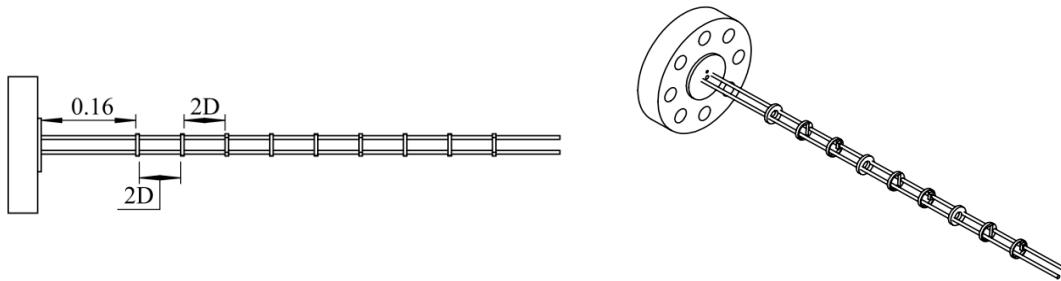


Figure 31. Obstacle layout for Experiment 7 – ring-shaped obstacles with a decreasing blockage ratio and a “uniform” obstacle distribution. The gap between the obstacles is $2D$. Units are given in meters.

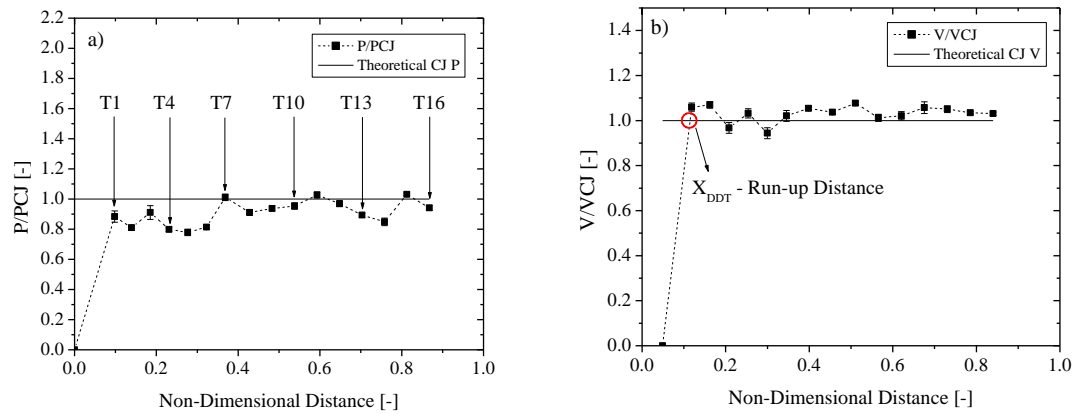


Figure 32. Summary of the results for Experiment 7—acetylene-oxygen mixtures with ring-shaped obstacles, decreasing BR, and a uniform obstacle distribution.

In this experiment, the pressures obtained in the congested area were lower than the CJ pressure, as seen in Figure 32a. However, as the combustion progresses into the unobstructed section of the detonation tube, a significant increase in the pressure is observed. For instance, at T7 the experimental pressure just exceeded the CJ value. After T7, a tendency for the pressure to fluctuate relatively close to the CJ pressure was observed.

The velocity shows a very similar response to the one obtained for the sixth experiment. For instance, in Figure 32b, the velocity already exceeded the CJ value between T1 and T2, followed by a constant velocity between T2 and T3. The detonation wave, then, decelerates, but the speed magnitude is close to the CJ value. The obstructed section of the detonation tube shows some fluctuations near the CJ speed. However, as the combustion progresses into the uncongested section of the detonation tube, the velocity shows a tendency to stabilize above the CJ value. This means that, with this obstacle configuration, an overdriven detonation takes place. Similar to the sixth experiment, it is believed that the unstable detonation is given by the formation of localized auto-explosions of compressed mass found right after the obstacles that have an 80% blockage ratio. For this experiment, the run-up distance was estimated to be at 0.31 m away from the ignition source.

6.8. Experiment 8

Experiment 8 utilized an acetylene-oxygen mixture with an array of half-washer-shaped obstacles. In this case, the blockage ratio configuration used was “*increasing*”; therefore, the blockage ratio was augmented from 25% to 80% within a set. The placement of the obstacles was “*staggered*”, which means that the ring-shaped obstacles were spaced at 1D followed by a 5D gap. This arrangement was made in three sets, each set consisting of three obstacles. Figure 33 shows a schematic of the layout of the obstacles for this experiment. Figure 34 shows the summary of the pressure and velocity profiles.

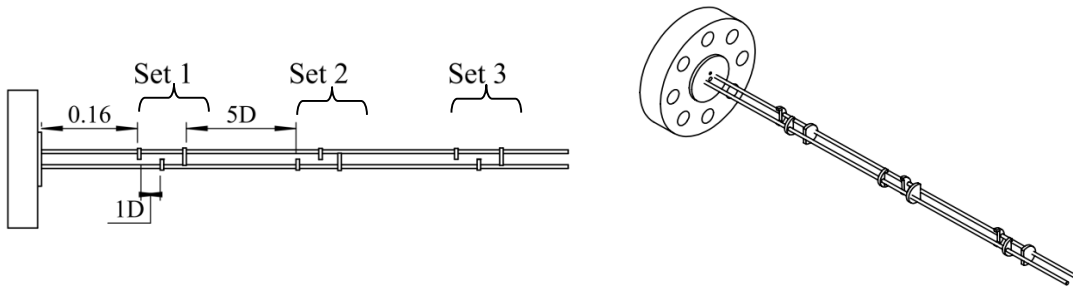


Figure 33. Obstacle layout for Experiment 8 – Half-washer-shaped obstacles with an increasing blockage ratio and a “staggered” obstacle distribution. The gap between the first three obstacles is 1D each. This is then followed by a gap of 5D. The location for the upcoming obstacles is repeated following the same order. Units are given in meters.

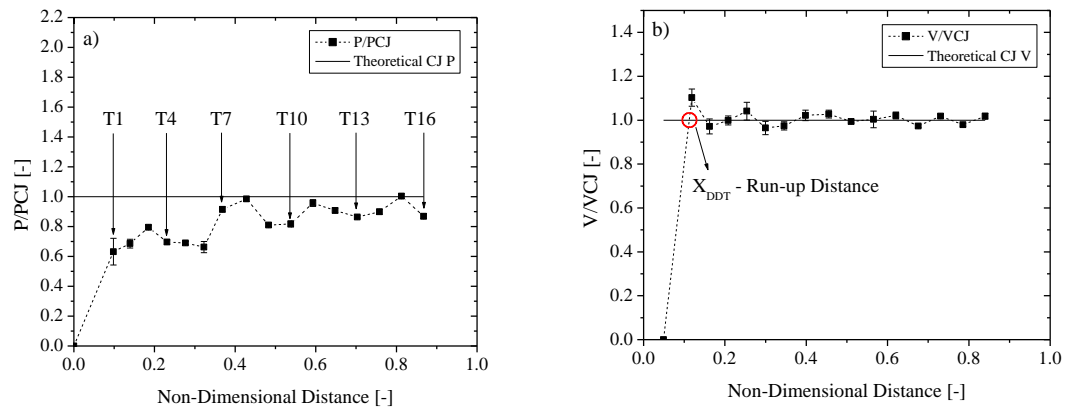


Figure 34. Summary of the results for Experiment 8— C_2H_2 - O_2 mixture with half-washer-shaped obstacles, increasing BR, and a staggered obstacle distribution.

As shown in Figure 34a, the experimental pressures obtained in the congested section of the detonation tube are again below the CJ value (between 0.5 to 0.8 times the CJ pressure). As the combustion progresses into the unobstructed section of the tube, the pressure increases to values close to the CJ pressure; however, this value is not achieved until T15. As the detonation wave moves downstream, a tendency for the pressure to stabilize below the CJ value is observed.

As for the velocity (Figure 34b) the experimental results show that between T1 and T2, the velocity exceeds the CJ value, followed by a detonation deceleration towards the CJ speed. In general, the obstructed section of the detonation tube shows small fluctuations near the CJ value. As the combustion front progresses into the uncongested region of the detonation tube, these oscillations seem to not be altered at all by the presence or absence of obstruction, as seen for the other configurations. Once DDT takes place, the detonation tends to stabilize at the CJ velocity. The run-up distance for this experiment was estimated to be at 0.31 m from the ignition source.

6.9. Experiment 9

The ninth experiment of the matrix consisted of igniting the $C_2H_2-O_2$ mixture with an array of block-shaped obstacles. In this case, the obstacles had a blockage ratio of 40%. The placement of the obstacles was “*variation*” and is described by the obstruction being placed once, twice, and three times the internal diameter of the detonation tube. Figure 35 shows a schematic of the layout of the obstacles for this experiment. Figure 36 shows the summary of the pressure and velocity profiles.

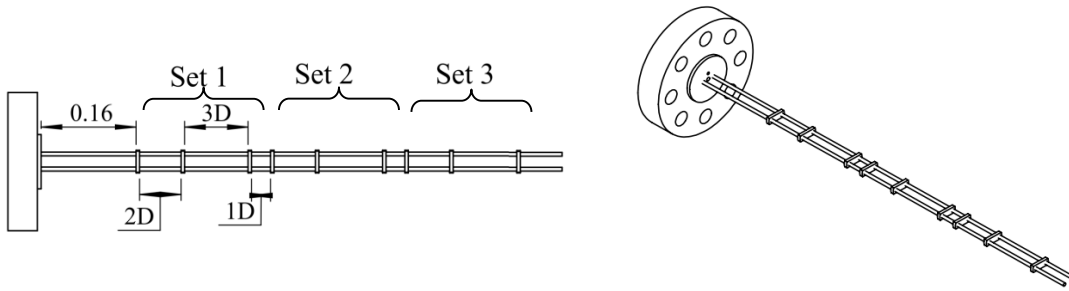


Figure 35. Obstacle layout for Experiment 9 – block-shaped obstacles with an equal blockage ratio and a “variation” obstacle distribution. The gap between the first two obstacles was $2D$. The gap between the second and third obstacle was $3D$. The gap between the next pair of obstacles was $1D$. The location for the upcoming obstacles is repeated following the same order. Units are given in meters.

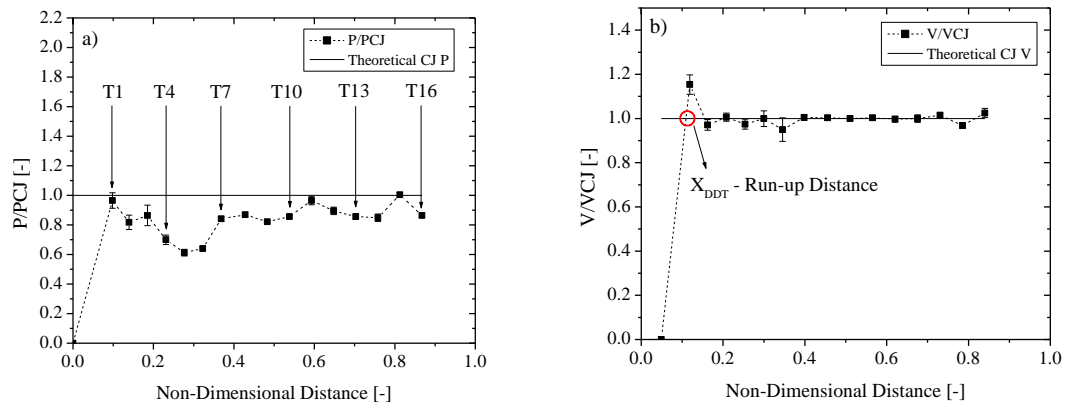


Figure 36. Summary of the results for Experiment 9—an acetylene-oxygen mixture with block-shaped obstacles, equal BR, and a variation obstacle distribution.

In this experiment, the pressures obtained in the congested area get close to the CJ pressure; however, this value is not reached in this section (Figure 36a). At T1, the pressure is very close to the CJ value; then at T2 a sudden decrease in the pressure magnitude is observed. Between T3 and T6, the pressure decays to nearly half the CJ value. At T7, an increase in the experimental pressure is observed, and from T7 to T10 the

pressure remains stable and below the CJ value. At T11, the pressure gets closer to the CJ value; however, this value was not reached. This behavior is followed by a minor decay in the pressure from T12 to T14. At T15, the pressure exceeds the CJ value, followed by a small decrease in the pressure magnitude. In summary, the experimental pressures showed a tendency to stabilize below the CJ pressure.

As seen in Figure 36b, the velocity shows a different behavior. For instance, between T1 and T2 the experimental speed exceeds the CJ value and is followed by a rapid deceleration of the detonation wave (between T2 and T3). From then on, the velocity shows a tendency to stabilize near the CJ value. When the combustion progresses into the uncongested region of the detonation tube, a sudden decrease in the speed is observed (between T6 and T7). However, as the detonation propagates downstream the stabilization tendency of the wave near the CJ value is maintained. In this case, the run-up distance for the onset of the detonation was estimated to be at 0.32 m away from the ignition source.

6.10. Discussion

6.10.1. Velocity Results

From the experimental data, several variables were analyzed: the maximum and minimum speed acquired throughout the experiment; the location at which these velocities were achieved; the average speed and the standard deviation for each experiment; the location in the detonation tube at which the detonation stabilized; the number of times the experimental velocity exceeded the CJ speed; and the run-up distance. Table 5 shows a summary of the experimental results obtained for the speed data, listed for each of the nine main experiments from the matrix. As it can be observed, the variables that deal with the

speed are normalized by the CJ values, and the variables that refer to any location are expressed in meters from the ignition plane.

Table 5. Summary of experimental results for the velocity data. Speeds are given relative to the calculated CJ velocity.

Exp. No.	Max Speed	Location Max V [m]	Min Speed	Location Min V [m]	Std Dev Speed	Run-up Distance [m]	Mean Speed	Stabilization Location [m]	No. Times V > VCJ
1	1.06	1.02	0.50	0.39	0.15	0.93	0.96	1.34	7
2	1.02	1.64	0.39	0.39	0.20	0.58	0.95	0.77	3
3	1.10	0.64	0.85	0.77	0.06	0.33	0.98	1.02	6
4	1.25	0.51	0.94	0.39	0.07	0.35	1.03	0.77	11
5	1.12	0.39	0.94	0.77	0.04	0.31	1.02	1.02	13
6	1.08	1.49	0.95	0.89	0.04	0.32	1.04	1.19	13
7	1.11	0.39	0.98	1.02	0.04	0.31	1.02	0.77	10
8	1.10	0.39	0.96	0.89	0.04	0.31	1.01	0.64	8
9	1.15	0.39	0.95	1.02	0.05	0.32	1.00	0.64	7

It is worth mentioning that, overall, the responses obtained for the run-up distance are very similar from the third to the ninth experiment. The authors believe that this occurred due to the high reactivity and ease for the mixtures utilized herein to undergo a DDT process; this tendency was enhanced with the addition of obstructions, which had a significant effect in reducing the distance at which detonation is achieved. Nonetheless, these data and the resulting statistical analysis provide excellent insight into what obstacle configurations enhance or have an adverse effect on flame acceleration, or perhaps have little effect at all.

The data were analyzed to determine which geometrical features are the key parameters that most affect the onset of the detonation, under the scope of the main variables considered for this study, *i.e.*, fuel, obstacle shape, blockage ratio, and the obstacle distribution. However, from the design of experiment matrix, more than one variable changes from experiment to experiment (Table 2). To perform a simple sensitivity analysis to determine the effect of the four main factors (with 3 levels each) on the measured response variables, the results for the response variable of interest are averaged over the experiments, which contained the same factor level. For instance, to determine the effect the fuel type has on the run-up distance, the data were analyzed by averaging the response obtained for each fuel, *i.e.*, for hydrogen it is the average of {0.93, 0.58, 0.33}, or 0.61. A similar procedure can be done for ethylene and acetylene. This methodology was applied to all the variables shown in Table 5 for each of the four main experimental factors. Figure 37 to Figure 40 show the graphical results of this sensitivity analysis. Recall that what is important in such an analysis are the relative changes in the variable over the different levels of the experiment factors.

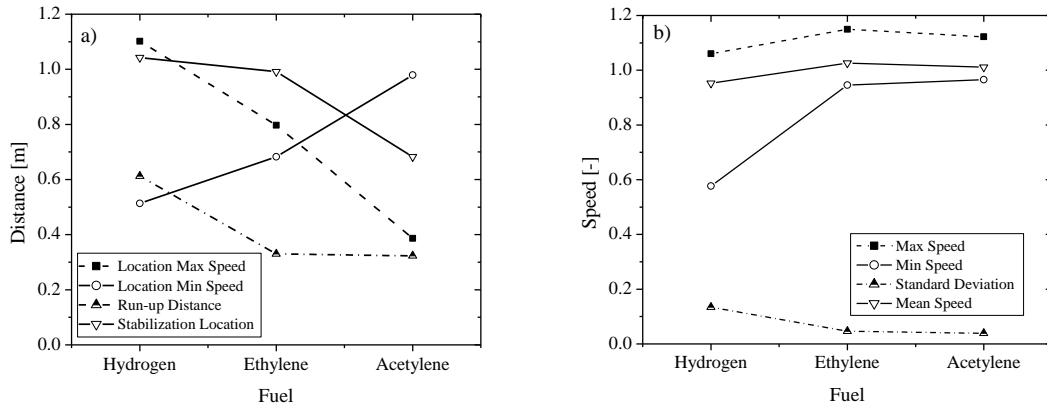


Figure 37. Sensitivity analysis for the wave velocity for different (a) location and (b) magnitude variables having fuel type as the parameter of interest.

As can be observed in Figure 37a, the fuel type had a large effect on each of the four velocity-related locations. As expected, the following locations were maximized with hydrogen-oxygen mixtures and minimized for acetylene-oxygen systems: the run-up distance, the location at which the velocity of the detonation stabilized near the CJ speed, and the location at which the maximum speed was obtained. As for the spot at which the velocity was the minimum, hydrogen-oxygen systems minimized the distance, while acetylene-oxygen mixtures maximized this distance. It is worth mentioning that for the hydrogen-oxygen mixtures, deflagration speeds were observed; however, for the other fuel-oxygen systems this did not occur. This is shown in Figure 37b, in which the minimum speed obtained for hydrogen is approximately 0.6 times the CJ velocity, while for the other mixtures the minimum speed was very close to the CJ value. The other variables studied in this analysis, *i.e.*, the maximum speed, the mean velocity and the standard deviation of the speed in a complete experiment, show that the effect of the fuel

is not significant, as the values are relatively close to each other. A similar analysis was carried out for the other three variables, *i.e.*, the obstacle shape, the blockage ratio, and the obstacle distribution. Figure 38 to Figure 40 show these results, respectively.

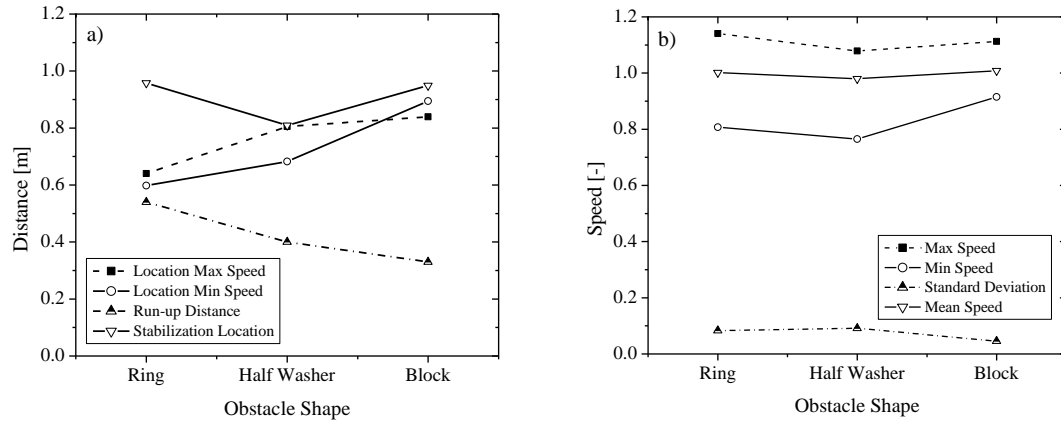


Figure 38. Sensitivity analysis for the wave velocity for different (a) location and (b) magnitude variables having obstacle shape as the parameter of interest.

Figure 38 summarizes the sensitivity analysis results for the three different obstacle shapes used in the experiments. From Figure 38a, one can see that the obstacle shape has some noticeable effect on the distances for achieving the key velocity markers (as evident in the variation in results across the 3 different shapes). As it can be noticed, the ring-shaped obstacles maximized the run-up distance and the distance necessary for the detonation to stabilize. However, they minimized the location at which the maximum and minimum speeds were obtained, while the block-shaped obstacles maximized these values. Additionally, this obstruction geometry maximized the run-up distance to obtain a

detonation. The half-washer obstacle results show that this shape minimizes the distance to obtain a stable detonation regime.

In contrast, Figure 38b shows that, in general, the obstacle shape does not have a significant effect on the magnitude-related values of the wave speed. For instance, the maximum, mean, and standard deviation of the velocity do not vary notably amongst the different obstacle shapes. However, the minimum velocity obtained shows a slight minimum when half-washer obstacle shapes were used and a maximum when the block geometry was employed.

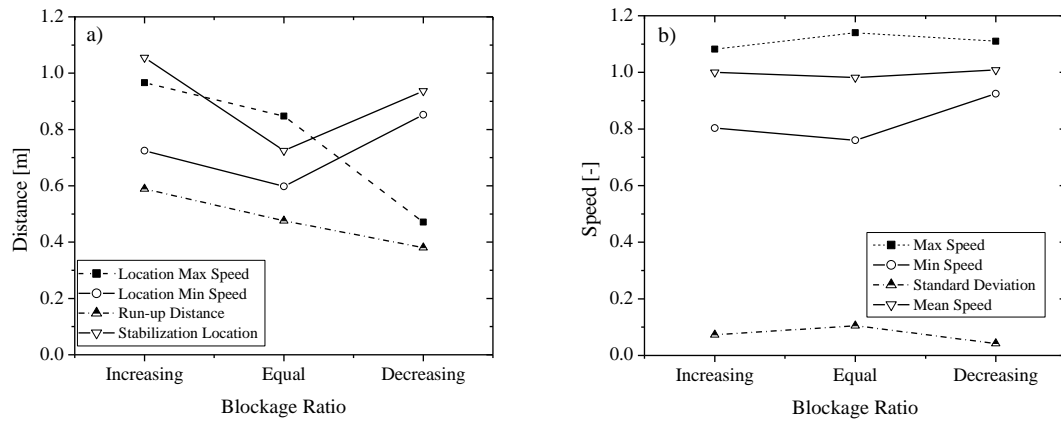


Figure 39. Sensitivity analysis for the wave velocity for different (a) location and (b) magnitude variables having blockage ratio as the parameter of interest.

As seen in Figure 39, the obstacle distribution played a noticeable role in most of the speed location-related variables, where the changes (variation, uniform, and staggered) induced differences in the measured locations. When the blockage ratio was increasing, the run-up distance, the location at which the maximum speed was attained, and the

distance at which the detonation stabilizes were all maximized. The largest value for the minimum speed was obtained when the blockage ratio was decreasing. Additionally, when the blockage ratio decreases, the run-up distance and the location at which the maximum speed was obtained were both minimized. When the blockage ratio was kept constant, the distance of the minimum speed and where the detonation was stable were both minimized.

As seen in Figure 39b, a similar behavior to the one described for the obstacle shape in Figure 38 is observed. For instance, the only velocity magnitude-related variable that was affected even slightly is the minimum speed (the lowest speed was obtained with an equal blockage ratio and maximized when the level of blockage was decreasing). As for the other parameters analyzed in this figure, no significant effect was observed when the blockage ratio was modified.

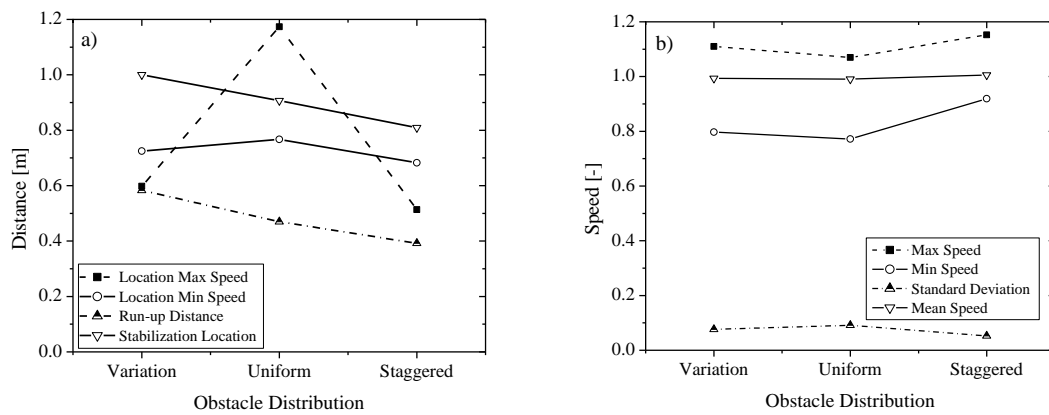


Figure 40. Sensitivity analysis for the wave velocity for different (a) location and (b) magnitude variables having obstacle distribution as the parameter of interest.

The effects that the obstacle distribution had on several parameters are shown in Figure 40. As for the other factors, the obstacle distribution had a significant influence on the various velocity-related distances, as seen in Figure 40a. For instance, it is possible to determine that the run-up distance and the location at which the detonation stabilizes is maximized by the “variation” obstacle distribution and minimized by a staggered obstruction configuration. Additionally, the distances at which the maximum and minimum speeds were achieved were favored by a staggered obstacle distribution. On the contrary, when a uniform obstacle distribution was used, the maximum and minimum speed locations were maximized.

Figure 40b illustrates a similar behavior to the effect described with the blockage ratio and obstacle shape. That is, there is no significant effect on the maximum and mean velocities, and the effect on the standard deviation of the speed is also negligible. However, the minimum speed obtained in the experiments show the smaller value being attained when a uniform obstacle distribution was used and maximized (slightly) when the obstacles were staggered.

Table 6. Ranking of variables as a function of the parameters modified in the experiments, where “1” is most significant and “4” is least significant.

Variables	Max Speed	Location Max V [m]	Min Speed	Location Min V [m]	Std Dev Speed	Run-up Distance [m]	Mean Speed	Stabilization Location [m]	No. Times V > VCJ
Fuel	1	1	1	1	1	1	1	1	1
Shape	3	4	3	2	3	2	2	4	3
BR	4	3	2	3	2	3	3	2	2
Dist.	2	2	4	4	4	4	4	3	4

The overall effect that each parameter has on the variables analyzed is ranked in Table 6. Not unexpectedly, the fuel is the most important factor; however, of more interest to the present study is the impact of the obstacle configuration. To this end, it was found that the impact of the configuration depends on the response being measured; these other parameters have different effects for each of the variables analyzed in this section. For instance, the obstacle distribution only seems to have a significant impact in the maximum speed and its location, as well as on the stabilization location. On the other hand, the parameters that have the largest overall effect on the detonation response variables related to the wave speed were identified to be the obstacle shape and the blockage ratio.

6.10.2. Pressure Results

Table 7 shows a summary of the experimental results obtained for the pressure data. The variables analyzed in this part of the study are: the maximum and minimum pressure obtained in the experiments; the location at which these pressures were attained; the average pressure and the standard deviation for each experiment; the number of times the pressure was greater than the CJ value; and the location at which the pressure exceeded the CJ value for the first time. As in Table 5, the variables that deal with the pressure are normalized to the CJ value, and the variables that refer to any location are expressed in meters.

Table 7. Summary of experimental results for the pressure data. Pressures are given relative to their respective CJ levels.

Exp. No.	Max Pressure	Location Max P [m]	Min Pressure	Location Min P [m]	Std Dev Pressure	Location first time P = PCJ [m]	Mean Pressure	No. Times P > 1
1	1.96	0.89	0.22	0.27	0.34	0.83	1.07	12
2	1.21	0.51	0.16	0.27	0.31	0.49	0.93	5
3	1.55	0.39	0.38	0.27	0.24	0.33	1.03	7
4	1.07	2.25	0.79	0.89	0.09	0.37	0.94	4
5	1.11	1.64	0.61	0.77	0.13	0.25	0.93	5
6	1.23	0.27	0.75	0.77	0.12	0.22	0.99	5
7	1.03	2.25	0.78	0.77	0.08	1.01	0.91	3
8	1.00	2.25	0.63	0.27	0.12	2.25	0.82	1
9	1.00	2.25	0.61	0.77	0.11	2.25	0.84	1

As with the wave speed, these pressure data were studied to determine which parameters affect the pressure magnitude, under the scope of the main variables considered for this study (*i.e.*, fuel, obstacle shape, blockage ratio, and obstacle distribution). A similar, simplified sensitivity analysis procedure to the one described for the speed subsection above was done for all the variables shown in Table 7 [50]. Figure 41 to Figure 44 show the graphical results of this analysis.

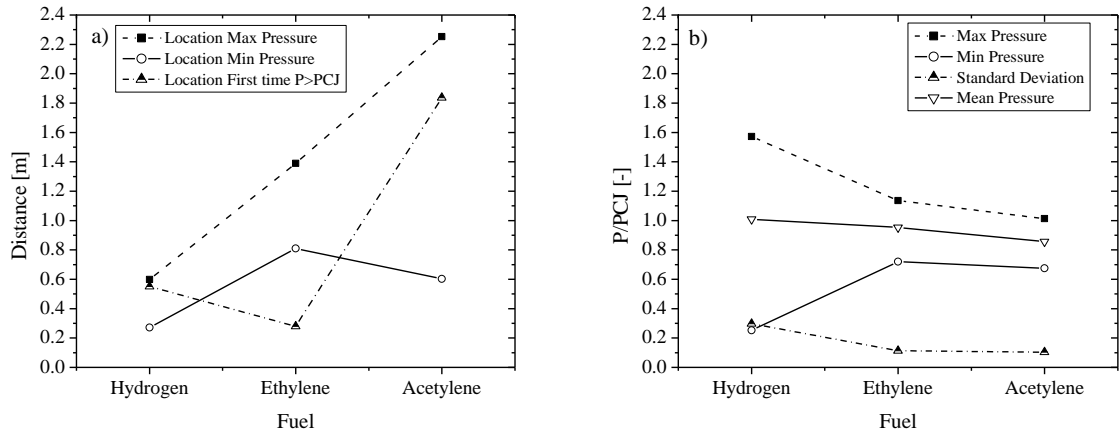


Figure 41. Sensitivity analysis for the pressure for different (a) location and (b) magnitude variables having fuel type as the parameter of interest.

Figure 41 shows the results obtained for the different fuels used in the experiments. As seen in Figure 41a, the fuel changes had a large effect on the locations of the various pressure variable, particularly for the maximum pressure and the location where $P > P_{CJ}$ for the first time. For instance, the maximum distance was obtained for acetylene-oxygen mixtures, and the minimum distance was observed for ethylene-oxygen systems, with a 1.4-m difference between the two. Additionally, the location of the maximum pressure is minimized for the hydrogen-oxygen mixture and maximized for the acetylene-oxygen case.

Figure 41b shows that the maximum pressure variable gave the largest value for hydrogen and the smallest value for acetylene. As for the minimum pressure, experiments with hydrogen reported the smallest pressures, while ethylene accounted for the largest values. The standard deviation and the mean pressure do not seem to be significantly affected by the fuels used in these experiments. In general, despite acetylene's high

reactivity, the presence of obstacles seems to reduce the pressure magnitude and, as expected, increase the flame acceleration process due to the increment in the turbulence and, consequently, reduce the run-up distance for the onset of the detonation.

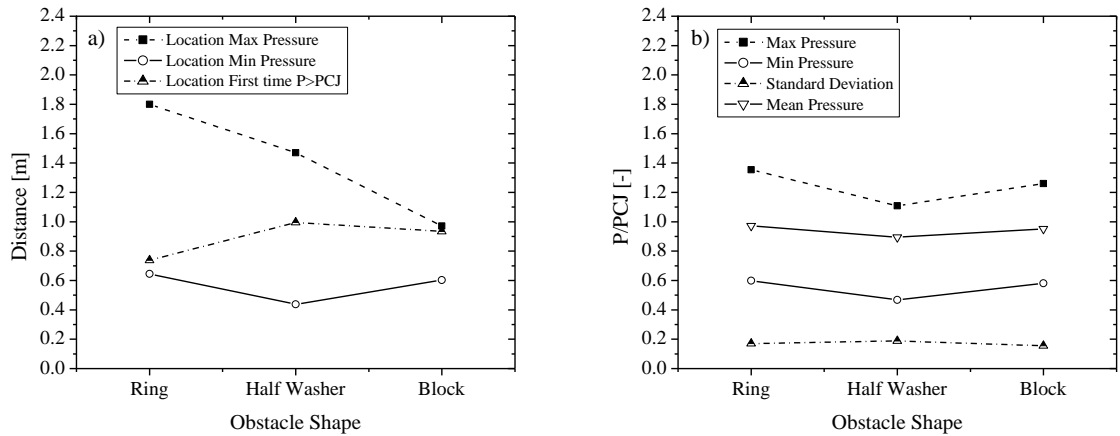


Figure 42. Sensitivity analysis for the pressure for different (a) location and (b) magnitude variables having the obstacle shape as the parameter of interest.

The effect that the different shapes of obstacles have on the pressure is shown in Figure 42. With regard to the pressure locations (Figure 42a), the location of maximum pressure is most influenced by the obstacle shape, while the other pressure-related distances are affected by obstacle shape to a lesser degree. As observed, the location of the maximum pressure is the greatest when the ring-shaped obstacles are used, and it is minimized for the block-shaped obstacles. A possible reason for this is that with the block-shaped obstacles, the flame has to fully divert to continue propagating. This diversion will enhance the creation of pockets of unburned and compressed mass that will be ignited via

shock interactions, leading to a localized auto explosion right after the obstacles. The first time the pressure exceeds the CJ pressure is also affected by the shape of the obstacle; however, it is not as significant as the maximum pressure location.

As for the standard deviation, the maximum, the minimum, and the mean pressures, the effect the obstacle shapes had on the pressure results were all similar. In general, there was no significant effect on the pressure magnitudes as a result of changes in the obstacle shape.

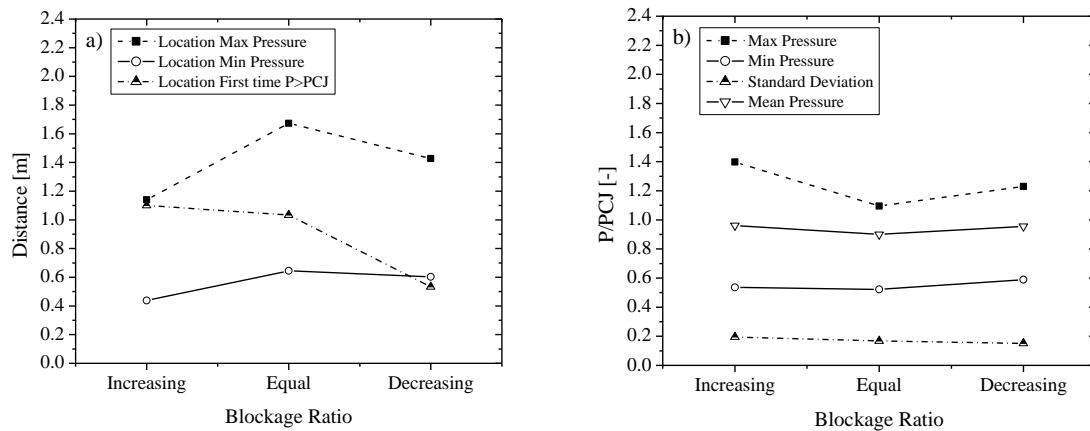


Figure 43. Sensitivity analysis for the pressure for different (a) location and (b) magnitude variables having the blockage ratio as the parameter of interest.

Figure 43 shows the pressure sensitivity results obtained for the different blockage ratio setups used in the experiments. From Figure 43a, the blockage ratio produced some significant changes in the location of the maximum pressure and where $P > P_{CJ}$ for the first time. In this case, the location of the first time in which the pressure exceeds the CJ

pressure is dependent on the blockage ratio setup, with the maximum distance occurring when the blockage ratio setup was “increasing”; the minimum distance was observed for the “decreasing” setup. Additionally, for the location of the maximum pressure the “increasing” blockage ratio setup gave the minimum distance, and this distance was the greatest when an “equal” blockage ratio setup was used. As for the other variables, the results show that there is no significant difference in the pressure magnitudes (Figure 43b) with the different blockage ratio setups.

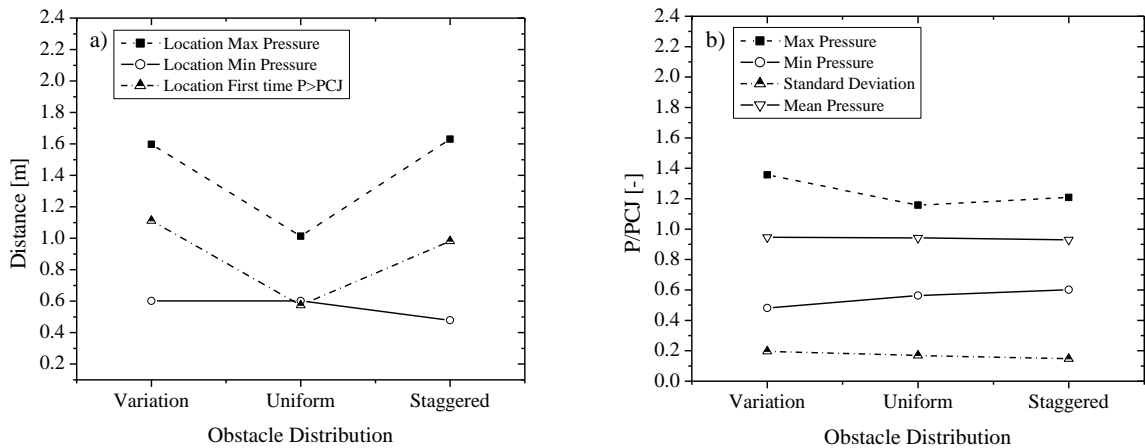


Figure 44. Sensitivity analysis for the pressure for different (a) location and (b) magnitude variables having the obstacle distribution as the parameter of interest.

As for the effect the obstacle distribution has on the pressure, Figure 44a indicates that the distance at which the pressure exceeds the CJ pressure for the first time and the location of the maximum pressure follow similar trends and are both influenced by the obstacle distribution. For instance, there is no significant difference between the

“variation” and “staggered” obstacle distribution; however, the “uniform” obstacle distribution shows a minimum for these distances. By observing the pressure effects given by the different obstacle distributions, it is again seen that there is no significant effect from the changing obstacle distributions (Figure 44b). Hence, the obstacle distribution does not affect the pressure magnitude.

Table 8. Ranking of experiment parameters for the various pressure response variables measured in the experiments.

Variables	Max Pressure	Location Max P [m]	Min Pressure	Location Min P [m]	Std Dev Pressure	Location first time P = PCJ [m]	Mean Pressure	No. Times P > 1
Fuel	1	1	1	1	1	1	1	1
Shape	3	2	2	2	4	4	2	2
BR	2	4	4	2	3	2	3	2
Distribution	4	3	3	3	2	3	4	3

The overall effect that each parameter has on the variables analyzed is ranked in Table 8. As with the velocity, the fuel type is the most important factor. The shape factor does not have a significant effect on the location at which the experimental pressure is equivalent to the CJ value for the first time; still, it is an important parameter that has a notable impact on the minimum pressure and, the location of the maximum and minimum pressures. On the other hand, the blockage ratio is a parameter that greatly affects the maximum pressure obtained in the experiments, the location at which the experimental pressure exceeds the CJ value for the first time and, the number of times that the pressure exceeds the CJ value. Finally, the obstacle distribution does not seem to have an overall

effect in the response of the selected variables. In general, it can be concluded that the importance of each parameter by analyzing the pressure responses can be organized as follows: 1) fuel, 2) blockage ratio, 3) obstacle shape and 4) obstacle distribution.

However, when looking at the ranking in Table 8, it is possible to determine that all the parameters have some effect on all the variables analyzed and there is no clear trend to determine that certain factor is more important than the other.

6.10.3. Summary

Not unexpectedly, the fuel type is the main parameter that affects both the pressure and the speed of the combustion process the most, both in terms of magnitude and location. However, the speed results show that the other variables, *i.e.*, obstacle shape, blockage ratio and obstacle distribution, affect the combustion process as well, but primarily in terms of the axial location. For instance, the run-up distance for the onset of the detonation was different for all the experiments. Table 9 shows the layouts of the experiments that maximized and minimized the run-up distance to trigger the detonation; in other words, the scenarios that presented the fastest and slowest flame acceleration, respectively.

Table 9. Maximum and minimum run-up distance scenarios.

	Maximum Run-up Distance Scenario	Minimum Run-up Distance Scenario
Fuel	Hydrogen	Acetylene
Obstacle Shape	Ring	Block
Blockage Ratio	Increasing	Decreasing
Obstacle Distribution	Variation	Staggered

The scenarios described in Table 9 show an experiment that has been completed in the design of experiment matrix (Table 2). The first experiment in the matrix consisted of a hydrogen-oxygen mixture with ring-shaped obstacles, an increasing blockage ratio, and a *variation* obstacle distribution. As for the minimum run-up distance, the layout describes Experiment 3 of the matrix. The only difference for this scenario is that in the matrix, the fuel used was hydrogen.

Additionally, the distance at which the detonation became stable at each experiment was another factor that was greatly affected by the configuration changes. In most of the experiments, the detonation stabilized within the first meter from the ignition source. The other variables analyzed in this study showed that there was no significant difference between the different parameters evaluated.

Furthermore, the pressure magnitude does not seem to be significantly affected by the other variables, *i.e.*, obstacle shape, blockage ratio, and obstacle distribution. However, the locations of the maximum and minimum pressures and the first time that the experimental pressure exceeds the CJ pressure are all greatly affected by the obstacle configuration. For instance, the configurations that gave the maximum and minimum values for the first time that the experimental pressure exceeds the CJ pressure are given in Table 10.

Table 10. Maximum and minimum distance when the experimental pressure exceeds the CJ pressure for the first time.

	Maximum Distance	Minimum Distance
Fuel	Acetylene	Ethylene
Obstacle Shape	Half washer	Ring
Blockage Ratio	Increasing	Decreasing
Obstacle Distribution	Variation	Uniform

From the statistical sensitivity analysis, it was possible to determine that the distance at which the detonation is triggered is affected by the parameters studied. However, the validity of these results had yet to be proven. To this end, the configurations that gave the maximum and minimum run-up distances were used, but in this case, it was imperative to consider all the fuels used in the study. By doing this, it was possible to determine that the overall tendency that was observed experimentally is independent of the fuel used in the experiments.

Additionally, comparing the experiments that had no obstruction with the tests that had obstructions, it was noticed that once the detonation is triggered in the congested section of the detonation tube, the pressure is adversely impacted and the velocity tends to remain constant and near the CJ value. This trend was observed for ethylene-oxygen and acetylene-oxygen mixtures. The authors believe that when the pressure wave interacts with the obstacle, a Mach-stem interacts with the flame, thus destabilizing the flame front. This leads to flame acceleration towards the unburned gas and a significant increase in the perturbations, which will ultimately add turbulence to the flame front via the Rayleigh-Markstein instability mechanism [19,60].

6.11. Validation

In order to determine if the experimental results obtained in the previous section are valid for different fuels, the configurations that gave the maximum and minimum run-up distances were used. However, in this case, all the proposed fuels in the matrix were used for each layout.

6.11.1. Maximum Run-up Distance Layout

In this case, the layout used consisted of ring-shaped obstacles with an increasing blockage ratio, and the obstacles are placed one, two, and three times the internal diameter (variation) of the detonation tube. As it is desirable, all the fuels used in the present study were tested. For instance, the first experiment in this matrix had the same layout and used hydrogen as the fuel. Figure 45 and Figure 46 show the experimental results obtained for this layout with ethylene and acetylene as the fuel, respectively.

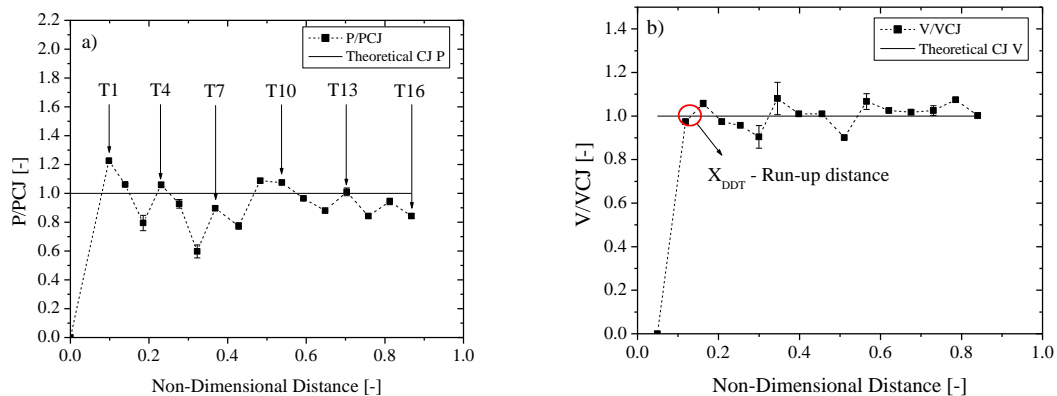


Figure 45. Results for the ethylene–oxygen mixture using the results for maximum run-up distance shown in Table 9.

As shown in Figure 45, the experimental results obtained for this layout are very different to the outcomes obtained for the ethylene-oxygen mixture experiments from the design of experiment matrix. For instance, the pressure reported at T1 and T2 are both above the CJ value, even at this early position. At T3, the pressure decays to approximately 0.8 times the CJ pressure, followed by a sudden increase in the pressure magnitude (above the CJ pressure at T4). At T5, the pressure magnitude decreases but remains relatively close to the CJ value. Once the combustion enters the uncongested region of the detonation tube, at T6, the pressure reaches its minimum (0.6 times the CJ value). After T9, the pressure reaches the CJ value and tends to fluctuate near this pressure.

As for the speed results, the velocity reported between T1 and T2 does not reach the CJ value. Between T2 and T3, the results show that the CJ speed is exceeded. In the obstructed section of the detonation tube, the velocity seems to decay progressively. However, as the detonation wave moves into the uncongested region of the tube, the velocity increases to values above the CJ speed with a deceleration of the detonation front between T9 and T10 and followed by the re-acceleration of the detonation wave. From then on, the velocity stabilizes near the CJ condition. The distance at which the onset of the detonation is observed is at 0.37 m away from the ignition source. Figure 46 shows the experimental results for the same layout, but with acetylene-oxygen mixtures.

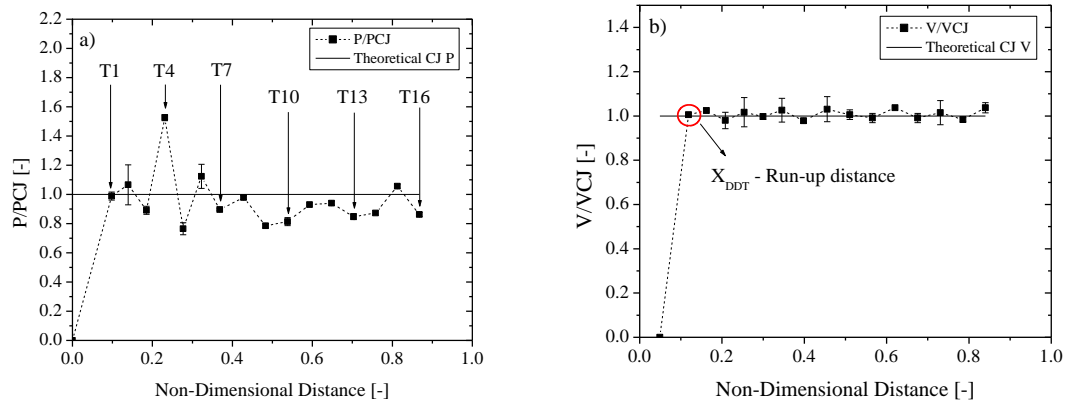


Figure 46. Results for the acetylene–oxygen mixture using the results for maximum run-up distance shown in Table 9.

As it can be observed in Figure 46, the experimental outcome obtained for both pressure and speed are completely different to the results obtained for the acetylene-oxygen mixture experiments from the design of experiment matrix. For instance, the pressure reported at T1 and T2 are above the CJ pressure. At T3, the pressure decays to approximately 0.9 times the CJ pressure. At T4, the pressure abruptly increases to nearly 1.5 times the CJ pressure. It is believed that a pocket of compressed mass is ignited; thus, an auto-explosion occurs between T3 and T4. At T5, a significant reduction in the pressure is observed. The reason for this behavior is that right after T5 a ring-shaped obstacle with an 80% blockage ratio is present; therefore, there is an excess of turbulence present at this point and the pressure is going to be significantly reduced. At T6, the detonation is already progressing into the uncongested section of the detonation tube; however, the pressure fluctuations in this scenario are significant and there is no sign that the pressure stabilizes throughout the experiment.

On the other hand, the speed results show a very rapid increase between T1 and T2. The speed reaches the CJ value and shows a tendency to stabilize near the CJ speed. As mentioned above, the run-up distance is the distance at which the onset of detonation due to DDT is observed [59]. In this case, the run-up distance is found at 0.33 m (between T1 and T2) from the ignition source.

In summary, the run-up distance for the fuel-oxygen mixtures in the detonation tube with ring-shaped obstacles, an increasing blockage ratio and a variation obstacle distribution are: a) $\text{H}_2\text{-O}_2$ is one meter, b) $\text{C}_2\text{H}_4\text{-O}_2$ is 0.43 m, and c) $\text{C}_2\text{H}_2\text{-O}_2$ is 0.39 m away from the ignition source. These results indicate that by utilizing the obstacle configuration that maximizes the run-up distance, the fuel-oxygen mixtures showed the expected behavior in which the distance at which the onset of the detonation is maximized with respect to the results shown in Table 5.

6.11.2. Minimum Run-up Distance Layout

The layout for this case consisted of block shape obstacles with a decreasing blockage ratio and the obstacles are spaced half the internal diameter of the detonation tube followed by a gap of three times the internal diameter of the detonation tube. This arrangement is made in three groups, each group consisting of three obstacles. This layout was utilized for the third experiment in the matrix developed for this study; however, the fuel used was hydrogen. Again, as for the maximum run-up distance layout, all the fuels in the matrix were used. Figure 47 and Figure 48 show the experimental results obtained for this layout with ethylene and acetylene as the fuel, respectively.

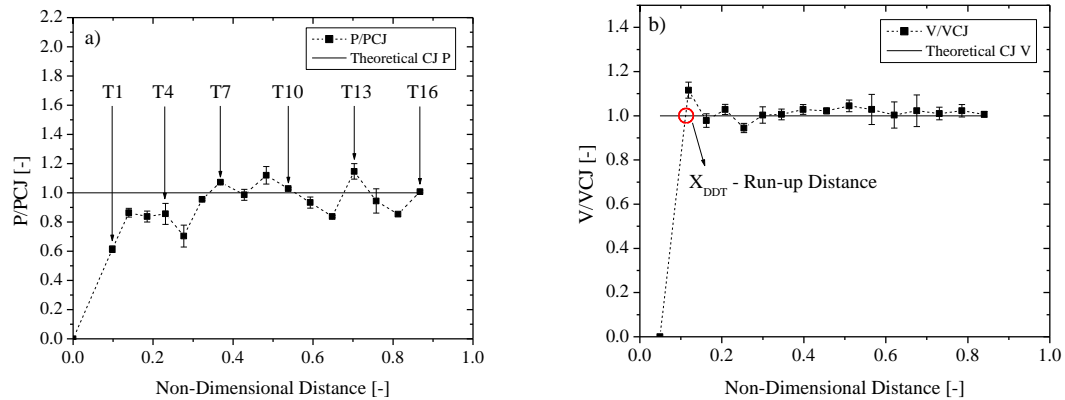


Figure 47. Results for the ethylene–oxygen mixture using the configuration for minimum run-up distance shown in Table 9.

The results shown in Figure 47 illustrate a different behavior compared to the experimental outcomes obtained in the tests established in the design of experiment matrix. For instance, with this layout the pressure does not exceed the CJ value until the combustion wave reaches the uncongested region of the detonation tube (at T6 and T7). At T1 the pressure reached is approximately 0.6 times the CJ value. From T2 to T4 the pressure stabilizes below the CJ value. At T5 a sudden decrease in the pressure magnitude is observed. This is followed by a rapid increase in the pressure as shown in T6 and T7. From then on the pressure fluctuates near the CJ value.

As for the speed results obtained for this layout, it is clear that the onset of detonation occurs between T1 and T2. As the combustion progresses into the obstructed region the velocity fluctuates near the CJ value and, actually shows a tendency to stabilize close to this value. As the detonation wave propagates into the uncongested region, the velocity shows a tendency to stabilize near the CJ speed; even though, in this case, some

of the values are above the CJ value. For this scenario, the estimated distance at which the onset of detonation occurs is at 0.30 m away from the ignition source.

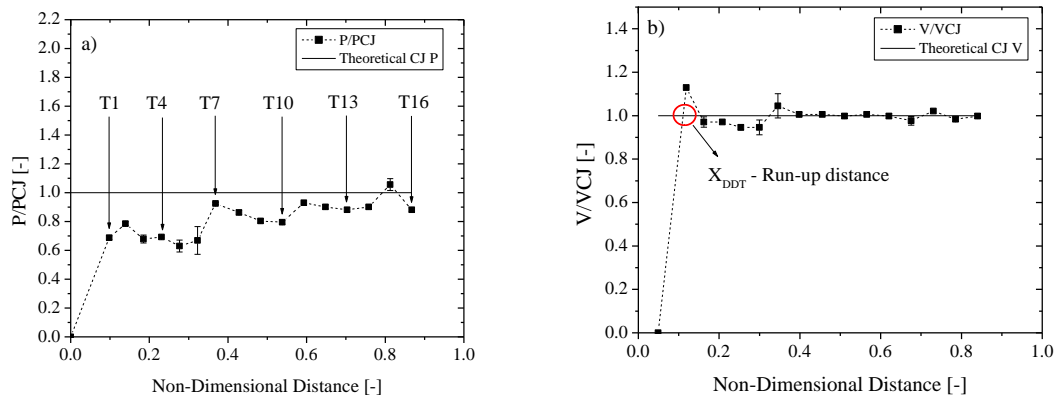


Figure 48. Results for acetylene–oxygen mixtures using the results for minimum run-up distance shown in Table 9.

As it can be observed in Figure 48, the experimental results obtained for the pressure and the speed show some similarities with the experimental outcomes obtained for the acetylene-oxygen mixture experiments from the design of experiment matrix. For instance, the pressure in the obstructed region in the detonation tube does not reach the CJ value; however, as the flame progresses into the uncongested section a significant increment in the pressure is observed (at T7). From then on, the pressure tends to stabilize below the CJ pressure, but at T11 there is a sudden increase. A tendency to stabilize below the CJ value is observed again; however, at T15 the pressure increases and exceeds the CJ pressure and is followed by an immediate decrease. In this experiment, the pressure does

not seem to stabilize; however, as the combustion moves into the uncongested section, an increasing tendency followed by a small decrease in the pressure is observed.

As for the speed, the velocity describes an overdriven detonation between T1 and T2. The speed magnitude decreases to a velocity slightly below the CJ value. While the combustion is propagating in the obstructed region of the detonation tube, the velocity shows a stabilization tendency, below the CJ speed. As the combustion moves into the uncongested section of the detonation tube, an overdriven explosion is observed (at T7). From then on, negligible fluctuations in the velocity magnitude are observed. In other words, the detonation stabilizes at approximately T8. In this case, the run-up distance for the onset of the detonation is between T1 and T2, more specifically at 0.30 m away from the ignition source.

In summary, the run-up distance for the fuel-oxygen mixtures in the detonation tube with block-shaped obstacles, a decreasing blockage ratio and a staggered obstacle distribution are: a) $\text{H}_2\text{-O}_2$ is 0.38 m, b) $\text{C}_2\text{H}_4\text{-O}_2$ is 0.38 m, and c) $\text{C}_2\text{H}_2\text{-O}_2$ is 0.37 m away from the ignition source. These results indicate that by utilizing the obstacle configuration that minimizes the run-up distance, the fuel-oxygen mixtures showed the expected behavior in which the distance at which the onset of the detonation is minimized with respect to the experimental results shown in Table 5.

6.12. Conclusions

As initially shown in this paper, with the current facility and data acquisition system, the experimental results obtained show a high repeatability, signifying that there was very little variation from the data. Once this was verified, the next step consisted of

the selection of the fuel. The criteria for the fuel selection was that the fuel-oxygen mixture was capable of detonating with no obstructions or if previous experiments with obstructions carried out at this facility showed a deflagration-to-detonation transition behavior. It was proven that hydrogen-oxygen mixtures with an equivalence ratio of 1.0 are able to detonate in a 2.77-m long and 3.86-cm internal diameter detonation tube. This result was validated with published data by Kuznetsov *et al.*, [52] on the detonation cell size for hydrogen-oxygen mixtures and the $D > 13\lambda$ criterion. Additionally, ethylene-oxygen and acetylene-oxygen mixtures showed that they are capable of undergoing a DDT in the smooth detonation tube. Nonetheless, this was also verified with data on the detonation cell size for these mixtures and an $\phi = 1.0$ [55,58].

Further on, an L9 design of experiments matrix based on Taguchi methods was proposed. With this matrix, it was possible to determine the effect that the non-uniform distribution of obstacles has on the combustion process. The experimental results showed in this thesis suggest that the non-uniform distribution of obstacles affect the flame acceleration and, consequently, the distance at which the onset of detonation is obtained. Additionally, the way the obstacles are placed in the detonation tube have little effect on the pressure magnitude and velocity of the detonation and the general propagation of the detonation wave throughout the detonation tube. These tests were performed with a wide range of obstacle geometries and configurations, and the experimental data suggest that the trials are extremely repeatable.

This thesis also demonstrates which layouts maximize or minimize the flame acceleration mechanism. For instance, the scenarios that present an increasing blockage

ratio (as described in this thesis), along the path of the combustion front will tend to maximize the run-up distance for the onset of DDT. On the other hand, when a decreasing blockage ratio configuration is utilized, this distance is minimized. This result indicates that the obstacle configuration does influence the timing and the location of the flame acceleration mechanism and, consequently, the features of the detonation, including the run-up distance.

7. DEFLAGRATION-TO-DETONATION TRANSITION (DDT): PREDICTING DDT IN HYDROCARBON-AIR MIXTURE EXPLOSIONS WITH DATA AVAILABLE FROM THE LITERATURE*

Deflagration to detonation transitions can possibly lead to explosion consequences orders of magnitude higher than their deflagration counterparts due to the severe overpressure associated with detonations, and more importantly, due to the potential contribution of the energy associated with flammable cloud outside of the congested and confined regions. For example, investigations have concluded that DDTs did indeed occur during the recent incidents of Buncefield [46], Sunrise Propane [61] and Jaipur [62]. Recent reports of the 2012 explosion at the Venezuela oil refinery have also hypothesized that a DDT had indeed occurred. These recent incidents further enforce the need to identify under what circumstances DDTs can occur in petrochemical and process facilities, and more importantly, what potential layout modifications or mitigation measures can be employed to help achieve an “inherently” safer design of a given facility.

Over the past couple of years, the development of 3D Computational Fluid Dynamics (CFD) models allows to study in detail the interaction between physical/chemical processes and geometry. FLACS has been focusing on explosion modelling since 1980. This has allowed the inclusion of several concepts, such as the

* This section has been reproduced with permission from “C. Rosas, S. Davis, D. Engel, P. Middha, K. Van Wingerden, M.S. Mannan. Deflagration to detonation transitions (DDTs): Predicting DDTs in hydrocarbon explosions, *Journal of Loss Prevention in the Process Industries*, Volume 30, July 2014, Pages 263-274, ISSN 0950-4230, <http://dx.doi.org/10.1016/j.jlp.2014.03.003>.” Copyright 2014, Elsevier

“distributed porosity” which allows to combine efficiency and accuracy when simulating dispersion and explosions in complex scenarios [63]. Additionally, FLACS has been extensively validated against hundreds of large-scale experiments, see for example [64].

Previous work has focused on the development of CFD models that accurately predict the conditions of the combustion process once DDT has been reached, *i.e.*, detonation wave speed, overpressure and run-up distance, considering incomplete combustion, allowing the formation of more by-products to the reaction; all which consequently increase the computational time to obtain a solution. However, these models have focused on simple systems, *i.e.*, detonation tubes, [65-67], and have not been applied to large-scale tests. In addition, these models do not simulate the deflagration, nor under what conditions the deflagration will transition to detonation.

FLACS is the only CFD code in widespread use that was specifically designed to evaluate the consequences of explosions in the oil and gas industry, which in recent years have included evaluating the likelihood of a given explosion scenario transitioning to a detonation (DDT). FLACS has been extensively applied for safety studies on petrochemical facilities, and has even been used to understand the causes of major incidents (see Figure 49). While, FLACS has been successfully validated and applied to numerous flammable gas release and explosion problems, it is imperative to extend its validation against experimental data involving DDTs in small, medium and large-scale tests; hence resulting in a more robust tool that accurately predicts whether or not DDTs can occur in real world scenarios.

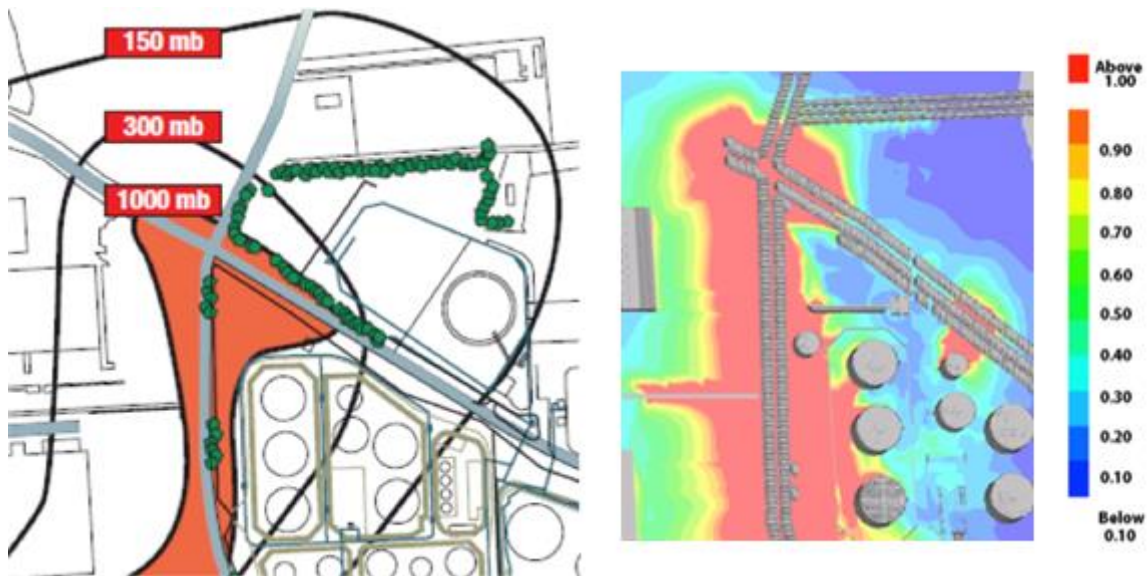


Figure 49. Estimated explosion overpressures based on blast damage (left) [46] and predicted using FLACS (right) for the Buncefield fuel storage depot explosion.

This section discusses the efforts to expand CFD predictions to include the prediction of deflagration to detonation transitions for various fuels including hydrogen, ethylene, propane and natural gas. The work is currently ongoing and includes validation against experiments conducted in a variety of configurations including: (1) closed pipes with obstacles; (2) other congested lab-scale geometries; (3) medium to large-scale 3-D obstacle configurations; and (4) large-scale geometries where DDT occurred upon flame propagation from confined to more open configurations. The results of a select body of experiments are presented next.

7.1. FLACS Background

FLACS utilizes the finite volume method to solve the compressible Reynolds-Averaged Navier-Stokes (RANS) equations on a 3D Cartesian grid [63]. Additionally, the

constants defined by Launder and Spalding (1974) [68] are used in the k - ϵ turbulence model. FLACS uses the flamelet-based combustion model with a one-step reaction kinetics. In this case, the laminar burning velocity determines how reactive a mixture is. An important characteristic of FLACS is that uses a sub-grid model capable to determine how the flame interacts with objects that are smaller than the grid size, allowing a more accurate description of the flame-object interaction [69]. The “distributed porosity” concept [70] allows to define the different objects by using a Cartesian grid, in which large objects are represented on-grid, while smaller objects are represented in the sub-grid.

The current commercial version of FLACS is capable of predicting fast deflagrations. However, it is not capable of predicting the DDT phenomenon. FLACS can accurately predict the behavior of a deflagration by allowing the combustion products to heat and ignite the unburned gas ahead of the flame front. The presence of obstacles creates turbulence and increases the flame speed and, consequently, the overpressures increase as well. If the flame accelerates to the point where transition to detonation is achieved (approximately 1,500-2,000 m/s flame speed), the combustion process changes and ignition of the gas occurs by means of shock wave propagation, rather than flame propagation. This new mechanism involves different physical phenomena whose governing equations are not presently included in FLACS [22].

Due to the potentially severe consequences of DDTs at petrochemical facilities, the capabilities of FLACS have been extended to include estimating the likelihood of having a DDT and the region where the onset of detonation is triggered. The likelihood of

DDT is expressed in terms of a non-dimensional spatial pressure gradient across the flame front ($DPDX$) [22].

$$DPDX = \left. \frac{dP}{dx} \right|_{Normalized} = \left. \frac{dP}{dx} \right|_{Actual} \frac{X_{CV}}{P_0} \quad (15)$$

Where P_0 is the initial pressure and X_{CV} represents the grid resolution. The $DPDX$ parameter allows one to establish when the reaction front captures the shock front, which is one of the main indicators of transition to detonation. This parameter has been extensively tested against hydrogen DDT experiments [22], and a set of criteria has been established to identify the likelihood of having a DDT in hydrogen-air mixtures:

- $DPDX < 0.5$: No DDT
- $0.5 < DPDX < 1.0$: DDT begins to be possible
- $1 < DPDX < 5$: DDT is possible
- $5 < DPDX < 10$: DDT is likely

However, when predicting the likelihood of DDT, this criterion should not be the only parameter considered. There are many variables that can affect DDT, such as geometry dimensions, initial pressure and temperature. Preliminary models have been implemented in FLACS comparing geometric sizes to experimentally determine detonation cell sizes. This is useful for small geometries as it has been proven to predict the occurrence of DDT. More specifically, a DDT Length Scale (DDTLS) variable is used to compare the geometric length scale (LSLIM) for a specific scenario with the detonation cell size (λ), which is an intrinsic parameter of the fuel-oxidizer region:

$$DDTLS = \frac{LSLIM}{\lambda} \quad (16)$$

It has been proposed that when DDTLS is equal to or greater than 7 the detonation front will propagate within obstructed tubes. For smooth tubes, it has been observed that when DDTLS is equal to 1 the propagation of the detonation front occurs.

7.2. Selection of Scenarios

This current project includes the comparisons against experimental data obtained in both confined geometries that are closed at one end and open at the other as well as those that are unconfined and open. For the selection of scenarios, an extensive literature review of previous experiments was performed [12-14,17,71-76]. Several experiments were identified; however, at this stage it was desirable to have experiments that contained as much data as possible for validation purposes. This not only allowed for more comparisons with the simulation results, but also helped to more accurately determine the run-up distances necessary to obtain detonations in both the experiments and simulations.

Depending on the mixture composition, the initial pressure and temperature conditions, the geometric configuration and, most importantly, the physical size (or scale) of the reactive system, flame accelerations that lead to detonations may or may not occur. The positive feedback mechanisms involving flame propagation and turbulence, which lead to flame accelerations and detonations, can substantially differ for very confined systems, like detonation tubes, and those for completely open yet highly congested (obstacle density) systems. Therefore, for the purpose of this section, two types of experiments were selected: (1) completely confined with both ends closed geometry and (2) a completely unconfined open geometry.

A confined geometry was selected to determine whether or not FLACS is able to account for flame accelerations and detonations under these types of tests, *i.e.*, detonation tubes, and establish general guidelines for determining the likelihood of DDT. The experiments described by Peraldi *et al.* (1988) [36] were utilized in the present study. In these experiments, the effect that uniform blockage ratio along the tube had on the transition to detonation was evaluated for various hydrocarbons at different concentrations. An additional advantage of this data set is that it comprised an extensive range of reactivity for the fuels studied, including those of high reactivity (hydrogen, acetylene, ethylene) and those with more moderate reactivity (propane and methane).

The second set of experiments included a much larger scale test series that was completely unconfined. Here the tests performed by BP/Shell/HSL [77] were simulated. These tests evaluated the flame acceleration and transition to detonation within a highly congested, unconfined test geometry. The tests were conducted by varying the equivalence ratio of the flammable mixture for both hydrogen and ethylene mixtures. These two vastly different experimental configurations were chosen for the validation to ensure that FLACS could not only accurately predict DDT under these conditions, but be applied to more realistic facilities.

Table 11 summarizes the experiments simulated and compared against FLACS calculations. This section highlights the preliminary results of some of the experiments. The following section describes the results of the two experiments chosen. It is worth mentioning that the highlighted experiments are going to be discussed in the following subsections.

Table 11. Summary of the scenarios simulated in FLACS.

Geometry	Author	Scale	Fuel	Comparison Parameters
Confined	Teodorczyk <i>et al.</i> [78]	<i>S</i>	H ₂	Average flame speed, DDT (yes/no)
	Blanchard <i>et al.</i> [44]	<i>L</i>	H ₂	Run-up distance, overpressure for ignition at 0.4 m, DDT (yes/no)
	Peraldi <i>et al.</i> [36]	<i>L</i>	H ₂ , C ₂ H ₂ , C ₂ H ₄ , C ₃ H ₈ and CH ₄	Average flame speed, DDT (yes/no)
	Kuznetsov <i>et al.</i> [79]	<i>L</i>	CH ₄	Flame speed, DDT (yes/no)
Unconfined	Kessler <i>et al.</i> [66]	<i>L</i>	CH ₄	DDT (yes/no)
	BP & HSL [77]	<i>L</i>	H ₂ , C ₂ H ₄	DDT (yes/no)
	Baker Risk [80]	<i>L</i>	C ₂ H ₄	DDT (yes/no)
	MERGE [81]	<i>L</i>	CH ₄ , C ₃ H ₈ , C ₂ H ₄	Overpressure, DDT (yes/no)
	Buncefield [46]	<i>L</i>	C ₃ H ₈	DDT (yes/no)
	Moen <i>et al.</i> (1982) [82]	<i>L</i>	CH ₄	Overpressure, DDT (yes/no)
	Mackay <i>et al.</i> [83]	<i>L</i>	C ₂ H ₂ , C ₂ H ₄ , C ₃ H ₈	Overpressure at the end of the tube, DDT (yes/no)
	Moen <i>et al.</i> (1985) [84]	<i>L</i>	C ₂ H ₂	DDT (yes/no)

S stands for small scale and *L* for large scale.

7.3. Results and Discussion

7.3.1. Confined Geometries

Peraldi *et al.* (1988) [36] defined criteria for transition to detonation in tubes. They concluded that in order to achieve DDT, the flame speed, prior the onset of detonation, has to be of the order of the speed of sound of the combustion products. Moreover, when dealing with ring-shaped obstacles, the ratio between the detonation cell size and the ring

orifice should be equal to or less than 1 ($\lambda/d \leq 1$). Additionally, localized auto explosions are required for transition to detonation to occur.

This study was performed in an 18 m long circular pipe with internal diameters of 0.05, 0.15 and 0.30 m. Experiments were conducted with various substances at different concentrations. Table 12 summarizes the experiments that were simulated.

Table 12. Experiments performed by Peraldi *et al.* [36].

Internal diameter (ID) [m]	Substance	ϕ [-]	CJ Pressure [bar]	DDT experimentally
0.15	C ₂ H ₂	0.5	13.64	Yes
	C ₂ H ₄	0.675	15.18	Yes
	C ₂ H ₄	2.235	17.67	Yes
	C ₃ H ₈	0.8	16.35	Yes
	C ₃ H ₈	1.38	18.48	Yes
	CH ₄	1	17.04	No
	H ₂	0.524	11.94	Yes
	H ₂	3.16	12.41	Yes
0.3	C ₂ H ₂	0.433	12.4	Yes
	C ₂ H ₄	0.56	13.52	Yes
	C ₂ H ₄	2.43	17.2	Yes
	C ₃ H ₈	0.71	15.23	Yes
	C ₃ H ₈	1.32	18.67	Yes
	CH ₄	1	17.04	No
	H ₂	0.455	11.06	Yes
	H ₂	3.58	11.85	Yes

Peraldi *et al.* (1988) [36] reported that there was DDT in all the experiments shown in Table 12 with the exception of both experiments that involved methane as the fuel.

Now, using the same methodology suggested above, it was found that FLACS was able to predict that DDT was going to occur in most of the experiments; however, using

the criteria used for hydrogen, FLACS did not predict DDT for rich ethylene. It is important to mention that the maximum overpressure predicted by FLACS in these cases was very close to the CJ pressure value (ID 0.3 - C₂H₄, $\phi = 2.43$). The results obtained from the simulations are summarized in Table 13.

Table 13. Summary of results from the simulations.

Internal diameter (ID) [m]	Substance	ϕ [-]	Maximum Pressure [barg]	Maximum <i>DPDX</i> [-]	DDT Prediction
0.15	C ₂ H ₂	0.5	20.62	9.62	Yes
	C ₂ H ₄	0.675	28.87	Greater than 10	Yes
	C ₂ H ₄	2.235	15.40	4.78	Possible
	C ₃ H ₈	0.8	28.93	Greater than 10	Yes
	C ₃ H ₈	1.38	23.81	7.34	Yes
	CH ₄	1	28.08	8.83	Yes
	H ₂	0.524	26.09	Greater than 10	Yes
	H ₂	3.16	32.60	Greater than 10	Yes
0.3	C ₂ H ₂	0.433	14.36	3.95	Yes
	C ₂ H ₄	0.56	14.90	4.11	Yes
	C ₂ H ₄	2.43	17.02	2.20	No
	C ₃ H ₈	0.71	16.39	5.36	Yes
	C ₃ H ₈	1.32	45.20	Greater than 10	Yes
	CH ₄	1	30.26	Greater than 10	Yes
	H ₂	0.455	29.61	Greater than 10	Yes
	H ₂	3.58	55.45	Greater than 10	Yes

It is worth mentioning that most of the DDT predictions by FLACS occurred near the end of the tube (see Figure 50 and Figure 51), with the exception of hydrogen. As it can be observed in Figure 52 and Figure 53, hydrogen presented a transition to detonation near where ignition occurred. Furthermore, it can be observed in Figure 51 and Figure 53 that obstacles not only play a very important role in flame acceleration, but also can contribute to localized explosions that can trigger DDT. In fact, these figures show that the *DPDX* variable locally increases to values greater than one near the top of many obstacles. This signifies that, as expected, obstacles increase the likelihood of DDT, which is also captured by FLACS.

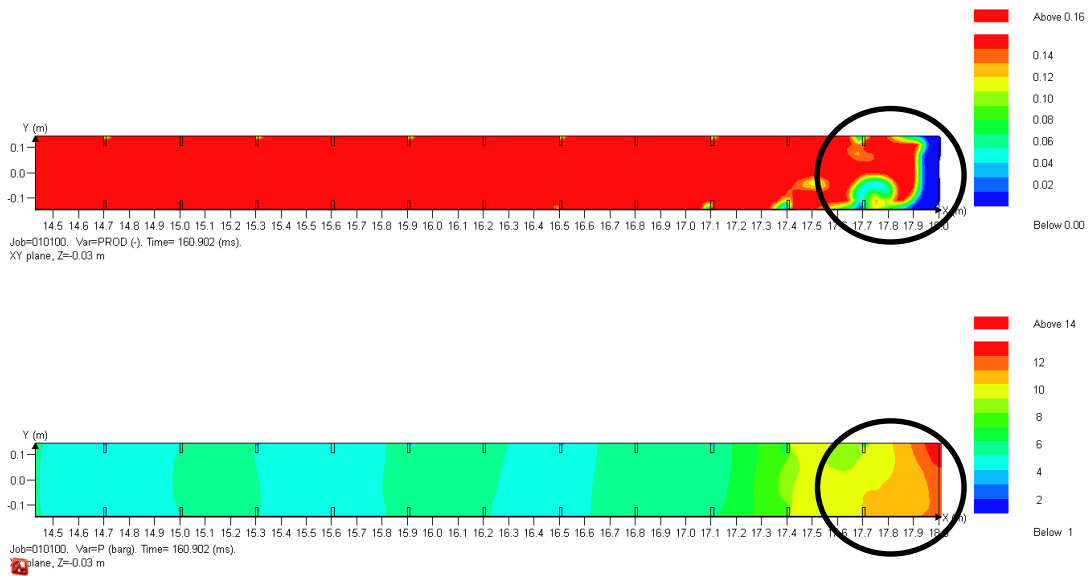


Figure 50. Flame front (top) and shock front (bottom) snapshots e (ID 0.3 – C₂H₄, $\phi = 0.56$) at 160.9 ms. Note that the flame front (interface between the red and blue in the top image) has reached the exit of the shock tube as well as the associated shock front (pressures > 12 barg locally) in the bottom image.

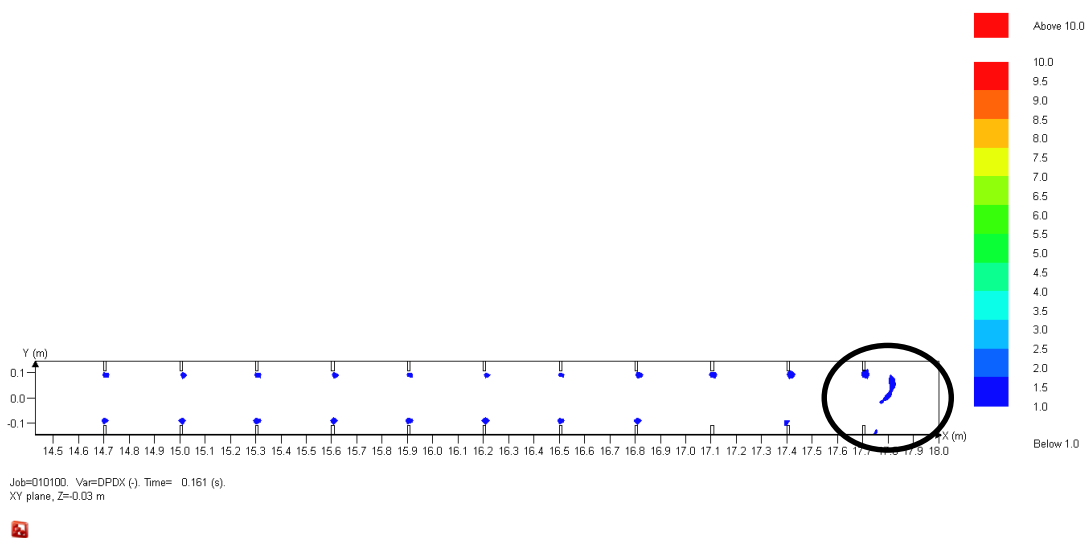


Figure 51. DPDX snapshot e (ID 0.3 – C₂H₄, $\phi = 0.56$) at 160.9 ms. Note that the lower threshold value for DPDX (dark blue) is given as 1.

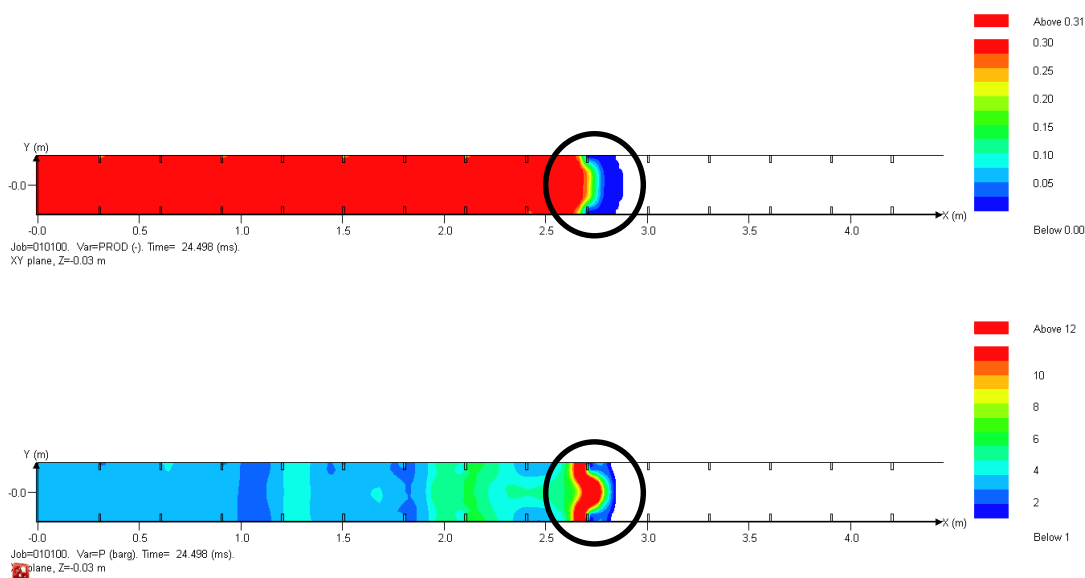


Figure 52. Flame front (Top) and Shock front (Bottom) snapshots - (ID 0.3 – H₂, $\phi = 3.58$) at ~24.5 ms. Note that the flame front (interface between the red and blue in the Top image) has reached approximately 2.7 m from end of the shock tube as well as the associated shock front (pressures >10 barg locally) in the bottom image.

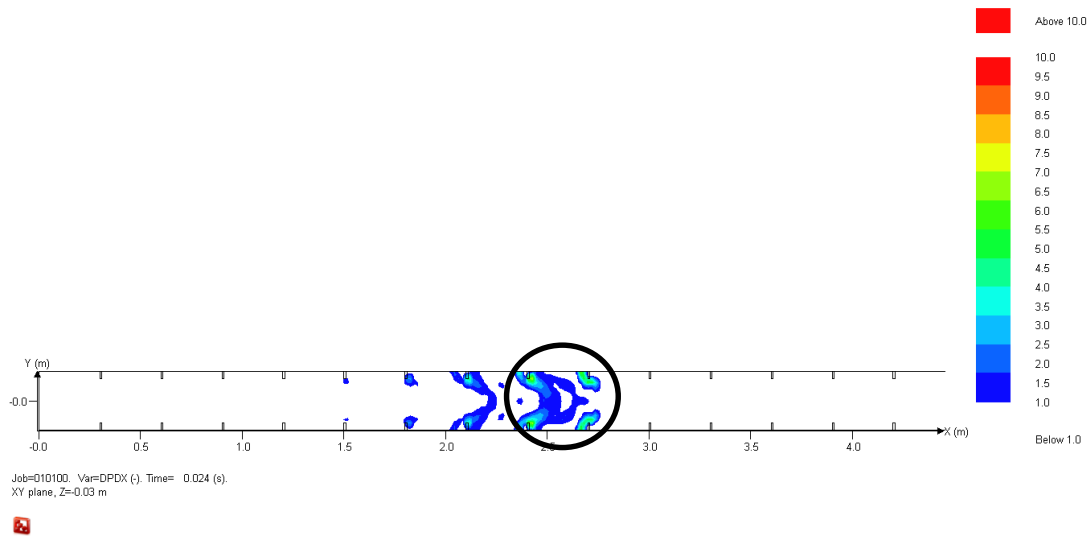


Figure 53. DPDX snapshot e (ID 0.3 – H₂, $\phi = 3.58$) at ~ 24.5 ms. Note that the lower threshold value for DPDX (dark blue) is given as 1. The image shows that a detonation is likely (*e.g.*, DPDX > 5).

The experiments also evaluated the onset of detonations versus the reactivity of the fuel. For instance, it is clear that hydrogen is easier to detonate than the other fuels used in the experiments due to its high reactivity. This is the main reason why hydrogen undergoes DDT in shorter run-up distances, *i.e.*, closer to the ignition point. It was also observed that methane, a lower reactivity fuel, did not result in detonations in the experiments evaluated. Based on the simulation results, it is clear that FLACS considers the reactivity of the different fuels.

For instance, it was also observed that methane, being a very difficult fuel to detonate, presented an overpressure greater than the CJ pressure; however, this occurred at the very end of the pipe and this could be due to either shock reflections or shock interactions. Still, based on the current guidance in FLACS simulations there is a potential

for DDT to occur in this configuration despite it not being observed in the experiments. The behavior observed in the simulations for the various fuels was as expected. For example, propane, acetylene and ethylene were not as difficult to transition to detonation as methane, yet the observed run-up distance to obtain detonation for these fuels was also much larger than that for hydrogen. In these cases, the maximum overpressures at the location of DDT were greater than the CJ pressure and *DPDX* fulfilled the proposed criteria for DDT to be considered likely.

7.3.2. Unconfined, Open Geometries

Shell/BP/HSL performed a series of experiments in a 3 m width, 3 m depth and 2 m height rig [77]. The rig was divided in two levels. The first one consisted of concentric vertical pipes and the second level contained horizontal pipes. Moreover, two different densities of obstacles were used, 4 and 7 rows of pipes in both levels. The two different layouts as represented in FLACS are shown in Figure 54 [77]. In general, it is expected to be more difficult to achieve DDT in the geometry with 4 rows of pipes than that with 7 rows of pipes, due to the decreased congestion density in 4 row setup.

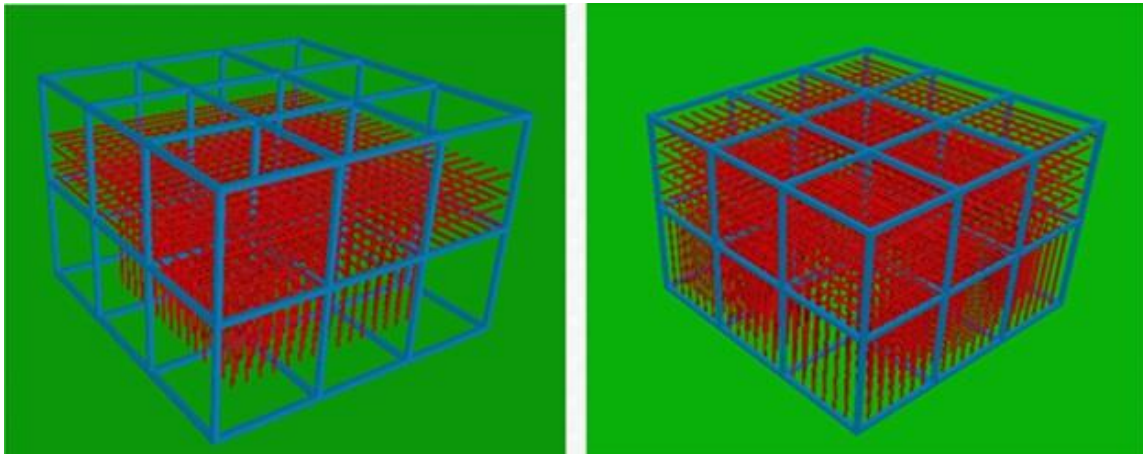


Figure 54. Layouts of the scenarios used by BP for their experiments (left 4 rows of pipes configuration and right 7 rows of pipes configuration). Adapted from [77].

Additionally, they performed experiments with hydrogen and ethylene with equivalence ratios ranging from 0.8 and 1.7 for each substance. For the purpose of this work, the scenarios with an equivalence ratio of 0.8, 1.0, 1.2, 1.4, 1.6 and 1.7 were simulated for both configurations. The simulations showed that none of the ethylene scenarios (both the 4 row and 7 row layouts) produced elevated overpressures and the *DPDX* values were below 0.5. This means that DDT is not expected to occur. Figure 55 and Figure 56 illustrate the results obtained for ethylene ($\phi = 1.0$) for both configurations. As can be observed, the maximum overpressure in both configurations is well below 1 barg and there is no indication of DDT ($DPDX < 0.5$). This leads to a conclusion that the dominant phenomenon is a deflagration with very low overpressure values, similar to what was observed in the experiments.

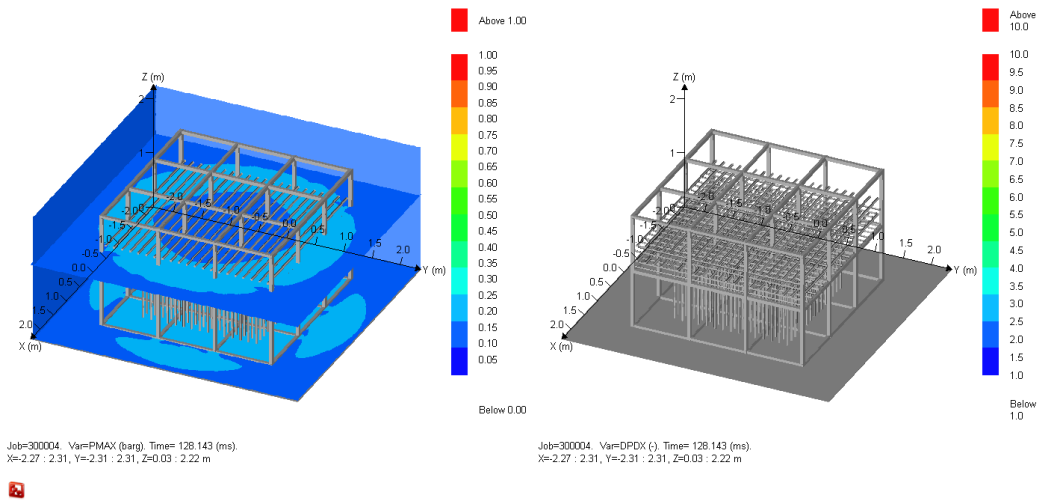


Figure 55. PMAX (Left) and DPDX (Right) snapshots - (4 rows of pipes configuration – C_2H_4 , $\phi = 1.0$) at ~129 ms. Note the pressures were observed to be less than 0.4 barg and no DDT was observed (DPDX < 1).

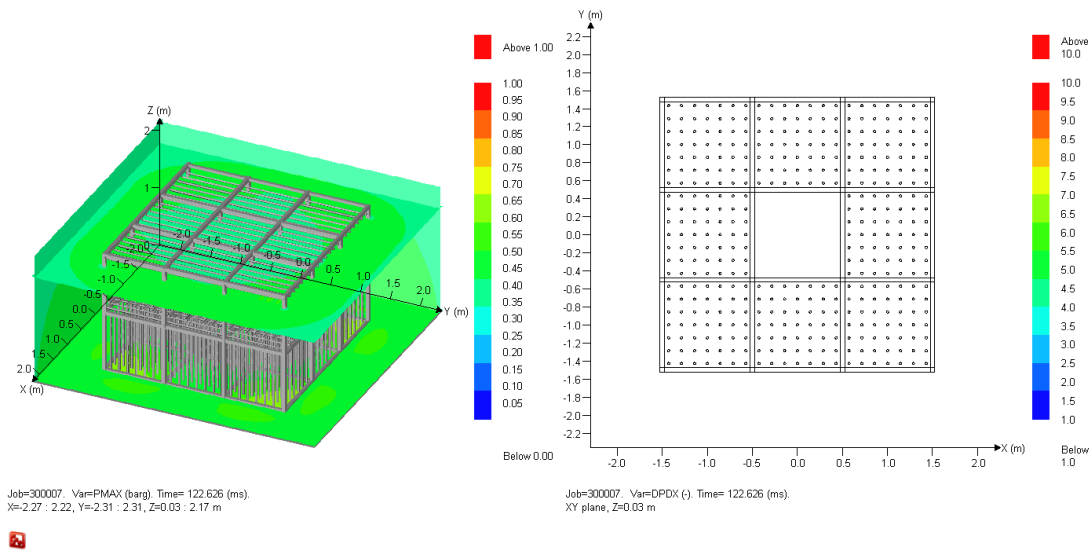


Figure 56. PMAX (Left) and DPDX (Right) snapshots - (7 rows of pipes configuration – C_2H_4 , $\phi = 1.0$) at ~123 ms. Note the pressures were observed to be less than 0.7 barg and no DDT was observed (DPDX < 1).

The simulations involving hydrogen were similar to those of ethylene for the geometry with 4 rows of pipes (*e.g.*, no evidence of DDT as shown in Figure 57 through Figure 61). More specifically, the obtained overpressures were below the hydrogen CJ pressure at the respective concentration and the values obtained for *DPDX* were small (generally less than one within the geometry). This signifies that a fast deflagration was the more likely scenario obtained in the performed simulations. Moreover, it was observed that the maximum overpressure was recorded at the end of the last row of horizontal pipes. When the equivalence ratio was 0.8, the maximum overpressure attained was the highest among all the cases. This suggests that as the mixture gets richer in hydrogen it will be more difficult to achieve DDT.

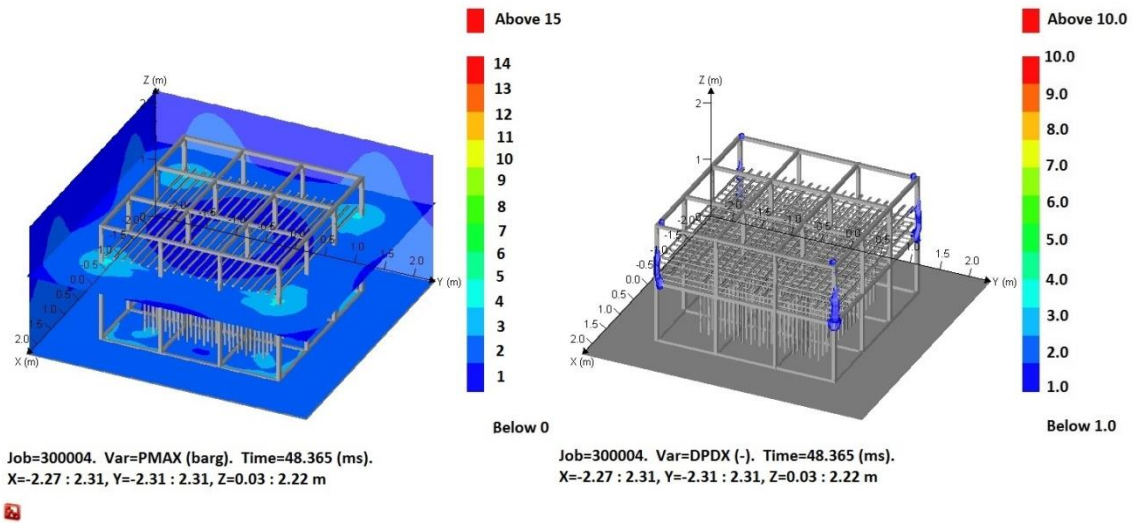


Figure 57. PMAX (Left) and *DPDX* (Right) snapshots - (4 rows of pipes configuration – H₂, $\phi = 0.8$) at ~48 ms. Note the pressures were observed to be less than 4 barg and no DDT was observed within the geometry (*DPDX* < 1).

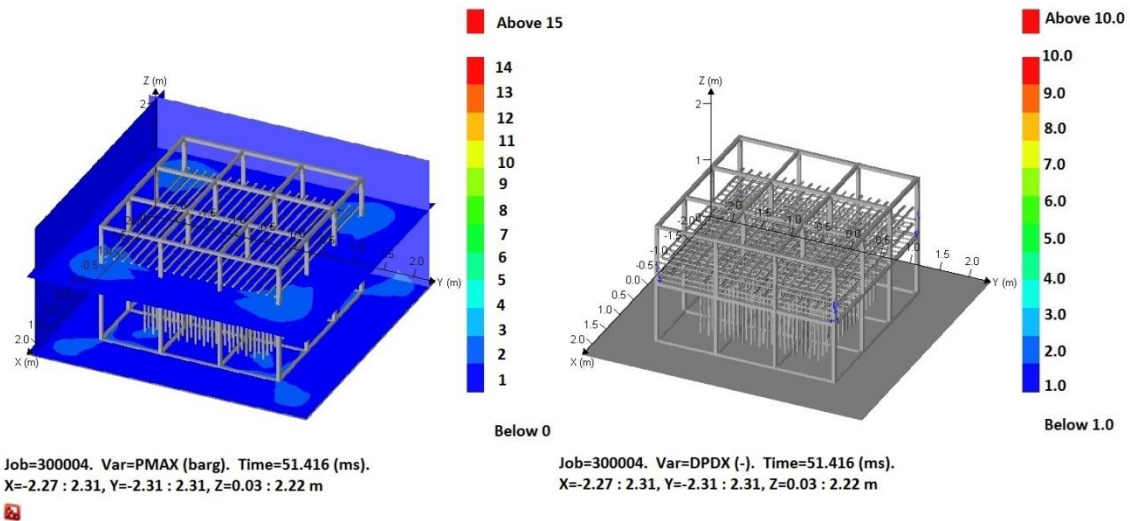


Figure 58. PMAX (Left) and DPDX (Right) snapshots - (4 rows of pipes configuration – H_2 , $\phi = 1.0$) at ~51 ms. Note the pressures were observed to be less than 3 barg and no DDT was observed within the geometry (DPDX < 1).

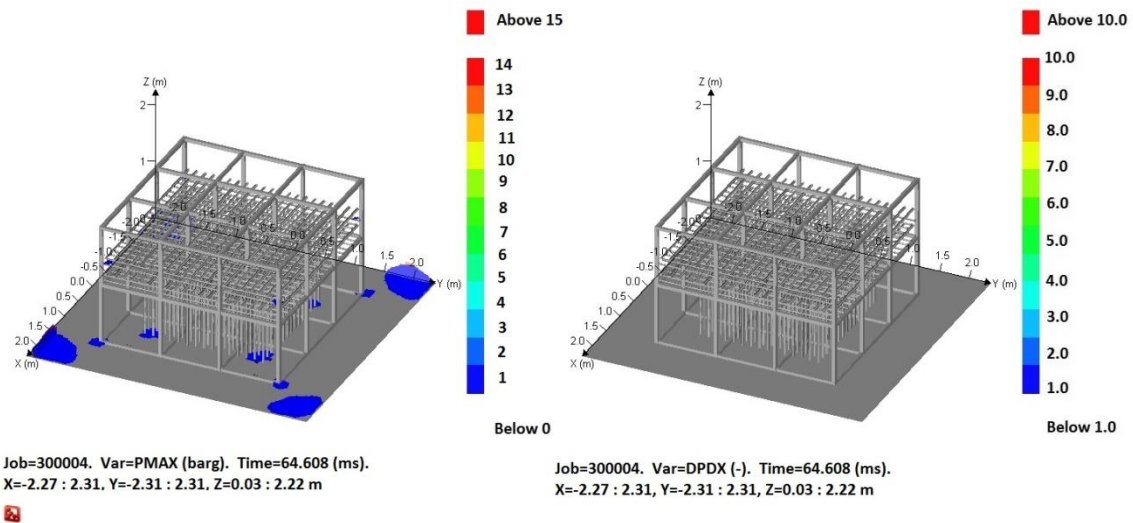


Figure 59. PMAX (Left) and DPDX (Right) snapshots - (4 rows of pipes configuration – H_2 , $\phi = 1.2$) at ~65 ms. Note the pressures were observed to be less than 2 barg and no DDT was observed within the geometry (DPDX < 1).

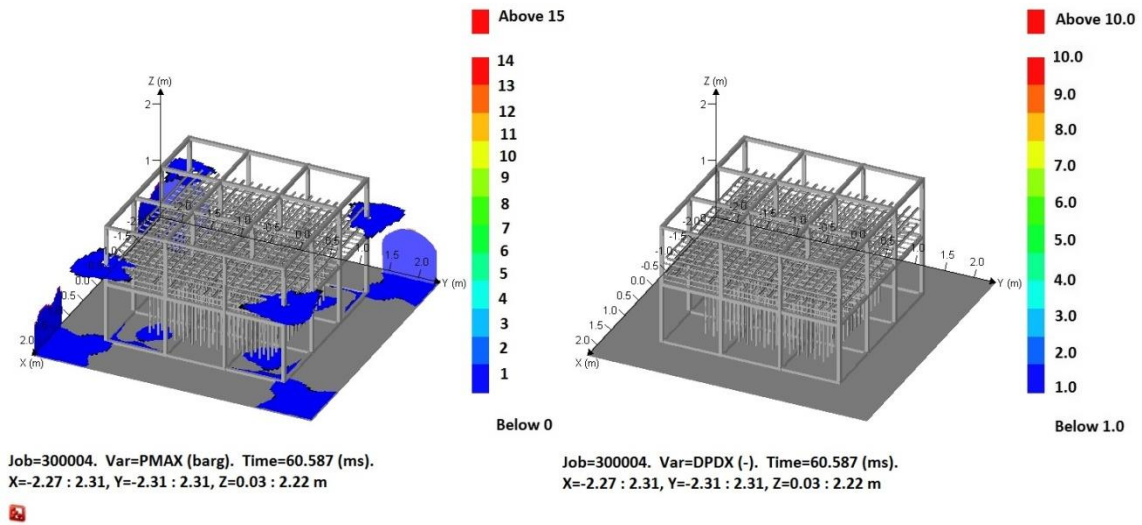


Figure 60. PMAX (Left) and *DPDX* (Right) snapshots - (4 rows of pipes configuration – H_2 , $\phi = 1.6$) at ~61 ms. Note the pressures were observed to be less than 2 barg and no DDT was observed within the geometry (*DPDX* < 1).

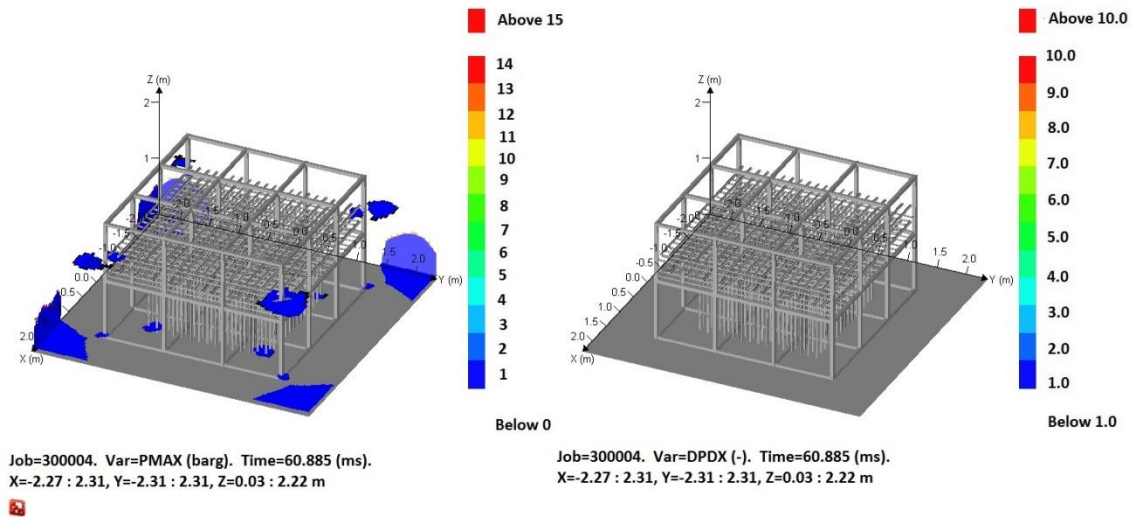


Figure 61. PMAX (Left) and *DPDX* (Right) snapshots - (4 rows of pipes configuration – H_2 , $\phi = 1.7$) at ~61 ms. Note the pressures were observed to be less than 2 barg and no DDT was observed within the geometry (*DPDX* < 1).

In contrast, the simulations involving hydrogen for the geometry with 7 rows of pipes showed that DDT was likely. In this configuration, very high overpressures were achieved, even greater than the corresponding CJ pressure for hydrogen at the specified concentrations. Table 14 summarizes the theoretical CJ pressure for hydrogen at different equivalence ratios.

Table 14. CJ pressure for different concentrations of hydrogen.

ϕ [-]	CJ pressure [bar]
0.8	14.5
1.0	15.4
1.2	15.6
1.4	15.3
1.6	15.0
1.7	14.8

Moreover, *DPDX* in all cases has values of 10 and even greater. This signifies that in most cases DDT should be expected. As is shown in Figure 62 – Figure 66, the maximum values of overpressure and *DPDX* are found at the corners of the rig. Moreover, the richer the mixture is in hydrogen, the smaller is the section where the higher overpressure was recorded.

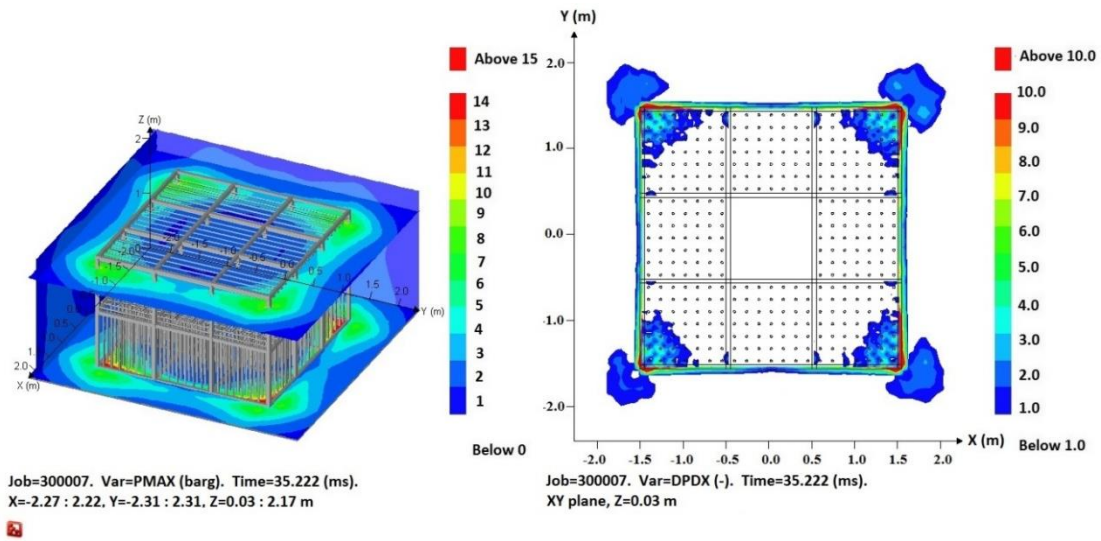


Figure 62. PMAX (Left) and DPDX (Right) snapshots - (7 rows of pipes configuration – H₂, $\phi = 0.8$) at ~35 ms. Note the pressures were observed to be greater than 14 barg and DDT is likely to occur (DPDX > 10).

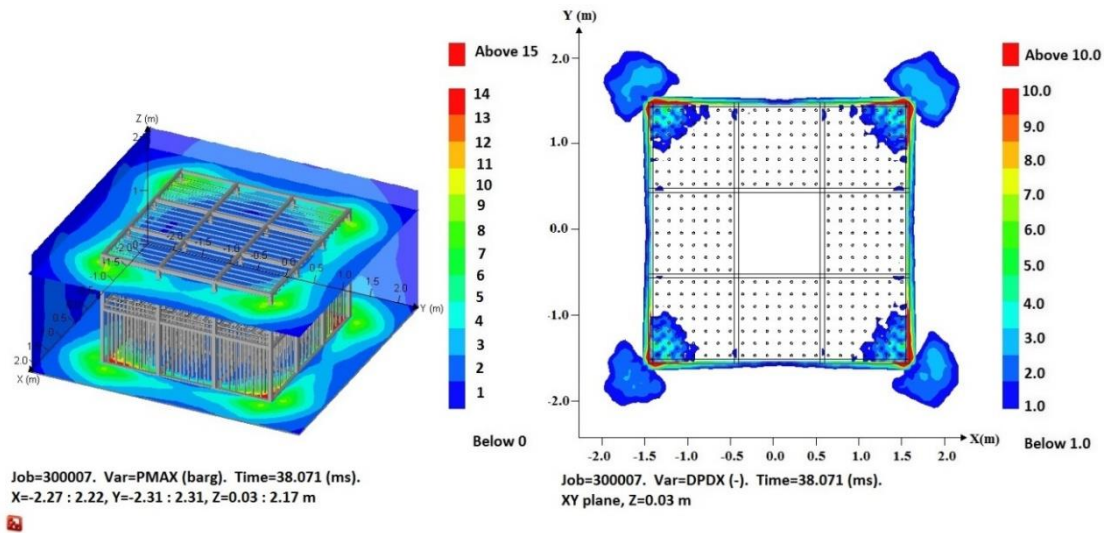


Figure 63. PMAX (Left) and DPDX (Right) snapshots - (7 rows of pipes configuration – H₂, $\phi = 1.0$) at ~38 ms. Note the pressures were observed to be greater than 10 barg and DDT is likely to occur (DPDX > 10).

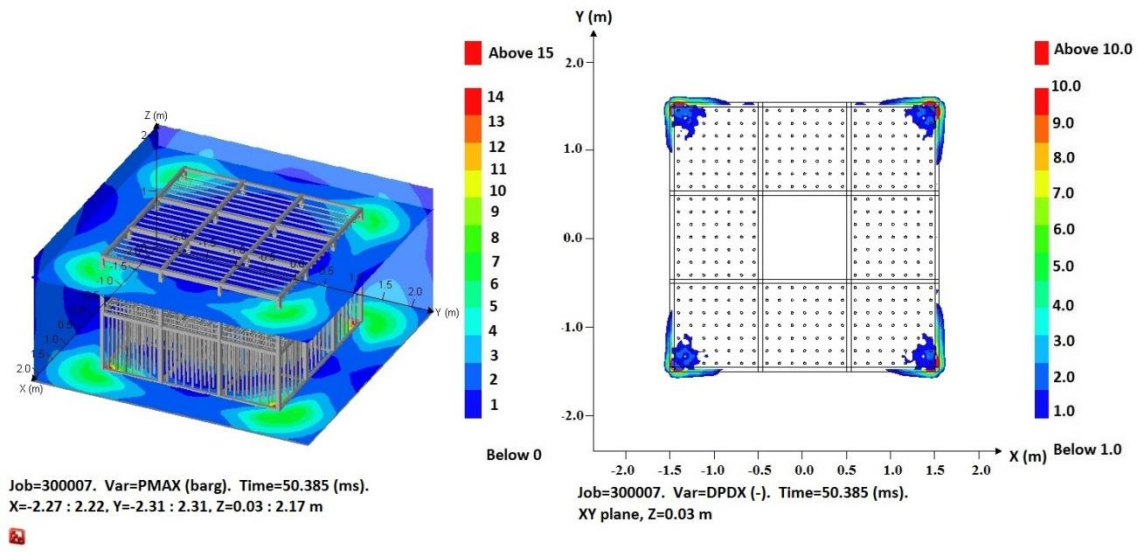


Figure 64. PMAX (Left) and *DPDX* (Right) snapshots - (7 rows of pipes configuration – H₂, $\phi = 1.2$) at ~50 ms. Note the pressures were observed to be greater than 10 barg and DDT is likely to occur (*DPDX* > 10).

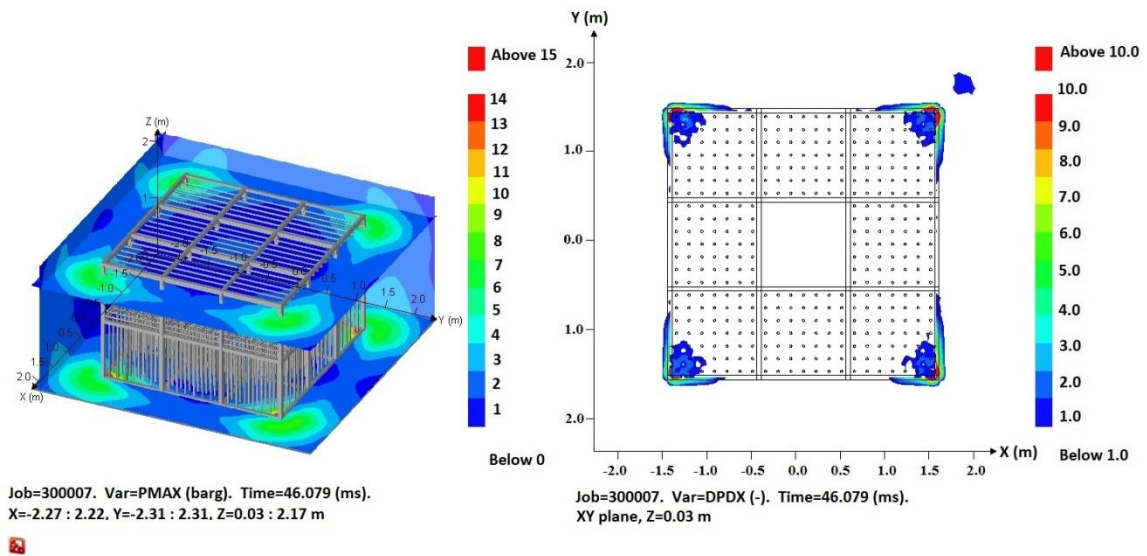


Figure 65. PMAX (Left) and *DPDX* (Right) snapshots - (7 rows of pipes configuration – H₂, $\phi = 1.6$) at ~46 ms. Note the pressures were observed to be greater than 10 barg and DDT is likely to occur (*DPDX* > 10).

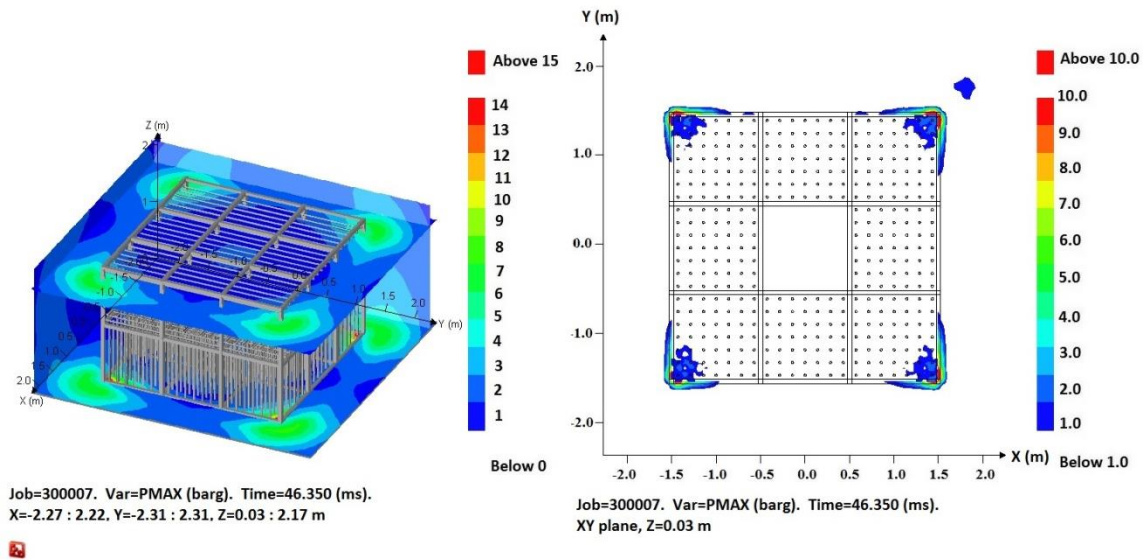


Figure 66. PMAX (Left) and *DPDX* (Right) snapshots - (7 rows of pipes configuration – H₂, $\phi = 1.7$) at ~46 ms. Note the pressures were observed to be greater than 9 barg and DDT is likely to occur (*DPDX* > 10).

Applying the same methodology proposed at the beginning of this section, it is possible to conclude that DDT occurs only for the configuration with 7 rows of pipes and hydrogen as the fuel. The other scenarios are not going to result in a transition from deflagration to detonation, mainly because there is not enough turbulence generated in the scenario or due to the intrinsic properties of the fuel. Experimentally, a similar behavior was reported, where DDT occurred in the scenario that had more level of obstruction, *i.e.*, 7 pipe configuration, with hydrogen as the fuel. Figure 67 compares the experimental and simulated overpressures for one of the hydrogen tests in the 4 rows of pipe configuration.

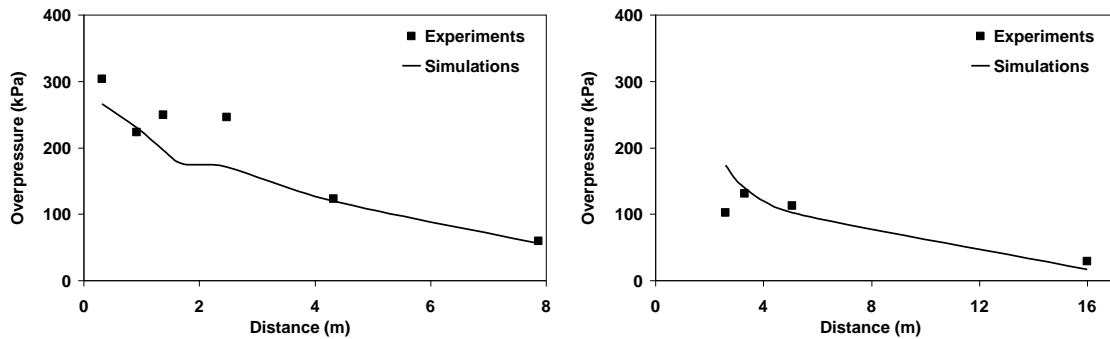


Figure 67. Overpressure for measurements parallel (left) and perpendicular (right) to wall 4 rows of pipes configuration – H_2 , $\phi = 1$).

7.4. Summary

This section presented preliminary work to expand the CFD models in FLACS to include the prediction of deflagration to detonation transitions for various fuels including hydrogen, ethylene, propane and natural gas. The work is currently ongoing and includes validation against experiments conducted in a variety of configurations including: (1) closed pipes with obstacles; (2) other congested lab-scale geometries; (3) medium to large-scale 3-D obstacle configurations; and (4) large-scale geometries where DDT occurred upon flame propagation from confined to more open configurations. It is worth mentioning that the current version of FLACS resolves the flame acceleration mechanisms leading to fast deflagrations; however, the detonation module is still not included. Consequently, ignition of the flammable gas ahead of the flame occurs by flame propagation and not by shock ignition. This means that the model is limited to predicting the onset of detonation and cannot predict the correct speed of the propagating detonation front. However, this work should lead to improved guidance on the likelihood of DDT when using FLACS.

Future research on this area should focus on the development of a detonation module that interacts together with the current FLACS flame acceleration module. This will enable one to predict not only the onset of DDT phenomena, but also the detonation front itself.

8. DEFLAGRATION-TO-DETONATION TRANSITION (DDT): PREDICTING DDT IN FUEL-OXYGEN SYSTEMS USING EXPERIMENTAL DATA

8.1. Methodology

As the validation of a model is an ongoing effort, in this section a new methodology is proposed. Although the model does not represent a detonation *per se*, it is capable of predicting how likely it is to obtain DDT in a particular scenario and indicates the regions where this might occur by calculating the non-dimensional spatial pressure gradient across the flame front (DPDX):

$$DPDX = \left. \frac{dP}{dx} \right|_{Normalized} = \left. \frac{dP}{dx} \right|_{Actual} \frac{X_{CV}}{P_0} \quad (17)$$

This DPDX parameter allows the determination of when the flame front catches up to the pressure front which, in general, is one of the main characteristics of a transition to detonation [22,23]. The following list provides the criteria for which were initially developed by Middha and Hansen [22] and expanded by Rosas, *et al.* [23]:

- $DPDX < 0.5$: No DDT
- $0.5 < DPDX < 1.0$: DDT begins to be possible
- $1 < DPDX < 5$: DDT is possible
- $5 < DPDX < 10$: DDT is likely

After the simulation is completed, a detailed “grid-by-grid” analysis was performed by examining the DPDX results. To consider the place at which the onset of the detonation took place, the DPDX has to be greater than five and be present

continuously over 20 cells. Once the specific place and time have been identified, the simulation is re-run to dump the simulation at the desired time. As the simulation results are dumped, then, the constant flame velocity is modified in the setup file to the CJ velocity and the simulation is re-run from that specific time (the time at which the simulation was dumped). The code that has to be introduced to modify the burning velocity is:

\$SETUP

KEYS="PS1=01"

COMBUSTION_MODEL = "BETA3 BURN=2748"

\$END

In this example, the burning velocity is fixed to a constant value of 2,748 m/s. It is worth mentioning that the fuels selected in the experimental section present no difficulty in reaching a detonation; therefore, the modification of the flame velocity in the simulations was performed towards the initial stages of the combustion process, at the location at which the criteria have been fulfilled.

The simulations performed were based on the experimental layout and the design of experiments illustrated in the Experimental section.

8.2. Simulation Results

In this section, the simulation results obtained from FLACS are presented. As a new methodology is being introduced a comparison between the experimental results, the results obtained with no modification in the flame velocity and the results in which the flame velocity was modified to the CJ velocity are shown. Additionally, the DPDX

outcome for each simulation is shown and discussed. With this information, it is possible to establish when and how likely is the detonation to occur. In this work, the run-up distance is referred to the distance at which the onset of detonation due to DDT is observed [59] unless otherwise noted. It is worth mentioning that the experimental results presented in the following sub-sections refer to the first maximum pressure obtained experimentally.

8.2.1. Scenario 1

Experimentally, in this scenario, the run-up distance was achieved at one meter away from the ignition source. Figure 68 shows the DPDX results obtained to determine the location at which the onset of detonation is expected.

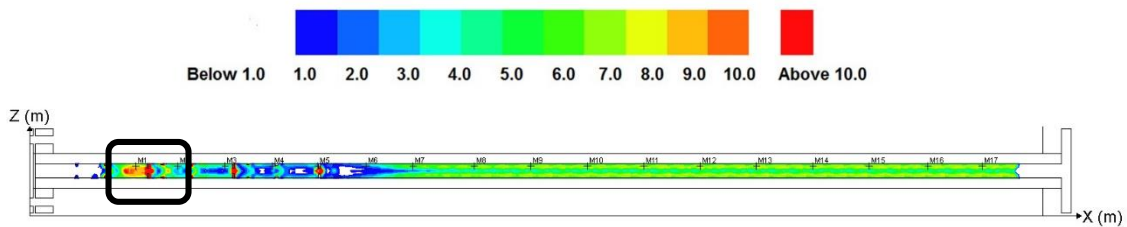


Figure 68. DPDX profile obtained using ring-shaped obstacles with an increasing blockage ratio and a “variation” obstacle distribution – Previous the modification of the flame velocity.

As can be observed in Figure 68, between the first and second monitor points, the DPDX value is greater than five and it remains like this for an extended section of the detonation tube (more than 20 cells). This high value means that it is very likely to have the onset of the detonation between T1 and T2 (between 0.4 and 0.5 meters away from the ignition source). However, as the combustion wave progresses, further into the congested

region, the DPDX variable decays to values below one, which means that the detonation is unlikely to occur. For instance, the presence of obstacles with high blockage ratio (80%), forces the DPDX estimations to increase to values greater than five right before the obstacle, due to an excessive generation of turbulence at that location and to wave interactions; however, after the combustion surpasses such obstacle, the DPDX decays to predict that is less likely to have a detonation at that point. As the combustion propagates into the uncongested region of the detonation tube, at T7, high DPDX values are obtained.

The preceding observations suggest that there is an initial attempt for the onset of the detonation, but it fails and, according to the results obtained in FLACS, a secondary effort for an onset of the detonation occurs toward the seventh monitor point (located at approximately 1.02 m away from the ignition source). This behavior was observed experimentally as well. For instance, the experimental results suggest that the detonation was obtained between the first two pressure transducers; however, due to the obstacle's layout the detonation failed to sustain and it was reinitiated right after the obstructed region, between T6 and T7.

After having modified the flame velocity to the CJ velocity of the hydrogen–oxygen mixture with an initial pressure of 20 kPa (2747 m/s), a new DPDX outcome is obtained. This is shown in Figure 69.

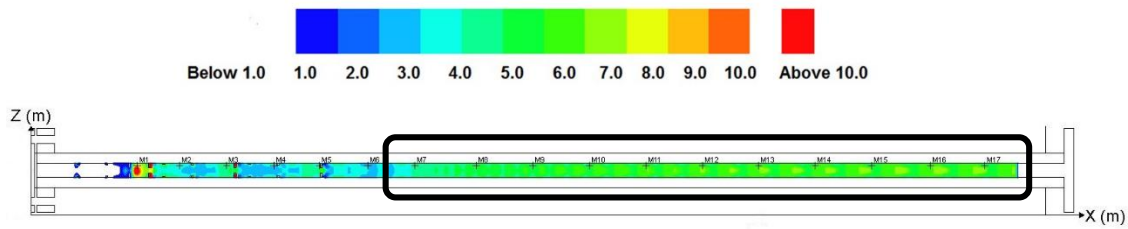


Figure 69. DPDX profile obtained using ring-shaped obstacles with an increasing blockage ratio and a “variation” obstacle distribution – After the modification of the flame velocity.

Figure 69 shows that there is a high likelihood to have the onset of detonation at T1; however, the DPDX estimations decay to values below five right after the obstacle. This means that the onset of detonation does not occur at that point, but it does further down the detonation tube (between T7 and T8 – at approximately 1.10 m away from the ignition point). Figure 70 shows the comparison between the experimental and the simulation results before and after the modification of the flame velocity.

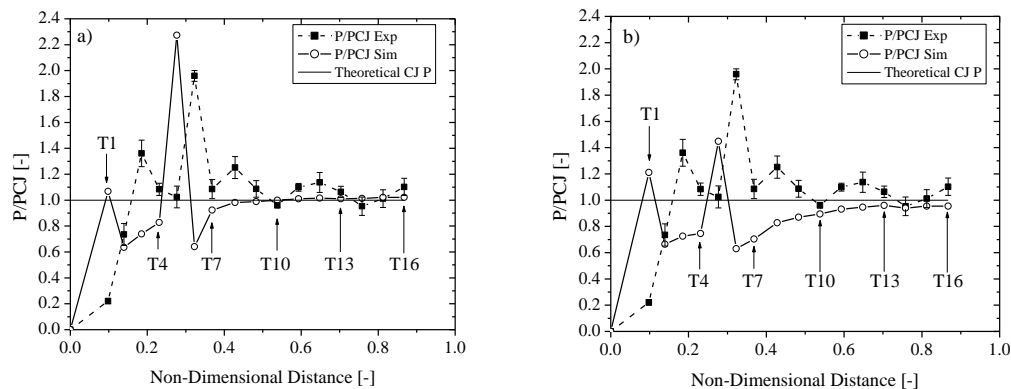


Figure 70. Comparison between the experimental and the simulation results for Scenario 1 – H_2 - O_2 mixtures with ring-shaped obstacles, an increasing BR, and a variation obstacle distribution. a) prior modification of the flame velocity, b) after the modification of the flame velocity.

As can be observed in Figure 70a, the initial stages of the explosion, in which a deflagration was observed experimentally, the simulation gives a similar tendency, with the exception of the pressure estimated at T1, in which FLACS calculates a pressure above the CJ value. At T2, the pressure computed by FLACS, shows a slight underprediction. At T3 FLACS significantly underpredicts the pressure. However, the pressure magnitude calculated by FLACS seems to follow the experimental trend, in which there is a pressure increase between T2 and T3. At T4, the experimental pressure shows a decay in the pressure magnitude, but FLACS does not capture this. On the contrary, it shows an increase in the calculated pressure. At T5, FLACS estimates a pressure approximately 2.2 times the CJ value. This is followed by a significant reduction in the pressure magnitude (nearly 0.6 times the CJ pressure). From then on, the results given by FLACS show a tendency to stabilize near the CJ pressure, similar to the experimental results.

Figure 70b shows the comparison between the experimental and the simulation (after the flame velocity was modified) results. In general, the calculated pressures by FLACS present a similar trend to that of the pressure results when the flame velocity was not modified (Figure 70a). However, when the estimated pressure exceeded the CJ value, the pressure magnitude was affected. For instance, the pressure reported by FLACS at T1 is approximately 1.2 times the CJ pressure (greater than the 1.1 times the CJ value reported when the flame velocity was not modified) and at T5 the pressure calculated is 1.45 times the CJ value (smaller than the 2.2 times the CJ pressure estimated by FLACS when the flame velocity was not modified). Another important difference between the results shown in Figure 70a and Figure 70b is that the overall tendency for the pressure to stabilize which,

for the case at which the flame velocity was modified, occurs below the CJ value. These results illustrate that FLACS is capable of estimating pressures above the CJ value even though its tendency is to replicate the behavior of a fast deflagration.

8.2.2. Scenario 2

Experimentally, in this scenario, the onset of the detonation occurred at 0.64 m away from the ignition source. Figure 71 shows the DPDX results obtained to determine the location at which the onset of detonation is expected.

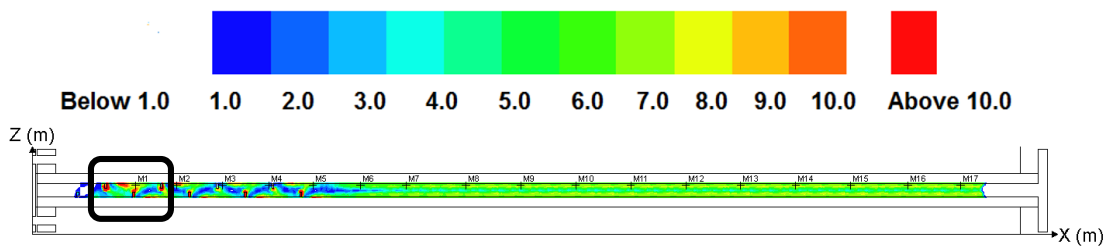


Figure 71. DPDX profile obtained using half-washer-shaped obstacles with an equal blockage ratio and a “uniform” obstacle distribution – Previous the modification of the flame velocity.

Figure 71 shows the DPDX variable with very high values (greater than five) for an extended section of the detonation tube (more than 20 cells) before the first pressure transducer. In this particular case, the DPDX variable is more noticeable and uniform throughout all the detonation tube. The obstacle’s layout provides a turbulence enhancement and forces the combustion wave to progress following a zig-zag trend; therefore, high DPDX values are expected. In this case, as the obstacles had the same blockage ratio (40%). This implies that there is no full obstruction of the flow of the flame,

as in the first scenario. Consequently, it seems that the detonation is more stable throughout the detonation tube, even in the obstructed region. As the combustion propagates into the uncongested section of the detonation tube, the DPDX variable starts to show a more uniform pattern which seems to describe an already stable detonation.

After having modified the flame velocity to the CJ velocity of the hydrogen–oxygen mixture with an initial pressure of 20 kPa (2747 m/s), a new DPDX outcome is obtained. This is shown in Figure 72.

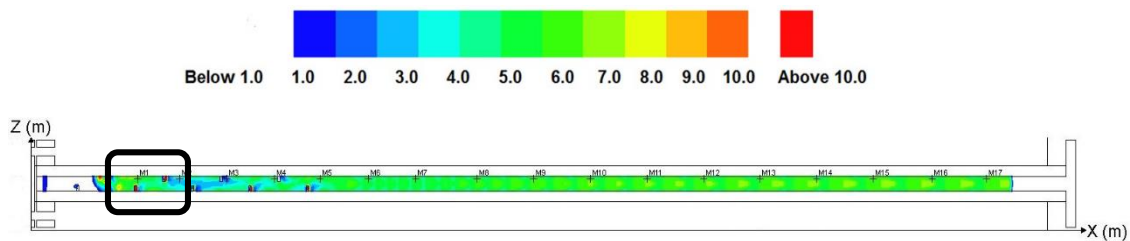


Figure 72. DPDX profile obtained using half-washer-shaped obstacles with an equal blockage ratio and a “uniform” obstacle distribution – After the modification of the flame velocity.

Figure 72 shows that there is a high likelihood to have the onset of detonation at T1; however, between T2 and T3, the DPDX estimations decay to values below five for an extended section of the tube. This means that the detonation is capable of sustain itself, despite the lower DPDX numbers obtained in this section of the detonation tube. Between T3 and T4 the DPDX values are greater than five, with no further sustained decay in the DPDX values. This means that the onset of the detonation occurs at approximately T1, 0.27 m away from the ignition point. Figure 73 shows the comparison between the

experimental and the simulation results before and after the modification of the flame velocity.

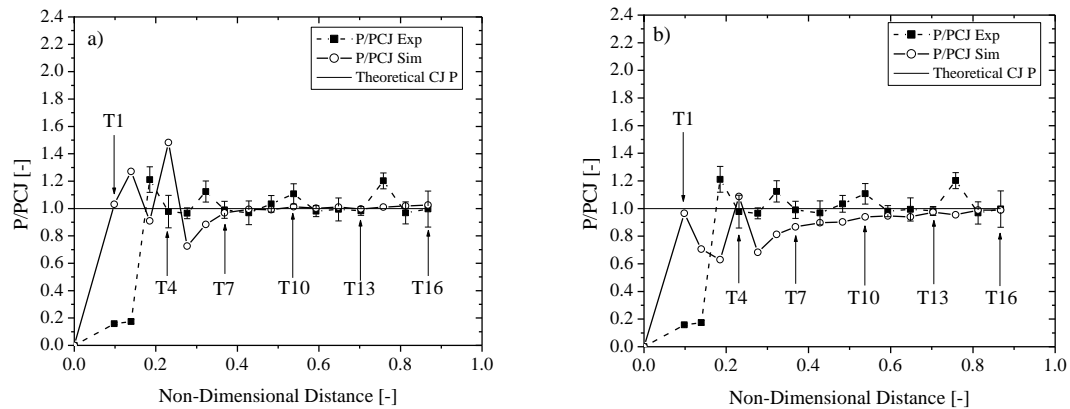


Figure 73. Comparison between the experimental and the simulation results for Scenario 2 – H₂-O₂ mixtures with half-washer-shaped obstacles, an equal BR, and a uniform obstacle distribution. a) prior modification of the flame velocity, b) after the modification of the flame velocity.

As shown in Figure 73a, at T1 FLACS estimates a pressure above the CJ value. At T2, the calculations go above the CJ pressure as well overpredicting the experimental results, followed by a sudden decay. At T4, the pressure reaches its maximum value (approximately 1.5 times the CJ value). The reason for this high pressure value is that one of the obstacles was located very close to this transducer. This proximity causes several shocks to interact with each other at that specific location, resulting in high pressure estimations. At T5, the pressure presents a significant reduction in magnitude and from then on, a gradual increase is observed until the pressure stabilizes near the CJ value.

The results shown in Figure 73b show a totally different behavior to the one described in Figure 73a. For instance, the pressure estimated by FLACS at T1 is slightly below the CJ value and still overpredicts the experimental pressure. At T2 and T3 a decay in the pressure magnitude is observed. At T4 the pressure increases and surpasses the CJ value, but the pressure is within the experimental range. At T5, a sudden decrease in the pressure is observed and the estimation is underpredicted. From then on, the pressure gradually increases until it stabilizes near the CJ value.

It is worth mentioning that for both cases, the pressure estimated at the monitor points located in the unobstructed region of the detonation tube, are within the experimental ranges obtained, except for the fourteenth monitor point, which is clearly underpredicted by FLACS.

8.2.3. Scenario 3

Experimentally, in this scenario, the onset of the detonation occurred at 0.38 m away from the ignition source. Figure 74 shows the DPDX results obtained to determine the location at which the onset of detonation is expected.

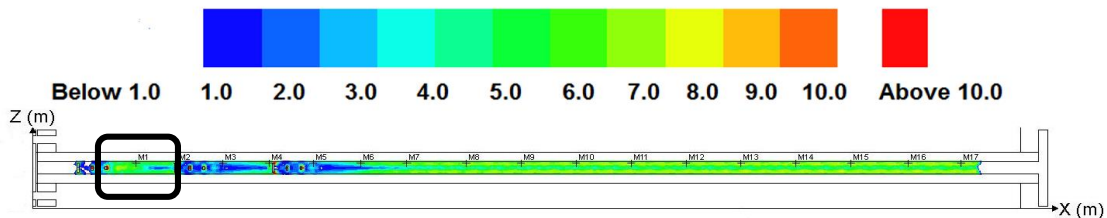


Figure 74. DPDX profile obtained using block-shaped obstacles with a decreasing blockage ratio and a “staggered” obstacle distribution – Previous the modification of the flame velocity.

As it can be observed in Figure 74, high values of DPDX are observed for an extended section of the detonation tube (greater than 20 cells), before and after the first monitor point. This means that it is very likely to have the onset of detonation before T1. As the combustion wave progresses further into the detonation tube, the DPDX variable decreases in its magnitude; however, it remains between one and five. The presence of block-shaped obstacles with high blockage ratio forces the flame flow pattern to be completely modified. For instance, the combustion wave has to split itself to successfully overcome the obstacle. Once the combustion wave surpasses the large blockage ratio obstruction, a pocket of unburned and highly compressed mass is left right after such obstacle. This unreacted mass will be ignited and create a localized auto-explosion via wave interactions and, consequently, accelerate the flame guiding the combustion process to a detonation. As the combustion propagates into the uncongested region of the detonation tube, the DPDX shows a more uniform pattern. This uniformity indicates that the detonation will tend to be stable in the uncongested region.

Comparing the results obtained between the first and third scenario, in the third scenario it is possible to observe a continuous DPDX with values greater than one. Even though the process becomes less likely right after the obstacles with large blockage ratio, the DPDX variable does not reach values below one and it is possible to determine that there is a tendency to form a stable detonation within the gap between the groups of obstacles.

After having modified the flame velocity to the CJ velocity of the hydrogen–oxygen mixture with an initial pressure of 20 kPa (2747 m/s), a new DPDX outcome is obtained. This is shown in Figure 75.

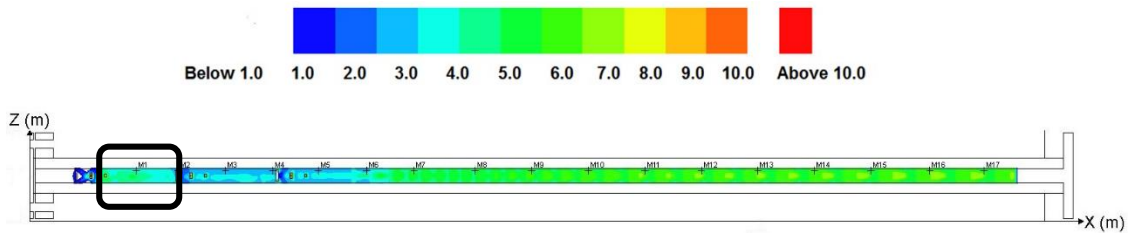


Figure 75. DPDX profile obtained using block-shaped obstacles with a decreasing blockage ratio and a “*staggered*” obstacle distribution – After the modification of the flame velocity.

Figure 75 shows that there is a high likelihood to have the onset of detonation before T1 (approximately 0.25 m away from the ignition source). Between T2 and T3, the DPDX estimations decay to values between three and five. This means that if a detonation was triggered before, the detonation might be able to sustain itself through this section. A similar situation is observed between T4 and T5. As the combustion propagates further into the uncongested section of the detonation tube (after the fifth monitor point) higher values of DPDX values are observed. This indicates that the detonation will tend to stabilize in the uncongested region of the detonation tube. Figure 76 shows the comparison between the experimental and the simulation results before and after the modification of the flame velocity.

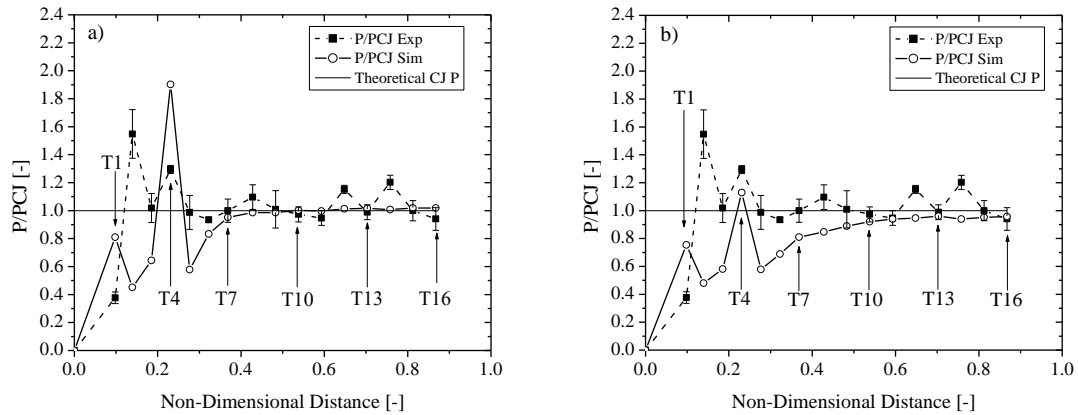


Figure 76. Comparison between the experimental and the simulation results for Scenario 3 – H₂-O₂ mixtures with block-shaped obstacles, decreasing BR, and a staggered obstacle distribution. a) prior modification of the flame velocity, b) after the modification of the flame velocity.

As can be observed in Figure 76a, the initial stages of the explosion, in which a deflagration was observed experimentally, the simulation shows an estimated pressure that overpredicts the actual experimental value. However, at T2 and T3 the calculations by FLACS significantly underpredict the experimental behavior. At T4 a very high pressure was estimated by the CFD model. The reason for this is that the fourth pressure transducer is located very close to an obstacle with an 80% blockage ratio. This means that several shock interactions are going to take place at this location. After T4, the pressure decays to approximately half the CJ value. From then on a gradual increase in the pressure is observed, until it stabilizes near the CJ pressure.

In Figure 76b, the simulation results show a similar trend to the ones described in Figure 76a. The main difference is observed at T4 in which, after the modification of the flame velocity to the CJ value, the pressure estimated by FLACS slightly underpredicts

the experimental value. At T5, the pressure magnitude decays to approximately 0.6 times the CJ value and, from then on a gradual increase in the pressure is observed, until it stabilizes near the CJ value.

8.2.4. Scenario 4

Experimentally, in this scenario, the onset of the detonation occurred at 0.41 m away from the ignition source. Figure 77 shows the DPDX results obtained to determine the location at which the onset of detonation is expected.

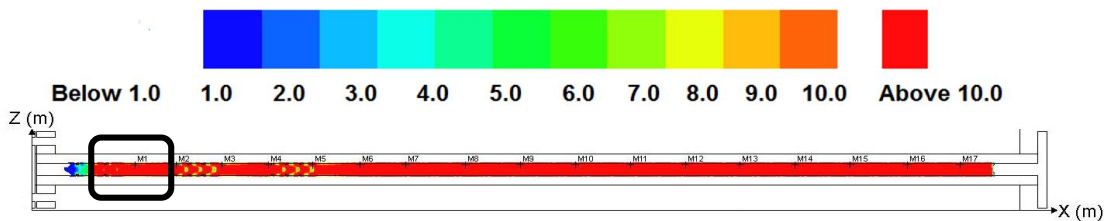


Figure 77. DPDX profile obtained using ring-shaped obstacles with an equal blockage ratio and a “staggered” obstacle distribution – Previous the modification of the flame velocity.

Figure 77 shows very high values of DPDX before the first monitor point for an extended section of the detonation tube (greater than 20 cells). This indicates that FLACS predicts the onset of detonation, even before the first pressure transducer. As it can be observed in Figure 77, as the combustion propagates into the first group of obstacles, the DPDX variable remains uniform with values above 10, which clearly indicates that the detonation is very likely to occur. As the combustion progresses into the second and third group of obstacles, it can be observed that the DPDX values estimated by FLACS decrease

to approximately 6, which still means that it is very likely to have a detonation. Further down in the detonation tube, the DPDX values remain high and constant throughout the detonation tube.

After having modified the flame velocity to the CJ velocity of the ethylene–oxygen mixture with an initial pressure of 16.7 kPa (2287 m/s), a new DPDX outcome is obtained. This is shown in Figure 78.

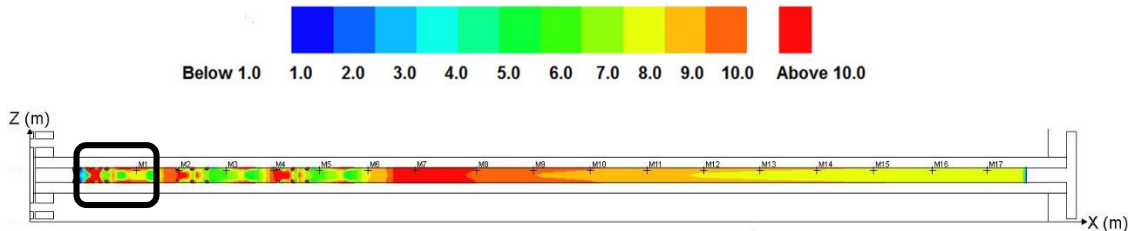


Figure 78. DPDX profile obtained using ring-shaped obstacles with an equal blockage ratio and a “*staggered*” obstacle distribution – After the modification of the flame velocity.

When the flame velocity is modified, the DPDX results changed significantly. This can be observed in Figure 78. For instance, the DPDX values show more variation and is not showing a constant and uniform pattern as the one observed in Figure 77. The results shown in Figure 78 allow one to visualize the onset of the detonation at approximately 0.2 m away from the ignition point. More importantly, the DPDX results show that, overall, the detonation is very likely to occur in both the obstructed and uncongested section of the detonation tube. However, when the combustion wave propagates into the unobstructed region of the tube the detonation shows an overall tendency to stabilize.

According to the DPDX results, FLACS estimates that the onset of the detonation occurs before the first monitor point at approximately 0.2 m away from the ignition source. Figure 79 shows the comparison between the experimental and the simulation results before and after the modification of the flame velocity.

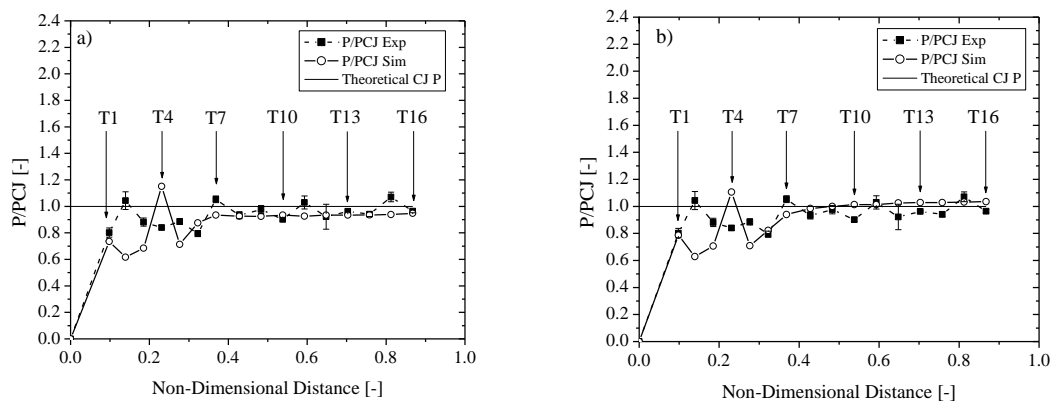


Figure 79. Comparison between the experimental and the simulation results for Scenario 4 – $C_2H_4-O_2$ mixtures with ring-shaped obstacles, an equal BR, and a staggered obstacle distribution. a) prior modification of the flame velocity, b) after the modification of the flame velocity.

As can be observed in Figure 79a, the experimental and calculated pressure at T1 are similar. However, at the second and third monitor point FLACS underpredicts the pressure. At T4, the opposite behavior occurs. For instance, the pressure estimated by FLACS is above the CJ value; while the experimental value obtained was below the CJ pressure. At T5 the pressure decays to approximately 0.7 times the CJ pressure. From then on, the pressure tends to stabilize below the CJ pressure.

Figure 79b shows the results after the flame velocity was modified. For instance, the results follow a similar trend to the results shown in Figure 79a. However, the pressure results obtained after modifying the flame velocity show better matching with the experimental results. As the combustion propagates into the uncongested region of the detonation tube, the pressure tends to stabilize near the CJ value and, more importantly, some of the experimental results match with the estimations made by the CFD model.

8.2.5. Scenario 5

Experimentally, in this scenario, the onset of the detonation occurred at 0.37 m away from the ignition source. Figure 80 shows the DPDX results obtained to determine the location at which the onset of detonation is expected.

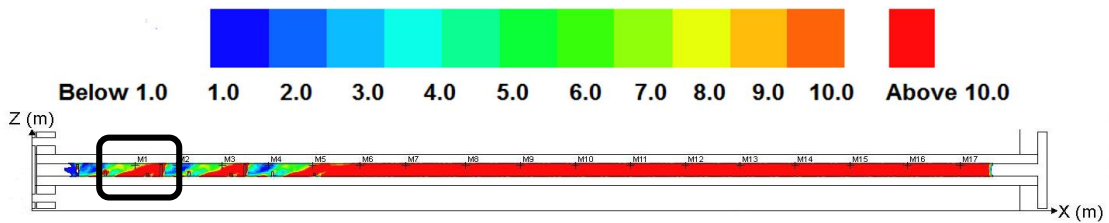


Figure 80. DPDX profile obtained using half-washer-shaped obstacles with a decreasing blockage ratio and a “variation” obstacle distribution – Previous the modification of the flame velocity.

Figure 80 shows that after the first obstacle there is an indication that a detonation might be likely as the DPDX results are greater than five and is shown for an extended section of the tube. As the combustion progresses and surpasses the second obstacle, the likelihood to have the onset of detonation increases to values above 10. This clearly

indicates that, according to FLACS predictions, the onset of the detonation occurs at approximately T1. As the fourth obstacle is surpassed (80% blockage ratio) the DPDX values calculated are significantly reduced; however, it does not reach values below one. This indicates that the high level of obstruction reduces the likelihood, but it does not suppress the overall possibility of having a detonation, as observed in the first scenario in which DPDX values below one were observed. A similar behavior is observed after the seventh obstacle (80% blockage ratio). From then on, the DPDX value gradually increases until it actually remains high and constant throughout the detonation tube.

After having modified the flame velocity to the CJ velocity of the ethylene–oxygen mixture with an initial pressure of 16.7 kPa (2287 m/s), a new DPDX outcome is obtained. This is shown in Figure 81.

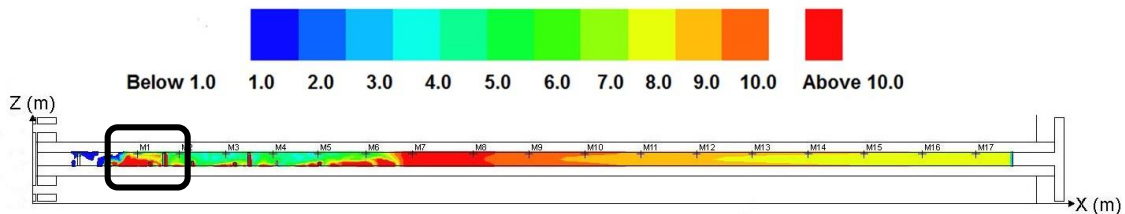


Figure 81. DPDX profile obtained using half-washer-shaped obstacles with a decreasing blockage ratio and a “*variation*” obstacle distribution – After the modification of the flame velocity.

After modifying the flame velocity, the DPDX results changed significantly, as shown in Figure 81. For instance, the calculations made by FLACS near the first obstacle illustrate that there is no chance for a detonation to take place at this location. As the

combustion progresses into the second and third obstacles the DPDX results show a significant increase in the likelihood of having a detonation within this section (at approximately T1 – 0.27 m away from the ignition point). The presence of obstacles with high blockage ratio induce to a reduction of the probability of having a detonation at that point; however, the reactivity of the mixture plays an important role and the detonation does not fail at any point with this layout, as shown by the DPDX results which are always greater than five. As the combustion wave propagates into the uncongested region, the detonation shows a tendency to behave as a stable detonation. Figure 82 shows the comparison between the experimental and the simulation results before and after the modification of the flame velocity.

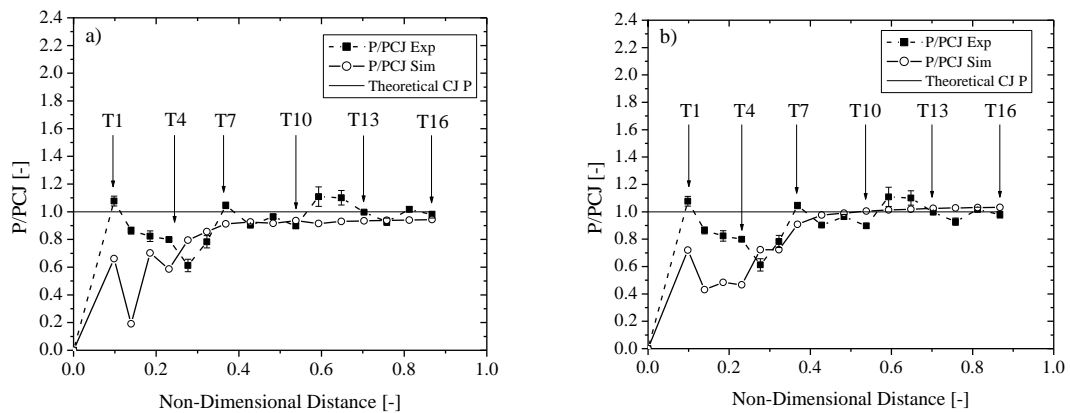


Figure 82. Comparison between the experimental and the simulation results for Scenario 5 – C₂H₄-O₂ mixtures with half-washer-shaped obstacles, decreasing BR, and a variation obstacle distribution. a) prior modification of the flame velocity, b) after the modification of the flame velocity.

As can be observed in Figure 82a, the calculated pressures between T1 and T4 are underpredicted. At T2 a sudden decrease of the pressure is estimated by FLACS. This occurs because right before T2 there is an obstacle with a very high blockage ratio; which actually obstructs the normal flow of the combustion wave and forces the pressure to significantly decay. A similar behavior is observed at T4; however, the pressure does not present a noticeable decrease as with T2. For instance, T4 is located farther away from the 80% blockage ratio obstacle than T2. As the combustion progresses, the estimated pressure magnitude gradually increases. Once the combustion wave reaches the uncongested section of the detonation tube the pressure shows a tendency to stabilize below the CJ value.

Figure 82b shows the pressure results obtained in FLACS after the flame velocity was changed. As can be noticed the pressures between T1 and T4 are still underpredicted; however, the pressure estimated at T2 is closer to the experimental value. As the combustion wave moves away from the ignition source, into the uncongested region of the detonation tube, a gradual increase in the pressure is observed, until it stabilizes near the CJ value.

8.2.6. Scenario 6

Experimentally, in this scenario, the onset of the detonation occurred at 0.39 m away from the ignition source. Figure 83 shows the DPDX results obtained to determine the location at which the onset of detonation is expected.

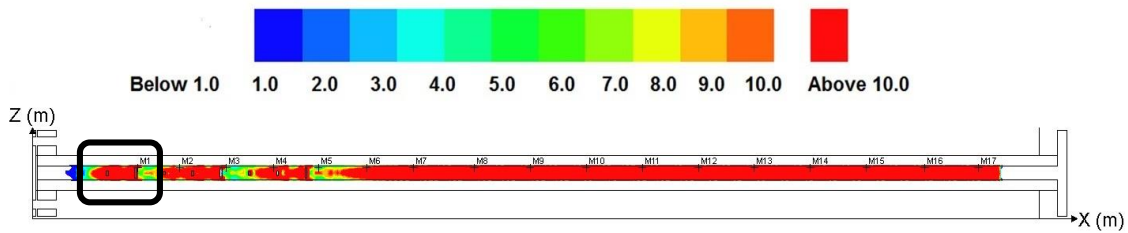


Figure 83. DPDX profile obtained using block-shaped obstacles with an increasing blockage ratio and a “uniform” obstacle distribution – Previous the modification of the flame velocity.

Figure 83 shows very high values of DPDX before the first monitor point (greater than 5) and for an extended section of the detonation tube (greater than 20 cells). This indicates that FLACS predicts a high likelihood to have the onset of detonation before the first monitor point. As it can be observed in Figure 83, this obstacle layout provides a gradual increase in the turbulence until the combustion wave reaches the third obstacle (with a blockage ratio of 80%). At this point, the combustion wave has to fully divert and engulf the obstacle, leaving a pocket of un-reacted mass right after the obstruction. This pocket of mass is then ignited via shock interactions, creating a localized auto-explosion. As can be noticed in Figure 83, the DPDX predictions given by FLACS do not decrease below five. This implies that the detonation is self-sustainable. As the combustion propagates into the uncongested region of the detonation tube, it is possible to observe that the DPDX results clearly describe a stable and high likely detonation.

After having modified the flame velocity to the CJ velocity of the ethylene–oxygen mixture with an initial pressure of 16.7 kPa (2287 m/s), a new DPDX outcome is obtained. This is shown in Figure 84.

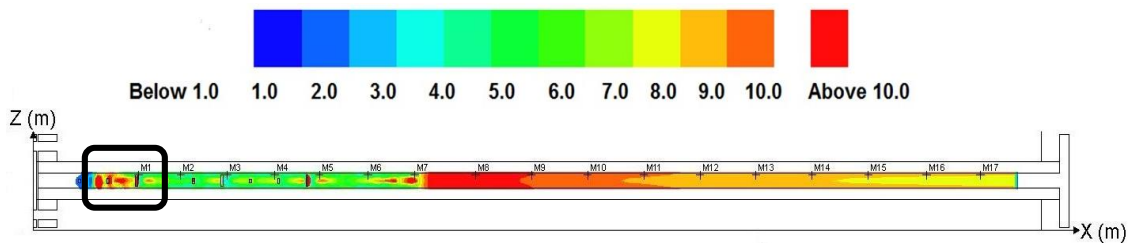


Figure 84. DPDX profile obtained using block-shaped obstacles with an increasing blockage ratio and a “uniform” obstacle distribution – After the modification of the flame velocity.

After having modified the flame velocity, the DPDX results changed significantly, as shown in Figure 84. For instance, a gradual increase in the DPDX is observed within the first two obstacles, with values greater than five. This clearly indicates that the detonation is highly expected to occur right before the first pressure transducer (at approximately 0.24 m away from the ignition source). As the combustion propagates and surpasses the third obstacle, the DPDX predictions by FLACS decay to values above five; which clearly indicates that the detonation is self-sustainable at that point. A similar tendency is observed in the next two groups of obstacles. As the combustion wave propagates into the uncongested region, a higher DPDX is observed, describing a stable detonation. Figure 85 shows the comparison between the experimental and the simulation results before and after the modification of the flame velocity.

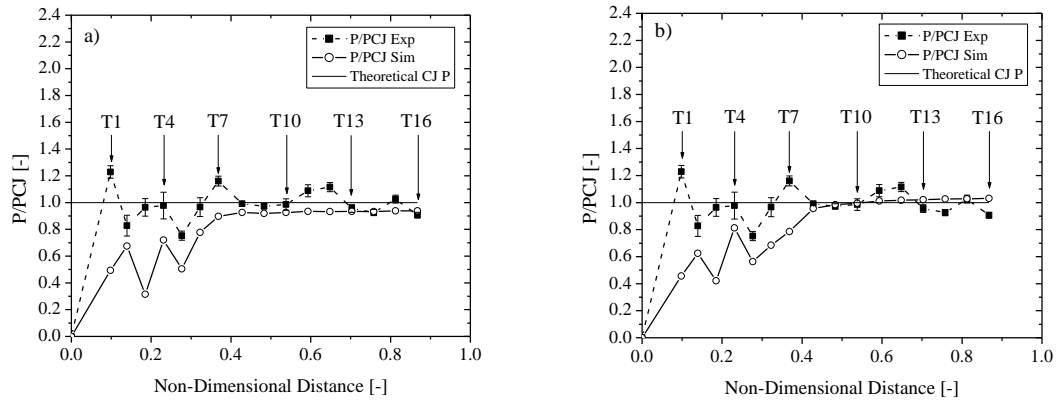


Figure 85. Comparison between the experimental and the simulation results for Scenario 6 – $C_2H_4-O_2$ mixtures with block-shaped obstacles, increasing BR, and a uniform obstacle distribution. a) prior modification of the flame velocity, b) after the modification of the flame velocity.

As described in Figure 85a, the pressures calculated by FLACS within the obstructed region of the detonation tube show a tendency to underpredict the experimental values obtained. For instance, the pressures reported by FLACS from T1 to T5 are underpredicted. As the combustion progresses into the uncongested region of the detonation tube, the estimated pressures show a tendency to stabilize near and below the CJ value. However, some of the calculated pressures are within the range of the experimental values, *i.e.*, T9 through T11.

As the flame velocity is changed to the CJ value, an improvement in the pressure calculations is observed, as depicted in Figure 85b. For instance, the pressure predicted at T3 is still underpredicted; however, the pressure magnitude increased from 0.3 times the CJ pressure (Figure 85a) to 0.4 times the CJ pressure (Figure 85b). Additionally, when the flame velocity is changed, the pressures estimated by FLACS are closer to the

experimental value. This can be seen in the obstructed section and in the uncongested region of the detonation tube. More importantly, as the combustion wave stabilizes near the CJ value, the predictions by FLACS give a better matching to the actual experimental values.

8.2.7. Scenario 7

Experimentally, in this scenario, the onset of the detonation occurred at 0.38 m away from the ignition source. Figure 86 shows the DPDX results obtained to determine the location at which the onset of detonation is expected.

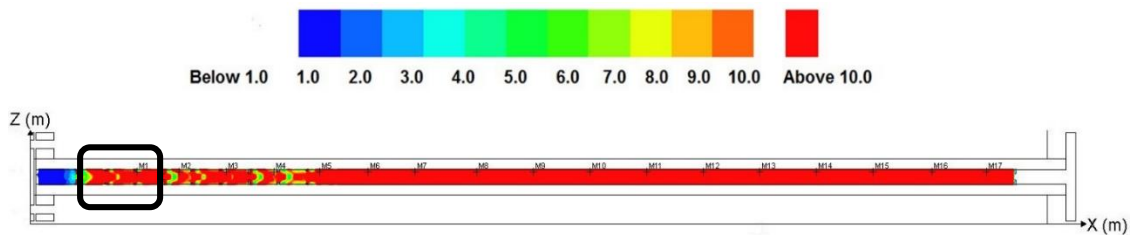


Figure 86. DPDX profile obtained using ring-shaped obstacles with a decreasing blockage ratio and a “uniform” obstacle distribution – Previous the modification of the flame velocity.

As can be observed in Figure 86, high values of DPDX are observed for an extended section of the detonation tube (greater than 20 cells), before the first monitor point. This means that it is very likely to have the onset of the detonation before T1. As the combustion wave progresses further into the detonation tube, the DPDX variable shows some variations in its response; however, the overall value of the DPDX does not decrease below five. The presence of the ring-shaped obstacles forces the flow of the flame

to keep on propagating through the axis, forcing no significant change in the overall propagation of the flame. Once the combustion wave propagates into the uncongested section of the detonation tube, the DPDX shows a very uniform pattern, indicating that the detonation will tend to be stable.

In general, the results obtained without the modification of the flame velocity, suggest that the acetylene-oxygen mixtures tend to form a very rapid detonation and that is self-sustainable throughout the detonation tube; even in the congested section of the tube.

After having modified the flame velocity to the CJ velocity of the acetylene–oxygen mixture with an initial pressure of 9.3 kPa (2296 m/s), a new DPDX outcome is obtained. This is shown in Figure 87.

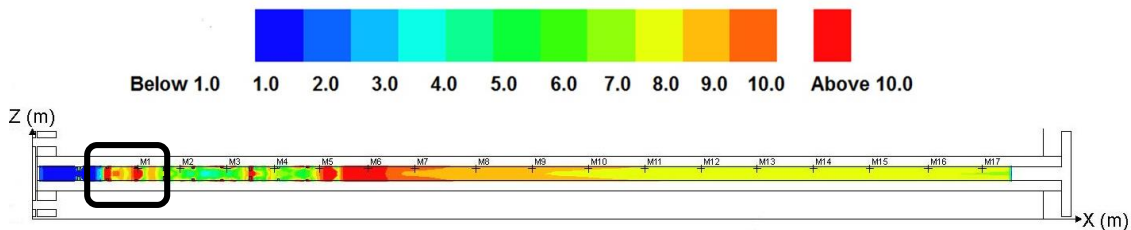


Figure 87. DPDX profile obtained using ring-shaped obstacles with a decreasing blockage ratio and a “uniform” obstacle distribution – After the modification of the flame velocity.

Figure 87 shows that as the acetylene-oxygen mixture is ignited, there is always a small chance to have a detonation. Thus, confirming the high reactivity of acetylene-oxygen mixtures. As the combustion propagates towards the second obstacle, a gradual

increase in the DPDX values is observed. More importantly, as the DPDX reaches a value of five, it does not go below that value. This implies that there is a very high likelihood to have a stable detonation throughout the obstructed region, as expected; however, the presence of the ring-shape obstacles tends to drag the turbulence towards the central axis of the detonation tube. This implies that the onset of detonation, according to FLACS, occurred before the first monitor point at approximately 0.25 m away from the ignition point. As the combustion propagates towards the uncongested region of the detonation tube, higher values of DPDX values are observed. This indicates that the detonation will tend to stabilize in the uncongested region of the detonation tube. Figure 88 shows the comparison between the experimental and the simulation results before and after the modification of the flame velocity.

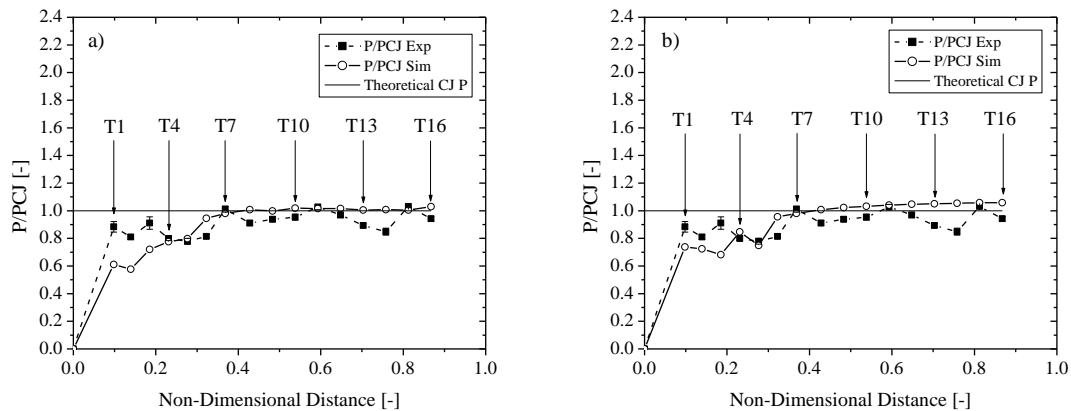


Figure 88. Comparison between the experimental and the simulation results for Scenario 7 – $C_2H_2-O_2$ mixtures with ring-shaped obstacles, decreasing BR, and a uniform obstacle distribution. a) prior modification of the flame velocity, b) after the modification of the flame velocity.

As can be observed in Figure 88a, the initial stages of the explosion, the simulation shows an estimated pressure that underpredicts the actual experimental value (between T1 through T3). As the combustion wave reaches T4 and T5, the simulation matches the experimental value. From then on, the simulation results show that there is a gradual increase in the pressure magnitude, until it stabilizes near the CJ value with slight overpredictions of the experimental pressures. Figure 88b shows a similar trend to the one described in Figure 88a. The main difference is that the pressures predicted by the model at the very beginning of the explosion are underpredicted, but closer to the experimental values than the case in which the flame velocity was not modified. As the combustion moves towards the uncongested region of the detonation tube, a gradual increase in the pressure magnitude is observed until it stabilizes above and near the CJ value. In general, when this occurs the pressure estimated by FLACS is overpredicted.

8.2.8. Scenario 8

Experimentally, in this scenario, the onset of the detonation occurred at 0.38 m away from the ignition source. Figure 89 shows the DPDX results obtained to determine the location at which the onset of detonation is expected.

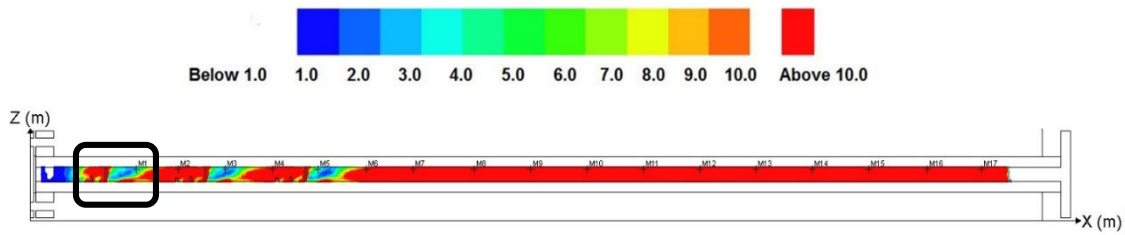


Figure 89. DPDX profile obtained using half-washer-shaped obstacles with an increasing blockage ratio and a “*staggered*” obstacle distribution – Previous the modification of the flame velocity.

Figure 89 shows that the DPDX variable starts showing right after the ignition point. As in the seventh scenario, the DPDX results show a gradual increase. In this case, the obstacles (half-washer-shaped obstruction) are lined up in an increasing blockage ratio. This implies that the turbulence provided by the obstacles is gradually increasing until the combustion wave reaches the third obstacle with a high blockage ratio (80%). In this case, the flame has only one direction to go (through the top of the obstacle). This means that the detonation will be suddenly blocked; however, due to the high reactivity of the mixture, the un-reacted gases can easily re-detonate. This is observed in the second and third groups of obstacles, in which the DPDX decays to values of approximately one and then increases to very high values (above five). As the combustion progresses into the uncongested region, the detonation seems to be more stable throughout the detonation tube.

After having modified the flame velocity to the CJ velocity of the acetylene–oxygen mixture with an initial pressure of 9.3 kPa (2296 m/s), a new DPDX outcome is obtained. This is shown in Figure 90.

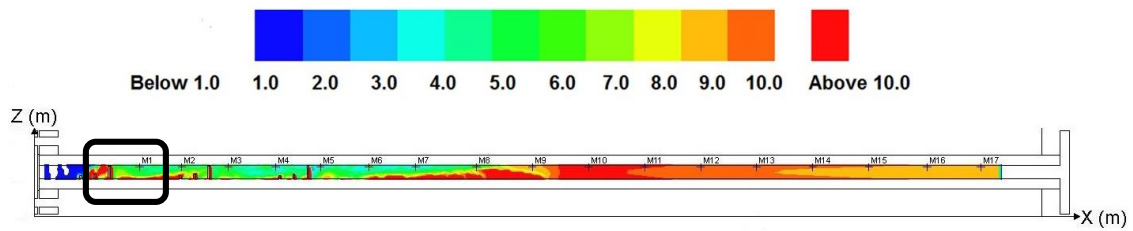


Figure 90. DPDX profile obtained using half-washer-shaped obstacles with an increasing blockage ratio and a “*staggered*” obstacle distribution – After the modification of the flame velocity.

Figure 90 shows a similar trend to the one just described for Figure 89. For instance, as the mixture is ignited the DPDX results start showing a possible onset of detonation; however, as the combustion propagates towards the first group of obstacles, DDT is very likely to occur. This implies that the onset of detonation, according to FLACS, occurred before the first monitor point (at approximately 0.2 m away from the ignition point). Once the first group of obstruction is surpassed, the gap between the first and second set of obstacles is sufficiently large to allow the likelihood to increase. A similar trend occurs between the second and third group of obstacles. As the combustion wave moves into the uncongested region of the detonation tube, higher values of DPDX are observed. This indicates that the detonation will be stable throughout the rest of the detonation tube. Figure 91 shows the comparison between the experimental and the simulation results before and after the modification of the flame velocity.

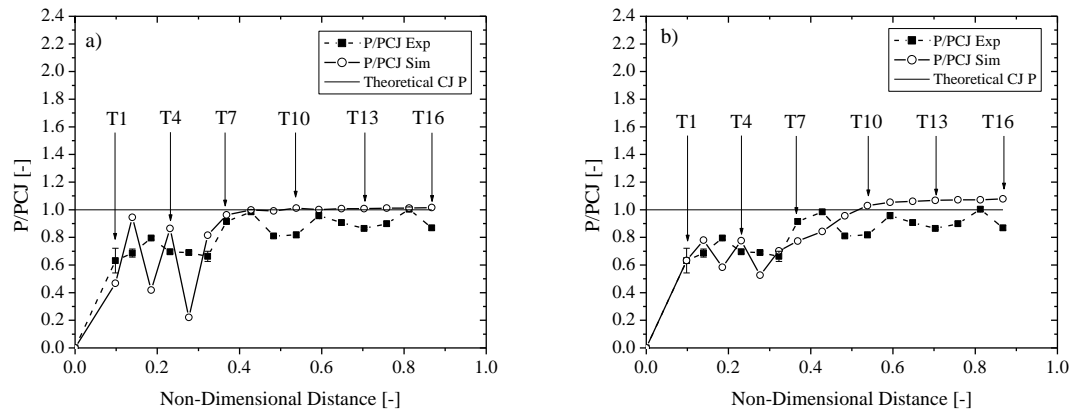


Figure 91. Comparison between the experimental and the simulation results for Scenario 8 – C_2H_2 - O_2 mixtures with half-washer-shaped obstacles, increasing BR, and staggered obstacle distribution. a) prior modification of the flame velocity, b) after the modification of the flame velocity.

As can be observed in Figure 91a, the estimations given by FLACS do not show a specific trend, and as a matter of fact, significantly underpredicts the experimental pressure for T1, T3 and T5; and overpredicts the pressure at T2 and T4. The main reason for this behavior is the obstacle's layout. For instance, T3 and T5 are right after an obstacle with a large blockage ratio (80%). This actually slows down the combustion wave significantly and as described in Figure 89, the detonation likelihood decays right after these high blockage ratio obstacles. Once the combustion wave surpasses the congested region and moves towards the uncongested section of the detonation tube, the pressure values estimated by FLACS show a tendency to stabilize near the CJ value.

On the other hand, when the flame velocity is changed to the CJ value, the pressure estimations by FLACS are significantly improved. For instance, at T1 the experimental and simulation results are well matched, but at T2 and T4 the simulation results slightly

overpredict the experimental results. As for T3 and T5, FLACS underpredicts the pressure. As the combustion moves away from the obstructed region, a gradual increase in the pressure estimations by FLACS is observed, with a tendency to stabilize above and near the CJ value.

8.2.9. Scenario 9

Experimentally, in this scenario, the onset of the detonation occurred at 0.38 m away from the ignition source. Figure 92 shows the DPDX results obtained to determine the location at which the onset of detonation is expected.

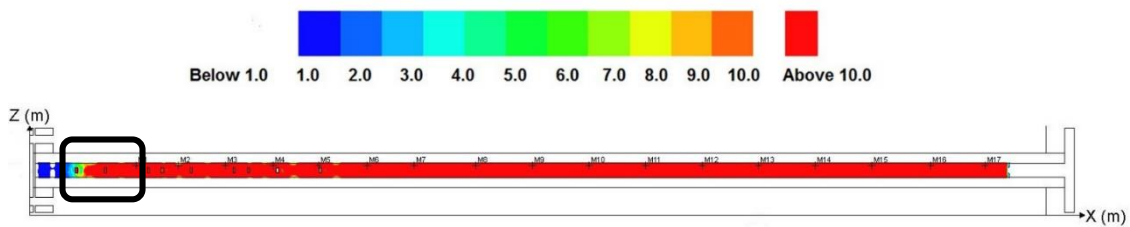


Figure 92. DPDX profile obtained using block-shaped obstacles with an equal blockage ratio and a “variation” obstacle distribution – Previous the modification of the flame velocity.

Figure 92 shows that the DPDX variable starts showing right after the ignition point. In this case, the block-shaped obstacles have the same blockage ratio (40%). Initially, the DPDX starts showing small values, but it progressively increases. For instance, as the combustion wave surpasses the first obstacle, the DPDX results are already exceeding five, which means that the DDT might occur at this point (well behind the first

monitor point). From then on, the detonation seems to be stable in the congested and unobstructed regions of the detonation tube.

After having modified the flame velocity to the CJ velocity of the acetylene–oxygen mixture with an initial pressure of 9.3 kPa (2296 m/s), a new DPDX outcome is obtained. This is shown in Figure 93.

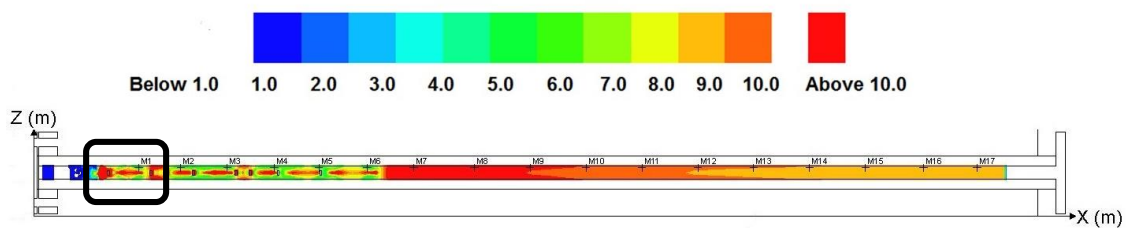


Figure 93. DPDX profile obtained using block-shaped obstacles with an equal blockage ratio and a “variation” obstacle distribution – After the modification of the flame velocity.

Figure 93 shows that as the mixture is ignited, the DPDX results begin appearing. However, the detonation starts becoming likely when the combustion wave reaches the first obstacle (at 0.17 m away from the ignition point). At this point, the DPDX is gradually increasing from five to ten and above. Having block-shaped obstacles forces the flame flow pattern to completely diverge and engulf the obstacle. Once the combustion wave surpasses the obstruction, a pocket of unreacted and highly compressed mass is left right after the obstacle. This mass will start to react via wave interactions and create a localized auto-explosion, which will accelerate the flame and guide the process to a successful and self-sustainable detonation. Once the combustion wave moves into the uncongested region of the detonation tube, higher values of DPDX are observed. This implies that the

detonation will be stable throughout the rest of the detonation tube. Figure 94 shows the comparison between the experimental and the simulation results before and after the modification of the flame velocity

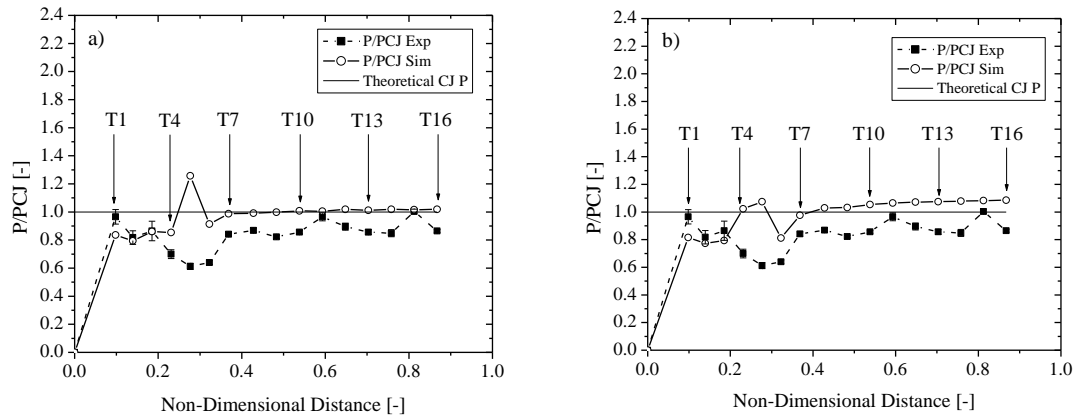


Figure 94. Comparison between the experimental and the simulation results for Scenario 9 – $C_2H_2-O_2$ mixtures with block-shaped obstacles, equal BR, and a variation obstacle distribution. a) prior modification of the flame velocity, b) after the modification of the flame velocity.

As depicted in Figure 94a, the calculations given by FLACS show a general overpredicting tendency. However, at T1 a slight underprediction is observed. At T2 and T3 the model agrees with the experimental values obtained. From then on, the pressures are over estimated. At T5 FLACS predicts a maximum pressure of approximately 1.3 times the CJ value. This occurs mainly because of the position of the monitor point which is right between the obstacle and the wall of the tube and several wave interactions occur in that position. From then on, the pressure estimated by FLACS shows a tendency to stabilize near the CJ value.

On the other hand, when the flame velocity is changed to the CJ value, the pressure estimations by FLACS are significantly improved in the near-field. For instance, the estimated pressure at T1 still underpredicts the experimental behavior, but at T2 and T3 the calculated pressure is within the experimental range. From then on, the pressures given by the model overpredict the experimental values and show a general tendency for the pressure to stabilize above the CJ value.

8.3. Discussion

From the numerical data, several variables were analyzed: the maximum and minimum pressures obtained in the simulations; the location at which these pressures were attained; the average pressure and the standard deviation for each simulation; the run-up distance at which DDT was triggered; and the number of times the pressure was greater than the CJ value. As in Table 15, the variables that deal with the pressure are normalized to the CJ value, and the variables that refer to any location are expressed in meters.

Table 15. Summary of the simulation results for the pressure data. Pressures are given relative to their respective CJ levels.

Exp No.	Max Pressure	Location Max P [m]	Min Pressure	Location Min P [m]	Std Dev Pressure	Run-up Distance [m]	Mean Pressure	No. Times P > 1
1	1.45	0.77	0.63	0.89	0.21	1.10	0.90	2
2	1.09	0.64	0.63	0.51	0.12	0.27	0.89	1
3	1.13	0.64	0.48	0.39	0.18	0.25	0.84	1
4	1.11	0.64	0.63	0.39	0.15	0.20	0.93	8
5	1.03	2.41	0.43	0.39	0.22	0.27	0.85	7
6	1.03	2.41	0.42	0.51	0.22	0.24	0.84	6
7	1.06	2.25	0.68	0.51	0.14	0.25	0.94	9
8	1.08	2.41	0.53	0.77	0.20	0.20	0.88	7
9	1.09	2.41	0.77	0.39	0.12	0.17	0.99	11

The data were analyzed to determine which geometrical features can affect the onset of the detonation, under the scope of the main factors considered for this study, *i.e.*, fuel, obstacle shape, blockage ratio and obstacle distribution. However, for the design of experiment matrix shown in Table 2, more than one variable changes from simulation to simulation. To perform a sensitivity analysis to determine the effect a main factor can have on a particular variable of interest, the result for the response variable are averaged over the simulations which contained the same factor level. For instance, to determine the effect the fuel has on the run-up distance, these data were analyzed by averaging the response obtained for each fuel, *i.e.*, for hydrogen the average is obtained from {1.10, 0.27 and 0.25} or 0.54. A similar procedure can be done for ethylene and acetylene. This methodology was applied to all the variables shown in Table 15 for each of the four factors [50]. Figure 95 to Figure 98 show the graphic results of this analysis.

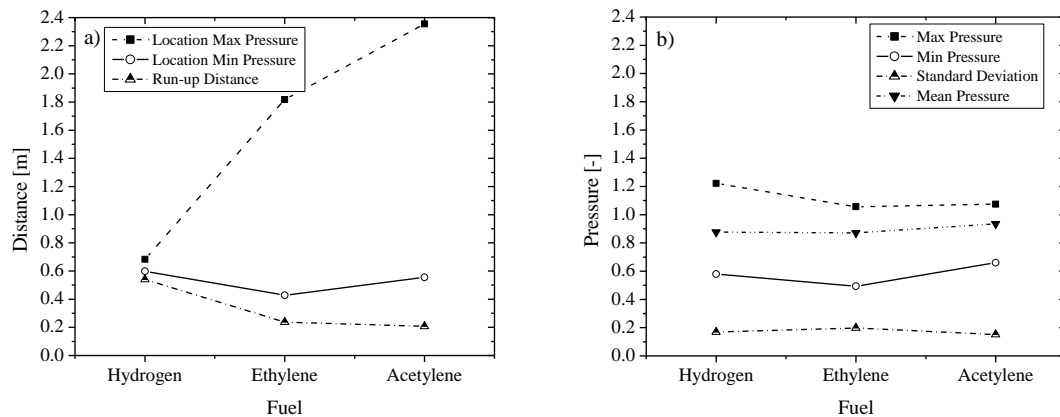


Figure 95. Sensitivity analysis for the pressure for different (a) location and (b) magnitude variables having fuel type as the parameter of interest.

The effect of different fuels on the pressure and the run-up distance to cause the onset of the detonation is shown in Figure 95. As can be observed in Figure 95a (distance vs. gas), the run-up distance is maximized with hydrogen-oxygen mixtures and minimized with acetylene-oxygen mixtures. However, the location at which the maximum pressure is observed presents the opposite behavior, in which hydrogen-oxygen mixtures show that the maximum pressure is obtained closer to the ignition source while acetylene-oxygen mixtures present the maximum pressure near the end of the detonation tube.

Figure 95b shows that, in general, the gas does not have a significant effect on the variables that evaluate the pressure, *i.e.*, maximum and minimum pressure, mean pressure and standard deviation. However, as it can be observed, the maximum pressure is obtained with hydrogen-oxygen mixtures and the minimum pressure is obtained with ethylene-oxygen mixtures. Additionally, there is no significant variation in the mean pressure.

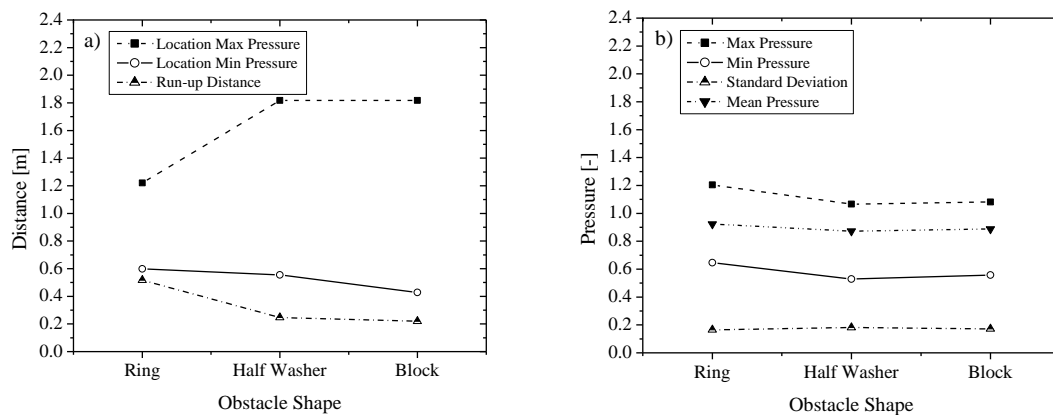


Figure 96. Sensitivity analysis for the pressure for different (a) location and (b) magnitude variables having the obstacle shape as the parameter of interest.

Figure 96a shows the effect that the obstacle shape has on the location of the maximum and minimum pressure and the run-up distance to obtain DDT. For instance, the location at which the maximum pressure is obtained is maximized with block-shaped obstacles and minimized with ring-shaped obstacles. The opposite behavior is observed with the location at which the minimum pressure is observed. However, this variable is not significantly affected. As for the run-up distance, the ring-shaped obstacles maximize the distance at which DDT is observed, while the block-shaped obstruction minimizes this distance.

The statistical analysis shown in Figure 96b describes that the obstacle shape, in general, does not have a significant effect in the variables evaluated. However, the maximum pressure is obtained with ring-shaped obstacles and the minimum pressure is achieved with half washer-shaped obstruction.

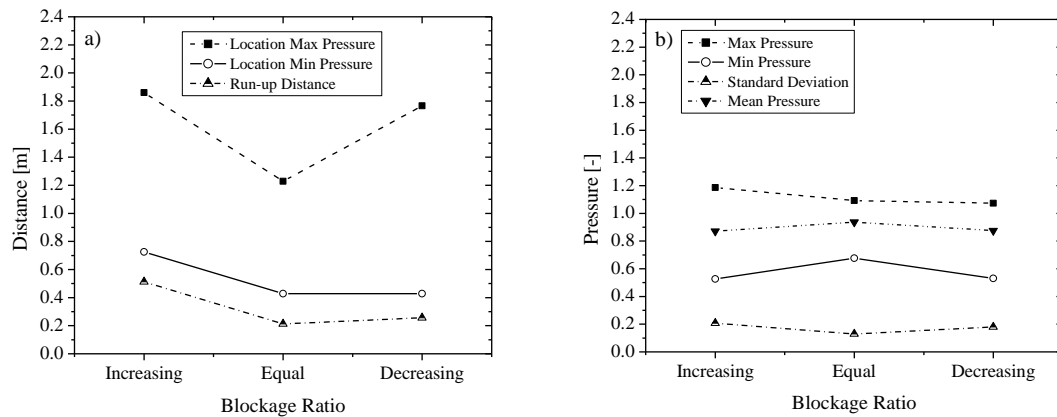


Figure 97. Sensitivity analysis for the pressure for different (a) location and (b) magnitude variables having the blockage ratio as the parameter of interest.

Figure 97a shows the effect that the different levels of congestion has on the location at which the maximum and minimum pressure are observed and the run-up distance to DDT. As it can be observed, the configuration that presents an increasing blockage ratio (from 25% to 80%) maximizes the location at which the maximum and minimum pressure are observed and the run-up distance at which DDT is achieved. The layout that uses an equal blockage ratio (40%) minimizes all these distances.

The statistical analysis shown in Figure 97b, it illustrates that the blockage ratio does not have a significant effect in the variables evaluated. It is worth mentioning that the maximum and minimum pressures are obtained with an increasing blockage ratio setup.

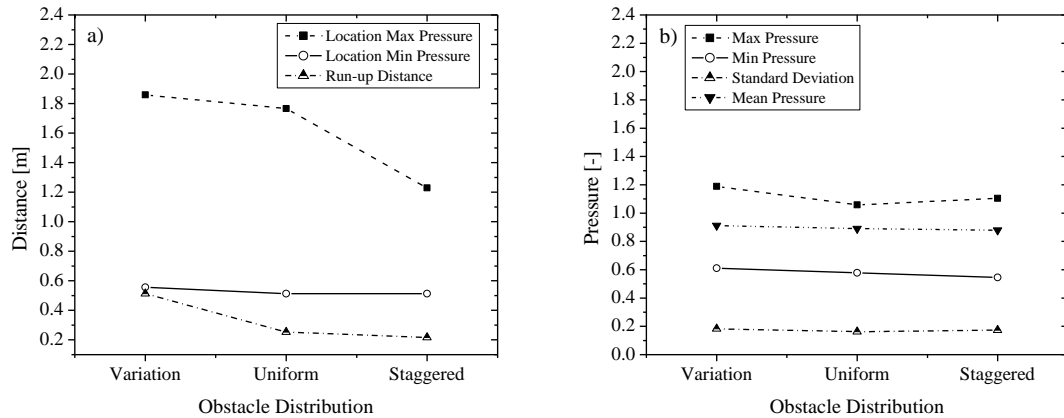


Figure 98. Sensitivity analysis for the pressure for different (a) location and (b) magnitude variables having the obstacle distribution as the parameter of interest.

Figure 98a shows the effect that the obstacle distribution has on the location at which the maximum and the minimum pressure are observed and the run-up distance to

obtain DDT. In this case, the “*variation*” obstacle distribution maximizes the run-up distance and the location at which the maximum and minimum pressure are observed. On the other hand, the “*staggered*” obstacle distribution minimizes all the variables just described.

The statistical analysis shown in Figure 98b illustrates that the obstacle distribution does not have a significant effect in the variables evaluated. It is worth mentioning that the maximum pressure is obtained with the “*variation*” obstacle distribution and the minimum pressure is obtained with the “*staggered*” obstacle distribution.

Table 16. Ranking of variables as a function of the parameters modified in the simulations, where “1” is most significant and “4” is least significant.

Variables	Max Pressure	Location Max P [m]	Min Pressure	Location Min P [m]	Std Dev Pressure	Run-up Distance [m]	Mean Pressure	No. Times P > 1
Gas	1	1	1	2	2	1	2	1
Shape	2	4	3	3	4	3	3	4
BR	4	2	2	1	1	2	1	2
Distribution	3	3	4	4	3	4	4	3

The overall effect that each parameter has on the variables analyzed is ranked in Table 16. As it was expected, the fuel is the most important factor; however, and as mentioned previously, the impact of the obstacle configuration is the focus of this study. For instance, according to the simulation results obtained in FLACS, the blockage ratio plays an important role in the run-up distance to obtain a detonation and it has a significant effect in the number of times in which the estimated pressure exceeded the CJ value.

Additionally, the average pressure value of a simulation is driven by the blockage ratio. As for the effect of the obstacle shape on the run-up distance to detonation and the maximum pressure it can be observed that when the overall flow of the combustion wave is not distorted, as it is with block and half-washer-shaped obstacles, the run-up distance tends to be maximized (having an adverse effect on the flame acceleration). Finally, the obstacle distribution does not seem to be a factor that significantly affects any of the variables studied in this analysis.

8.4. Summary

As expected, the fuel type is the main parameter that affects the outcome of all the variables evaluated in the previous section. However, the results also suggest that the other parameters, *i.e.*, obstacle shape, blockage ratio and obstacle distribution, affect the simulation results and play an important role on variables such as the run-up distance for the onset of the detonation. Table 17 shows the layouts that maximized and minimized the run-up distance to DDT.

Table 17. Maximum and minimum run-up distance scenarios.

	Maximum Run-up Distance Scenario	Minimum Run-up Distance Scenario
Gas	Hydrogen	Acetylene
Obstacle Shape	Ring	Block
Blockage Ratio	Increasing	Equal
Obstacle Distribution	Variation	Staggered

Comparing the results shown in Table 17 with the outcome obtained in Chapter VI, the scenario that maximizes the run-up distance is the same to the one obtained experimentally and the scenario that minimizes the run-up distance differs in the blockage ratio, *e.g.*, FLACS predicts an equal blockage ratio while experimentally a decreasing blockage ratio was obtained.

8.5. Conclusions

The experimental results suggest that the non-uniform distribution of obstacles affects the flame acceleration and, consequently, the run-up distance to obtaining DDT, the pressure magnitude and the general propagation of the detonation wave throughout the detonation tube. This work also demonstrates the use of the FLACS code to predict the likelihood of a detonation occurring by tracking the DPDX variable along the propagation path. Additionally, this work suggests the estimation of the run-up distance to obtain DDT based on the DPDX results and includes a new methodology to predict the onset of the detonation. As it was shown in all the scenarios, the detonations were very likely to occur within the first meter of the detonation tube. In general, this outcome agrees with the experimental results; however, it is important to recall that FLACS only represents a fast deflagration and once the DPDX is greater than five for an extended section of the simulation volume (greater than 20 cells), the flame velocity has to be modified to the CJ value and the simulation must be re-run from that specific location. This correction improves the pressure and DPDX results significantly and allows the user to get a better visualization of how the obstruction affects the overall progression of the combustion wave.

9. CONCLUSIONS AND FUTURE WORK

9.1. Conclusions

This dissertation reports the rig characterization study that was carried out to determine if the current facility and methodologies employed produced similar pressures and velocities for several repeat experiments under the same conditions. This study was performed with stoichiometric H₂-O₂ mixtures and with lean H₂-O₂ mixtures ($\phi = 0.25$) and the variables attained in this study were: 1) pressure; 2) velocity; and, 3) run-up distance to obtain a detonation. The experimental pressure and velocity results were normalized with their corresponding CJ values, and the distance was normalized with the length of the detonation tube. The results indicated that experiments show good repeatability, as similar trends in pressure and velocity were obtained for all the experiments and there was no significant variation in the run-up distances obtained for all the experiments.

Additionally, this dissertation reports the effect that the randomization of obstructions has on the flame acceleration and, consequently, on the onset of the detonation. For this purpose, a Taguchi design of experiments matrix was implemented to consider a wide range of obstacle configurations. This work was based on a Taguchi L9 matrix, having four parameters at three levels each, namely 1) the fuel; 2) the obstacle shape; 3) the blockage ratio; and, 4) the obstacle distribution. As for the fuel selection, it was desirable that the fuel utilized was capable of detonating in the tube. Therefore, the fuels were selected if at least one of these criteria were satisfied: 1) if the fuel detonated

in previous research performed by Polley [48]; 2) if the fuel detonated in the smooth detonation tube, *e.g.*, no obstruction was included in the tube. The fuels selected for this study were hydrogen, ethylene and acetylene. Three obstacle shapes were machined for this study: 1) block-shaped; 2) ring-shaped; and, 3) half-washer-shaped, and three different sizes were manufactured to have 25%, 40%, and 80% blockage ratios. The categories for blockage ratio defined in this project were: 1) increasing (from 25% to 80%); 2) equal (40%); and, 3) decreasing (from 80% to 25%) blockage ratio. As for the obstacle distribution, the three categories defined in this project were: 1) variation (one, two, and three times the internal diameter of the detonation tube); 2) uniform (a spacing twice the internal diameter of the detonation tube); and, 3) staggered (all obstacles were spaced one internal diameter of the detonation tube followed by a gap of five times the internal diameter of the tube). From the experimental data, a sensitivity analysis was performed in which several variables were analyzed. One of the most important variables selected in this study is the run-up distance to obtain a detonation. For instance, it was found that when using ring-shaped obstacles with an increasing blockage ratio and a “*variation*” obstacle distribution, the run-up distance to obtain a detonation is maximized (adverse effect on the flame acceleration). In contrast, block-shaped obstacles with a decreasing blockage ratio and a “*staggered*” obstacle distribution minimized the run-up distance (promotes the flame acceleration).

As part of this dissertation, a numerical study was performed to determine if the CFD model used in this research was able to capture the run-up distance to obtain a detonation, despite the fact that this model is used without resolving precisely the details

of the DDT structure. This was done by utilizing the non-dimensional spatial gradient pressure (DPDX). This variable allows to determine the likelihood of having a DDT based on a detonation attribute, *i.e.*, the reaction front couples together with the pressure front. First, a basic methodology in which the likelihood of the detonation was dependent on the DPDX numerical value was validated against data found in the literature:

- $DPDX < 0.5$: No DDT
- $0.5 < DPDX < 1.0$: DDT begins to be possible
- $1 < DPDX < 5$: DDT is possible
- $5 < DPDX < 10$: DDT is likely

Then, an expansion to this methodology was proposed. For instance, it was found that when a “*grid-by-grid*” analysis is performed, a total of 20 or more continuous cells have to have a DPDX value equal to or greater than five. This methodology was implemented and validated with the experimental data attained in this project.

The results obtained with the validation of this expanded methodology were: when using ring-shaped obstacles with an increasing blockage ratio and a “*variation*” obstacle distribution the run-up distance to obtain a detonation is maximized (adverse effect on the flame acceleration). In contrast, block-shaped obstacles with an equal blockage ratio and a “*staggered*” obstacle distribution minimized the run-up distance (promotes the flame acceleration).

9.2. Future Work

The methodology implemented in this study to analyze the effect of the non-uniform obstacle distribution can be extended to include the effect of different obstruction

shapes keeping the blockage ratio as a fixed parameter. Additionally, the modification of the blockage ratio and the obstacle shape in the same experiments should also be accounted for. This study will complete a more robust analysis in the effect on the flame acceleration and, consequently, the onset of the detonation due to the randomization of the obstruction. The inclusion of flow visualization is also recommended as it will provide: 1) a better understanding of how the onset of detonation is being affected by the inclusion of a randomized obstacle configuration; and, 2) a more complete insight on how the turbulence plays an important role once a detonation is triggered.

Another important study that could be carried out with the current facility is to develop a database that has information about the limits of detonation for different fuel-oxygen and/or fuel-air mixtures at different initial conditions in a smooth detonation tube. Fuels such as hydrogen, ethylene and acetylene have been widely studied; however, the data are very limited towards the initial pressure and the equivalence ratio of the mixture [56]. This will significantly expand the current knowledge of detonations and the different combustion regimes.

Further research developed in this area should account for the inclusion of more pressure transducers along the detonation tube (opposite to the location of the current pressure transducers temperature acquisition). This will provide more information on the type of the detonation that is being obtained in the detonation tube, and it would be interesting to study how spinning detonations behave in terms of pressure.

From a safety perspective, research should be conducted towards techniques to mitigate the effects of a detonation. For instance, current research is looking at the effect

a detonation would have if it is counteracted by a secondary explosion, triggered at an opposite location from where the initial detonation was formed. Additional efforts should be driven towards the development of a numerical tool that accounts for the overall combustion process within the same program, *i.e.*, deflagration, DDT and, detonation. This tool can be validated by utilizing all the data that have been collected though this project and forthcoming research.

REFERENCES

- [1] S.B. Dorofeev, Flame acceleration and explosion safety applications, Proceedings of the Combustion Institute. 33 (2011) 2161-2175.
- [2] D.K. Pritchard, Review of explosion mitigation measures for platform legs, HSL/2006/64 (2006).
- [3] I. Glassman, R.A. Yetter, N.G. Glumac, Combustion, 5th ed., Academic Press, Burlington, 2014.
- [4] J.H.S. Lee, I.O. Moen, The mechanism of transition from deflagration to detonation in vapor cloud explosions, Progress in Energy and Combustion Science. 6 (1980) 359-389.
- [5] J.H.S. Lee, The Detonation Phenomenon, Cambridge University Press, Montreal, 2008.
- [6] R.J. Martin, A. Reza, L.W. Anderson, What is an explosion? A case history of an investigation for the insurance industry, J Loss Prev Process Ind. 13 (2000) 491-497.
- [7] K. Terao, Irreversible Phenomena: Ignitions, Combustion, and Detonation Waves, 1st ed., Springer, Yokosuka, Japan, 2007.
- [8] V. Bychkov, V. Akkerman, Explosion triggering by an accelerating flame, Physical Review E. 73 (2006) 066305.
- [9] G.H. Markstein, Nonsteady Flame Propagation, Published for and on behalf of Advisory Group for Aeronautical Research and Development, North Atlantic Treaty Organization by Pergamon Press, 1964.
- [10] V. Parasram, Impact of the explosion and fire at Caribbean petroleum tank terminal in Bayamon Puerto Rico, (2013).
- [11] C. Chan, I.O. Moen, J.H.S. Lee, Influence of confinement on flame acceleration due to repeated obstacles, Combustion and Flame. 49 (1983) 27-39.
- [12] G. Ciccarelli, Critical tube measurements at elevated initial mixture temperatures, Combustion Science and Technology. 174 (2002) 173-183.
- [13] G. Ciccarelli, C.J. Fowler, M. Bardon, Effect of obstacle size and spacing on the initial stage of flame acceleration in a rough tube, Shock Waves. 14 (2005) 161-166.

- [14] G. Ciccarelli, S.B. Dorofeev, Flame acceleration and transition to detonation in ducts, *Progress in Energy and Combustion Science*. 34 (2008) 499-550.
- [15] M. Donato, The influence of confinement on the propagation of near limit detonation waves, *ProQuest Dissertations and Theses*. (1982).
- [16] S.B. Dorofeev, Hydrogen flames in tubes: Critical run-up distances, *International Journal of Hydrogen Energy*. 34 (2009) 5832-5837.
- [17] V.N. Gamezo, T. Ogawa, E.S. Oran, Flame acceleration and DDT in channels with obstacles: Effect of obstacle spacing, *Combustion and Flame*. 155 (2008) 302-315.
- [18] H. James, *Basic Phenomenology of Deflagration, DDT and Detonation*, 2013 (2002).
- [19] S. Kumagai, I. Kimura, The effect of turbulence on flame propagation in gases, *Symposium (International) on Combustion*. 4 (1953) 667-669.
- [20] I.O. Moen, M. Donato, R. Knystautas, J.H.S. Lee, Flame acceleration due to turbulence produced by obstacles, *Combustion and Flame*. 39 (1980) 21-32.
- [21] A. Teodorczyk, J.H.S. Lee, R. Knystautas, The structure of fast turbulent flames in very rough, obstacle-filled channels, *Symposium (International) on Combustion*. 23 (1991) 735-741.
- [22] P. Middha, O.R. Hansen, Predicting deflagration to detonation transition in hydrogen explosions, *Process Saf. Prog.* 27 (2008) 192-204.
- [23] C. Rosas, S. Davis, D. Engel, P. Middha, K. Van Wingerden, M.S. Mannan, Deflagration to detonation transitions (DDTs): Predicting DDTs in hydrocarbon explosions, *J Loss Prev Process Ind.* 30 (2014) 263-274.
- [24] I.O. Moen, Transition to detonation in fuel-air explosive clouds, *J. Hazard. Mater.* 33 (1993) 159-192.
- [25] J.F. Clarke, Fast flames, waves and detonation, *Progress in Energy and Combustion Science*. 15 (1989) 241-271.
- [26] B.E. Gelfand, S.M. Frolov, M.A. Nettleton, Gaseous detonations: A selective review, *Progress in Energy and Combustion Science*. 17 (1991) 327-371.
- [27] D.L. Chapman, On the rate of explosion in gases, *Philosophical Magazine*. 47 (1889) 90-104.
- [28] E. Jouguet, Sur l'onde explosive, *C. R. Acad. Sci. Paris*. 140 (1904) 1211.

- [29] P. Laffite, Sur la propagation de l'onde explosive, *Comptes Rendues*. 176 (1923) 1392-1395.
- [30] W.R. Chapman, R.V. Wheeler, VI.-The propagation of flame in mixtures of methane and air. Part V. The movement of the medium in which the flame travels, *Journal of the Chemical Society*. (1927) 38-46.
- [31] K.I. Shchelkin, Effect of roughness of the surface in a tube on origination and propagation of detonation in gases, *Journal of Experimental and Theoretical Physics*. 10 (1940) 823-827.
- [32] H. Guenoche, N. Manson, Influence des Conditions aux Limites Transversales sur la Propagation des Ondes de Choc et de Combustion, *Revue de l'Institut Français du Pétrole*. 2 (1949).
- [33] C. Brochet, Contribution a l'étude des détonations instables dans les mélanges gazeux, (1966).
- [34] A. Teodorczyk, J.H.S. Lee, R. Knystautas, Propagation mechanism of quasi-detonations, *Symp. Int. Combust.* 22 (1988) 1723-1731.
- [35] A. Teodorczyk, Scale effects on hydrogen-air fast deflagrations and detonations in small obstructed channels, *J Loss Prev Process Ind.* 21 (2008) 147-153.
- [36] O. Peraldi, R. Knystautas, J.H.S. Lee, Criteria for transition to detonation in tubes, *Symposium (International) on Combustion*. 21 (1988) 1629-1637.
- [37] G.A. Lyamin, V.V. Mitrofanov, A.V. Pinaev, V.A. Subbotin, Propagation of Gas Explosion in Channels with Uneven Walls and in Porous Media, in: A.A. Borissov (Ed.), *Dynamic Structure of Detonation in Gaseous and Dispersed Media*, Dordrecht ; Boston : Kluwer Academic Publishers, 1991], 1991, pp. 51-75.
- [38] A. Makris, The propagation of gaseous detonation in porous media, Doctorate's Thesis, McGill University. (1993).
- [39] A. Makris, H. Shafique, J.H.S. Lee, R. Knystautas, Influence of mixture sensitivity and pore size on detonation velocities in porous media, *Shock Waves*. 5 (1995) 89-95.
- [40] M. Kuznetsov, V. Alekseev, A. Bezmelnitsyn, W. Breitung, S. Dorofeev, I. Matsukov, A. Vesper, Y. Yankin, Effect of obstacle geometry on behavior of turbulent flames, Institut für Kern- und Energietechnik Projekt Nukleare Sicherheitsforschung. (1999).

- [41] S.Y. Lee, J. Watts, S. Saretto, S. Pal, C. Conrad, R. Woodward, R. Santoro, Deflagration to Detonation Transition Processes by Turbulence-Generating Obstacles in Pulse Detonation Engines, *Journal of Propulsion and Power*. 20 (2004) 1026-1036.
- [42] M. Cross, G. Ciccarelli, DDT and detonation propagation limits in an obstacle filled tube, *J Loss Prev Process Ind.* 36 (2015) 380-386.
- [43] M.A. Nettleton, *Gaseous Detonations: Their Nature, Effect and Control*, Springer Netherlands, 1987.
- [44] R. Blanchard, D. Arndt, R. Grätz, S. Scheider, Effect of ignition position on the run-up distance to DDT for hydrogen–air explosions, *J Loss Prev Process Ind.* 24 (2011) 194-199.
- [45] D. Bjerketvedt, J.R. Bakke, K. van Wingerden, *Gas explosion handbook*, 52 (1997) 1-150.
- [46] Buncefield Major Incident Investigation Board, *The Buncefield Incident, 11 December 2005: The Final Report of the Major Incident Investigation Board*, Health and Safety Executive, 2008.
- [47] M. Girdhar, Jaipur Fire and its Environmental effects, *ESRI India User Conference*. (2011).
- [48] N.L. Polley, M.Q. Egbert, E.L. Petersen, Methods of re-initiation and critical conditions for a planar detonation transforming to a cylindrical detonation within a confined volume, *Combust. Flame*. 160 (2013) 212-221.
- [49] N. Polley, *Detonation Diffraction into a Confined Volume*, Master's thesis, Texas A&M University. Available electronically from <http://hdl.handle.net/1969>. (2010).
- [50] P.J. Ross, *Taguchi Techniques for Quality Engineering*, McGraw-Hill, New York, New York, 1996.
- [51] S. Kitano, M. Fukao, A. Susa, N. Tsuboi, A.K. Hayashi, M. Koshi, Spinning detonation and velocity deficit in small diameter tubes, *Proceedings of the Combustion Institute*. 32 (2009) 2355-2362.
- [52] M. Kuznetsov, V. Alekseev, I. Matsukov, S. Dorofeev, DDT in a smooth tube filled with a hydrogen-oxygen mixture, *Shock Waves*. 14 (2005) 205-215.
- [53] H. Matsui, J.H. Lee, On the measure of the relative detonation hazards of gaseous fuel-oxygen and air mixtures, *Symp. Int. Combust.* 17 (1979) 1269-1280.

- [54] F. Pintgen, J.E. Shepherd, Detonation diffraction in gases, *Combust. Flame*. 156 (2009) 665-677.
- [55] R.A. Strehlow, Multi-dimensional detonation wave structure, *Acta Astronautica*. 15 (1970) 345-357.
- [56] S. Browne, J. Ziegler, J.E. Shepherd, Shock and Detonation Toolbox, GALCIT - Explosion Dynamics Laboratory. (2008).
- [57] J. Card, D. Rival, G. Ciccarelli, DDT in fuel-air mixtures at elevated temperatures and pressures, *Shock waves*. 14 (2005) 167-173.
- [58] D. Desbordes, Transmission of Overdriven Plane Detonations: Critical Diameter as a Function of Cell Regularity and Size, in: *Anonymous Dynamics of Explosions*, American Institute of Aeronautics and Astronautics, 1988, pp. 170-170-185.
- [59] S. Browne, J. Ziegler, J.E. Shepherd, Glossary on Explosion Dynamics, 2015 (2008).
- [60] A. Teodorczyk, Fast deflagrations and detonations in obstacle-filled channels, *Institute of Heat Engineering - Warsaw University of Technology*. 79 (1995) 145-178.
- [61] Ontario Fire Marshall, Sunrise Propane explosion investigation report, Inv. No.:212-007-2008 (2010).
- [62] D.M. Johnson, Characteristics of the Vapour Cloud Explosion Incident at the IOC Terminal in Jaipur, Noble Denton Report 11510 (2011).
- [63] B.H. Hjertager, Computer Simulation of Turbulent Reactive Gas Dynamics, *Modeling, Identification and Control*. 5 (1984) 211-236.
- [64] C. Selby, B. Burgan, Blast and fire engineering for topside structures, phase 2, final summary report, SCI-P--253 (1988).
- [65] A.M. Khokhlov, E.S. Oran, G.O. Thomas, Numerical simulation of deflagration-to-detonation transition: the role of shock-flame interactions in turbulent flames, *Combustion and Flame*. 117 (1999) 323-339.
- [66] D.A. Kessler, V.N. Gamezo, E.S. Oran, Simulations of flame acceleration and deflagration-to-detonation transitions in methane-air systems, *Combustion and Flame*. 157 (2010) 2063-2077.
- [67] T. Ogawa, V.N. Gamezo, E.S. Oran, Flame acceleration and transition to detonation in an array of square obstacles, *Journal of Loss Prevention in the Process Industries*. 26 (2013) 355-362.

- [68] B.E. Launder, D.B. Spalding, The numerical computation of turbulent flows, *Computer Methods in Applied Mechanics and Engineering*. 3 (1974) 269-289.
- [69] R.G. Abdel-Gayed, D. Bradley, M. Lawes, Turbulent Burning Velocities: A General Correlation in Terms of Straining Rates, *Proceedings of the Royal Society of London A: Mathematical, Physical and Engineering Sciences*. 414 (1987) 389-413.
- [70] B.J. Arntzen, Modeling of turbulence and combustion for simulation of gas explosions in complex geometries, PhD Thesis (1998).
- [71] R. Knystautas, J.H.S. Lee, J.E. Shepherd, A. Teodorczyk, Flame acceleration and transition to detonation in benzene-air mixtures, *Combustion and Flame*. 115 (1998) 424-436.
- [72] S.B. Dorofeev, V.P. Sidorov, M.S. Kuznetsov, I.D. Matsukov, V.I. Alekseev, Effect of scale on the onset of detonations, *Shock Waves*. 10 (2000) 137-149.
- [73] M. Silvestrini, B. Genova, G. Parisi, F.J. Leon Trujillo, Flame acceleration and DDT run-up distance for smooth and obstacles filled tubes, *Journal of Loss Prevention in the Process Industries*. 21 (2008) 555-562.
- [74] M.A. Liberman, M.F. Ivanov, A.D. Kiverin, M.S. Kuznetsov, A.A. Chukalovsky, T.V. Rakhimova, Deflagration-to-detonation transition in highly reactive combustible mixtures, *Acta Astronautica*. 67 (2010) 688-701.
- [75] D. Valiev, V. Bychkov, V. Akkerman, C.K. Law, L.E. Eriksson, Flame acceleration in channels with obstacles in the deflagration-to-detonation transition, *Combustion and Flame*. 157 (2010) 1012-1021.
- [76] A.V. Gaathaug, K. Vaagsaether, D. Bjerketvedt, Experimental and numerical investigation of DDT in hydrogen-air behind a single obstacle, *International Journal of Hydrogen Energy*. 37 (2012) 17606-17615.
- [77] M. Royle, L.C. Shirvill, T.A. Roberts, Vapour Cloud explosions from the ignition of methane/hydrogen/air mixtures in a congested region, In *Proceedings of 2nd International Conference on Hydrogen Safety*. (2007).
- [78] A. Teodorczyk, P. Drobniak, A. Dabkowski, Fast turbulent deflagration and DDT of hydrogen-air mixtures in small obstructed channel, *International Journal of Hydrogen Energy*. 34 (2009) 5887-5893.
- [79] M. Kuznetsov, G. Ciccarelli, S.B. Dorofeev, V. Alekseev, Y. Yankin, T.H. Kim, DDT in methane-air mixtures, *Shock Waves*. 12 (2002) 215-220.

[80] J.K. Thomas, M.L. Goodrich, R.J. Duran, Propagation of a vapor cloud detonation from a congested area into an uncongested area: Demonstration test and impact on blast load prediction, *Process Safety Progress*. 32 (2013) 199-206.

[81] W.P.M. Merx, Modelling and experimental research into gas explosions. Overall final report of the MERGE project, STEP-CT-0111 (SSMA).

[82] I.O. Moen, J.H.S. Lee, B.H. Hjertager, K. Fuhre, R.K. Eckhoff, Pressure development due to turbulent flame propagation in large-scale methane-air explosions, *Combustion and Flame*. 47 (1982) 31-52.

[83] D.J. Mackay, S.B. Murray, I.O. Moen, P.A. Thibault, Flame-jet ignition of large fuel-air clouds, *Symposium (International) on Combustion*. 22 (1989) 1339-1353.

[84] I.O. Moen, D. Bjerketvedt, A. Jenssen, P.A. Thibault, Transition to detonation in a large fuel-air cloud, *Combustion and Flame*. 61 (1985) 285-291.